



4

5

7

8

9

10

11

12

13

14

15

16

17

18

19

20

21

22

23

24

25

26

27

28 29

30

31

32

33

34

35

36

37

38

39

Review

# Recent advances in mitigating catalyst deactivation of CO<sub>2</sub> hydrogenation to light olefins

Daniel Weber<sup>1</sup>, Tina He<sup>2</sup>, Mathew Wong<sup>3</sup>, Christian Moon<sup>1</sup>, Axel Zhang<sup>4</sup>, Nicole Foley<sup>1</sup>, Nicholas J. Ramer<sup>1,\*</sup> and Cheng Zhang<sup>1,\*</sup>

- Chemistry Department, Long Island University (Post), Brookville, NY 11548, USA; Emails: <u>Daniel.weber4@my.liu.edu</u> (D.W.); <u>Christian.moon@my.liu.edu</u> (C.M.); <u>nicole.foley2@my.liu.edu</u> (N.F.).
- <sup>2</sup> College of Natural Science, The University of Texas at Austin, Austin, TX 78712, USA; E-mail: tinah00@utexas.edu (T.H.).
- 3. College of Engineering, Cornell University, Ithaca, New York, NY 14850, USA; Email: <a href="mwong0127@gmail.com">mwong0127@gmail.com</a> (M.W.)
- 4. College of Science, John Jay University, New York, NY 11200, USA; Email: axelzhang59@gmail.com (A.Z.)
- \* Author to whom correspondence should be addressed; Email: nicholas.ramer@liu.edu (N.R.); Tel.: 01-516-299-3034; cheng.zhang@liu.edu (C.Z.); Tel.: 01-516-299-2013; Fax: 01-516-299-3944.

Abstract: Catalytic conversion of CO<sub>2</sub> to value-added chemicals and fuels has been long regarded as a promising approach to mitigate CO<sub>2</sub> emissions if green hydrogen is used. Light olefins, particularly ethylene and propylene, as building blocks for polymer and plastics are currently produced primarily from CO<sub>2</sub>-generating fossil resources. Identifying highly efficient catalysts with selective pathways for light olefin production from CO<sub>2</sub> is a high-reward goal but has serious technical challenges, such as low selectivity and catalyst deactivation. In this review, we first provide a brief summary of the two dominant reaction pathways (CO<sub>2</sub>-Fischer-Tropsch and MeOH-mediated), mechanistic insights and catalytic materials for CO<sub>2</sub> hydrogenation to light olefins. Then we list the main deactivation mechanisms caused by carbon deposition, water formation, phase transformation and metal sintering/agglomeration. Finally, we detail the recent progress on catalyst development for enhanced olefin yields and catalyst stability by the following catalyst functionalities: 1) promoter effect; 2) support effect; 3) bifunctional composite catalyst effect; and 4) structure effect. Our main focus of this review is to provide a useful resource for researchers to correlate the catalyst deactivation and recent research effort on catalyst development for enhanced olefin yield and catalyst stability.

**Keywords:** CO<sub>2</sub> hydrogenation, light olefins, catalyst deactivation, CO<sub>2</sub>-Fischer-Tropsch (CO<sub>2</sub>-FT), iron based catalysts, methanol to olefins, bifunctional composite catalysts, SAPO-34.

Citation: Lastname, F.; Lastname, F.; Lastname, F. Title. *Catalysts* **2021**, *11*, x. https://doi.org/10.3390/xxxxx

Academic Editor: Firstname Lastname

Received: date Accepted: date Published: date

**Publisher's Note:** MDPI stays neutral with regard to jurisdictional claims in published maps and institutional affiliations.



Copyright: © 2021 by the authors. Submitted for possible open access publication under the terms and conditions of the Creative Commons Attribution (CC BY) license (https://creativecommons.org/license s/by/4.0/).

#### 1. Introduction

1.1 General aspects

While carbon-rich fossil fuels like coal, oil, and natural gas have been powering human civilization, the massive emission of CO<sub>2</sub> as a greenhouse gas has caused severe and harmful effects on the ecological environment [1]. For example, the rise of sea levels is accelerating, the number of large hurricanes and wildfires is growing, dangerous heat waves and more severe droughts are occurring in many areas [2]. CO<sub>2</sub> concentration in the atmosphere had climbed to 415 ppm by 2020 (Figure 1), an increase of more than 40% relative to the pre-industrial era [3]. CO<sub>2</sub> concentration in the atmosphere will continue to

rise to ~570 ppm by the end of the century if no measures are taken [4]. Therefore, there is an urgent need to control CO<sub>2</sub> emission to mitigate its negative impact on the environment. In recent years, technologies for capturing and storing

the CO<sub>2</sub> released from the burning of fossil fuels have emerged and developed in potential commercial scale applications [5] [6] [7]]. To close the carbon gap, transforming the captured gas into value-added fuels and chemicals has become an urgent task for CO<sub>2</sub> remediation [8] [9]].

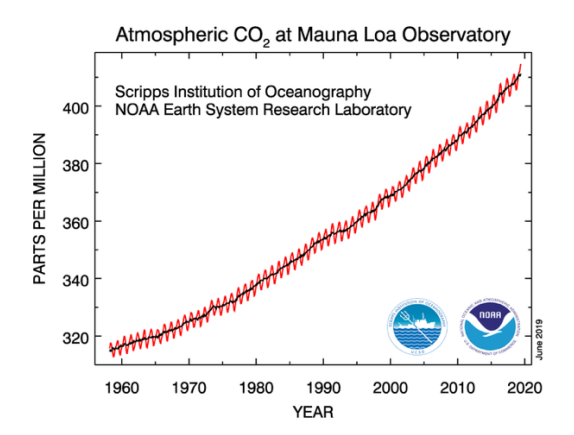
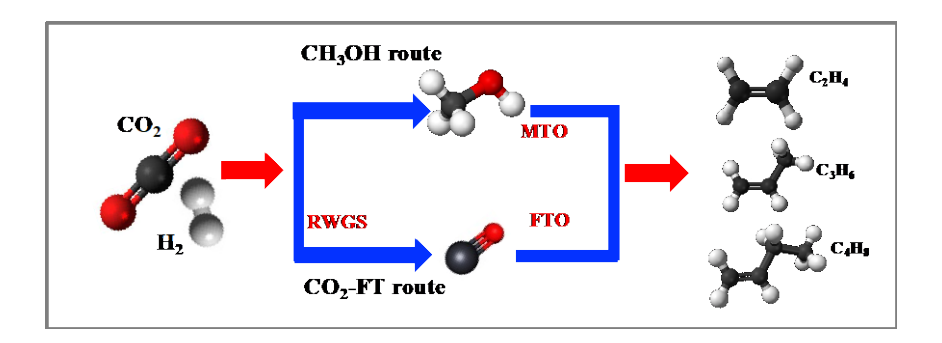


Figure 1. Trends in atmospheric CO<sub>2</sub> concentration (ppm) [3]

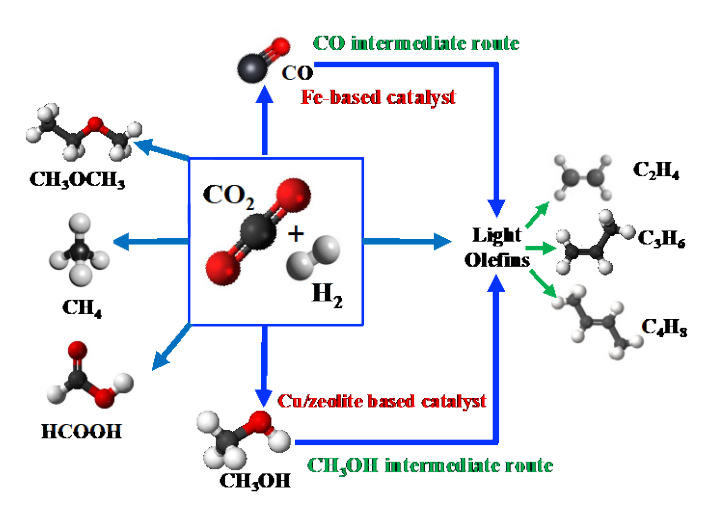
Catalytic conversion of CO<sub>2</sub> is a promising approach to mitigate CO<sub>2</sub> emissions by producing chemicals and fuels [8] [10] [11] [12] [13] [14] [15] [16] [17]]. Light olefins such as ethylene, propylene and butylene (C<sub>2</sub>--C<sub>4</sub>-), currently among the top petrochemicals, are the building blocks for the production of a wide variety of polymers, plastics, solvents, and cosmetics [8] [13] [18] [19] [20] [21]]. Moreover, light olefins can be oligomerized into long-chain hydrocarbons as fuels, making them a desirable product with high potential for utilizing up to 23% of CO<sub>2</sub> emissions [8]. A highly promising route is the selective CO<sub>2</sub> hydrogenation to produce light olefins [10]. The huge market demand for the lower olefins offers a great opportunity for the target technology to profoundly impact the scale of CO<sub>2</sub> utilization once it is developed with renewable hydrogen. The current chemical industry relies heavily on petroleum (steam cracking of naphtha) for the production of light olefins [22]. The depletion or movement away from refining of petroleum and the gap between supply and demand of light olefins call for a new strategy to synthesize light olefins from alternative carbon sources [18] [19] [20] [21] [23] [24]. One-step process for converting CO<sub>2</sub> to light olefins is a promising approach to address the "3Rs" (reduce, reuse, and recycle) associated with ever-increasing CO<sub>2</sub> levels, and solving the paradox between supply and demand of light olefins [25].



Scheme 1. Reaction route for CO<sub>2</sub> hydrogenation to light olefins

Currently, there are two primary pathways as shown in **Scheme 1** to produce light olefins from  $CO_2$  reduction by hydrogen (H<sub>2</sub>) in a one-step process: (1)  $CO_2$ -Fischer-Tropsch ( $CO_2$ -FT) route consists of two consecutive processes, the reverse water-gas shift (RWGS) reaction (eqn 1) and subsequent Fischer-Tropsch synthesis (FTS) (eqn 2). (2) Methanol (MeOH) mediated route consists of two consecutive processes:  $CO_2$ -to-MeOH (eqn 3) and a subsequent MeOH-to-

olefins (MTO) (eqn 4). The complex reaction network in scheme 2 indicates the competing reactions (i.e. eq.5) with the formation of light olefins. Controlling the selectivity of CO<sub>2</sub> hydrogenation to the desired olefin product requires the design of catalysts for reaction pathways that are compatible with favorable thermodynamics and a good understanding of the reaction kinetics [26]. The thermodynamic values in equations (eqn 1-5) indicates that lower temperatures favor FTS (eqn 2), methanol (eqn 3), and methane synthesis (eqn 5), while higher temperatures are needed to activate CO<sub>2</sub> (eqn 1) for fast reaction rates [27]. The complex reaction network in Scheme 2 and thermodynamics suggest that design and synthesis of catalysts for a one-step process to selectively produce olefins is challenging.



Scheme 2. Complex reaction network for CO<sub>2</sub> conversion to chemicals through hydrogenation

CO<sub>2</sub>-FTS reaction pathway:

Reverse water-gas shift reaction (RWGS):

$$CO_2 + H_2 \rightarrow CO + H_2O \triangle H_0^{298} = 41.1 \text{ kJmol}^{-1}$$
 (1)

Fischer-Tropsch synthesis to olefins (FTS):

$$nCO + 2nH_2 \rightarrow (CH_2)_n + nH_2O \quad \triangle H_0^{298} = -210.2 \text{ kJmol}^{-1} \text{ (n=2)}$$
 (2)

Methanol mediated reaction pathway:

Methanol synthesis

$$CO_2 + 3H_2 \rightarrow CH_3OH + H_2O \triangle H_0^{298} = -49.3 \text{ kJmol}^{-1}$$
 (3)

Methanol to Olefins (MTO)

$$nCH_3OH \rightarrow (CH_2)_n + H_2O \qquad \triangle H_0^{298} = -29.3 \text{ kJmol}^{-1} (n=2)$$
 (4)

CO<sub>2</sub> methanation

$$CO_2 + 4H_2 \rightarrow CH_4 + 2H_2O \qquad \Delta H_0^{298} = -165.0 \text{ kJmol}^{-1}$$
 (5)

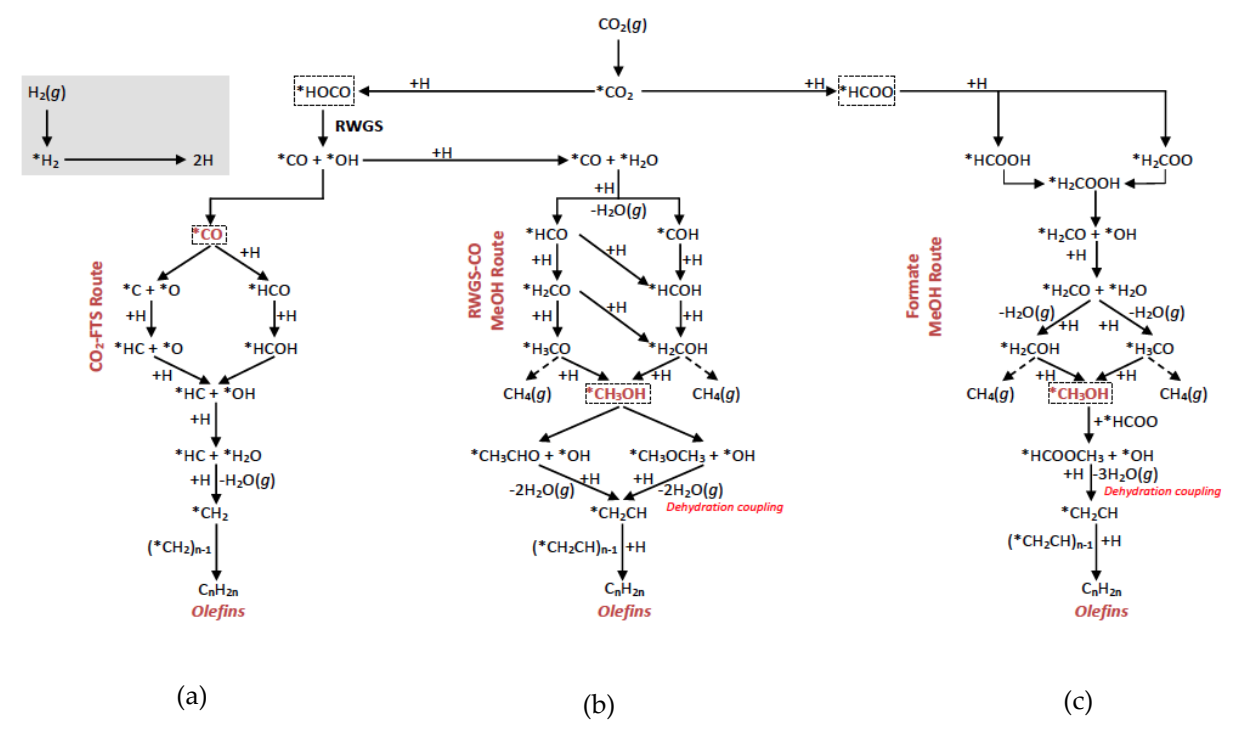
## 1.2 Mechanistic insights for CO2 converstion to light olefins

In light of the formation mechanism of light olefins, the key point is to control the active H/C to an appropriate ratio, wherein too much surface H\* will lead to excessive hydrogenation and methane formation, while the opposite

condition will offset the hydrogenation ability and reduce the activity of CO<sub>2</sub> conversion. The crucial step of light olefins synthesis by CO<sub>2</sub> hydrogenation is C–C bond formation and C–O bond cleavage [28].

Fe-based catalysts are extensively studied for CO<sub>2</sub>-FTS route due to their relatively high activity for both the RWGS and FTS reactions. During CO<sub>2</sub>-FTS over Fe-based catalysts, the initial Fe<sub>2</sub>O<sub>3</sub> phase is reduced by hydrogen to Fe<sub>3</sub>O<sub>4</sub> or a mixture of Fe<sub>3</sub>O<sub>4</sub> and FeO. The Fe<sub>3</sub>O<sub>4</sub> is the active phase for the RWGS reaction and can be further reduced to form metallic Fe [27]. The reaction mechanism for the CO<sub>2</sub>-FTS pathway is suggested as shown in Scheme 3a. CO<sub>2</sub> is first absorbed and activated on the RWGS active phases (e.g., Fe<sub>3</sub>O<sub>4</sub>) to form carboxylate species (\*CO<sub>2</sub>, \* representing the adsorption state). These \*CO<sub>2</sub> can be hydrogenated by adsorbed H to form an \*HOCO intermediate, which then dissociates into \*OH and \*CO species. The \*OH is hydrogenated into \*H<sub>2</sub>O and \*CO either desorbs as gaseous CO or reacts further via successive FTS. To form hydrocarbons, the \*CO species are first hydrogenated into \*HCO and then undergo hydrogenation, dissociation, and dehydration processes to form \*CH<sub>x</sub> species, which are the precursors for the formation of olefins. In an alternative mechanism, \*CO dissociates into \*C and \*O. Some \*C can diffuse into the metal lattice to form metal carbides such as  $\chi$ -Fe<sub>5</sub>C<sub>2</sub>, the active phase for the FTS reaction [27]. The C\* on the  $\chi$ -Fe<sub>5</sub>C<sub>2</sub> surface is then hydrogenated to CH<sub>x</sub>\* species. C\*+CH<sub>x</sub>\* and CH<sub>x</sub>\*+CH<sub>x</sub>\* were the most likely coupling pathways [28].

As mentioned above, \*CO can dissociate into \*C and \*O during the FTS reaction, and these \*C species diffuse into the  $\alpha$ -Fe lattice, potentially forming Fe<sub>7</sub>C<sub>3</sub>,  $\chi$ -Fe<sub>5</sub>C<sub>2</sub>,  $\theta$ -Fe<sub>3</sub>C,  $\epsilon'$ -Fe<sub>2</sub>2C, and  $\epsilon$ -Fe<sub>2</sub>C phases under different reaction conditions [27]. Fe carbides play an important role in CO hydrogenation/dissociation and C–C coupling. Some researchers propose that  $\chi$ -Fe<sub>5</sub>C<sub>2</sub> is the active phase, while  $\theta$ -Fe<sub>3</sub>C is less active and can cause catalyst deactivation due to transformation to graphitic carbon, which is stable under the FTS conditions and might block other active phases [27][29].



Scheme 3. Reaction mechanism for CO<sub>2</sub> hydrogenation to light olefins (modified from [27] and requested with permission)

Alternatively, the reaction mechanism for the MeOH pathway is suggested as shown in Scheme 3b-c. There are two main pathways for the synthesis of methanol: (1) CO-mediated, in which the \*CO intermediate produced from the RWGS reaction via the carboxyl (\*HOCO) species is hydrogenated to methanol via \*HCO and \*COH. and (2) formate-

mediated, in which the formate (\*HCOO) species is formed by hydrogenation of the carboxylate intermediate (\*CO<sub>2</sub>), which is further reacted to form \*H<sub>2</sub>COOH, \*H<sub>2</sub>CO, \*H<sub>2</sub>COH, and \*H<sub>3</sub>CO. The methanol then undergoes dehydration coupling to form \*CH<sub>2</sub>CH and subsequent hydrogenation into olefins [27].

## 1.3 Catalysts for CO<sub>2</sub> conversion to light olefins

Various catalysts have been utilized for CO<sub>2</sub> hydrogenation to olefins through both the CO<sub>2</sub>-FTS and MeOH routes. In the CO<sub>2</sub>-FT path, Fe is one of the most widely used components in the catalysts as they offer less methanation activity under high reaction temperatures. It was reported that the Fe<sub>3</sub>O<sub>4</sub> was responsible for RWGS, the metallic Fe and iron carbides could activate CO and produce hydrocarbons [30] [31]. When modified with alkali promoters, Fe-based catalysts exhibit higher olefin selectivity. The alkali metals perform as electron donors to Fe metal centers, facilitating CO<sub>2</sub> adsorption while lowering their affinity with H<sub>2</sub>, and consequently lead to higher olefins yield [32] [33] [34]. Doping the catalyst with a second metal may promote olefin yields by forming a highly active interface. The second metal components account for tuning the CO<sub>2</sub> and H<sub>2</sub> adsorption and activation, shifting the product distribution towards desired hydrocarbons. Supporting the Fe-based species on supports such as silica (SiO<sub>2</sub>), alumina (Al<sub>2</sub>O<sub>3</sub>), titania (TiO<sub>2</sub>), zirconia (ZrO<sub>2</sub>) and carbon materials (i.e., carbon nanotubes (CNTs), carbon nanospheres (CNSs), graphene oxide (GO)) may enhance the catalytic performance by improving the active metal dispersion and retarding the sintering of the active particles [35] [36]. Controlling hydrocarbon chain growth to achieve a desired carbon range (i.e., C<sub>2</sub>-C<sub>4</sub>) remains a challenge for CO<sub>2</sub> conversion due to the product selectivity limit governed by the Anderson–Schulz–Flory (ASF) distribution with a maximum achievable C<sub>2</sub>-C<sub>4</sub> hydrocarbons selectivity of less than 60 % as shown in Figure 2 [37] [38].

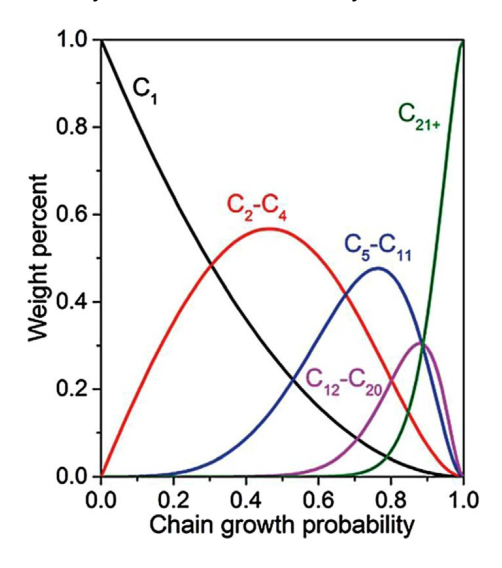


Figure 2. Product distribution according to the Anderson-Schulz-Flory(ASF) model. Reproduced with permission from [37].

Alternatively, in the MeOH path, light olefins can be synthesized with selectivity as high as 80-90 % among hydrocarbons, exceeding the ASF product distribution limit for FTS reactions [39] [40] [41] [42]. Possible reasons for the reported ASF distribution deviation are the blockage of surface polymerization by intermediates, such as ketene (CH<sub>2</sub>CO), space confinement, or the use of bifunctional catalysts with two types of active sites [27]. The deviation from the ASF distribution offers opportunities to increase the selectivity to olefins [2]. Several recent studies have reported to combine MeOH synthesis catalysts (i.e., In<sub>2</sub>O<sub>3</sub>, In-Zr, ZnGa<sub>2</sub>O<sub>4</sub>, MgGa<sub>2</sub>O<sub>4</sub>, ZnAl<sub>2</sub>O<sub>4</sub>, MgAl<sub>2</sub>O<sub>4</sub>, ZnZrO and In<sub>2</sub>O<sub>3</sub>-ZnZrO<sub>2</sub>) with MTO catalyst (i.e., SAPO-34, SSZ-13 and ZSM-5) for producing light olefins with enhanced selectivity

from CO<sub>2</sub> hydrogenation [43] [44] [45] [46]. The secondary functionality of acid-base sites on supports can significantly impact the light olefins selectivity. For example, passivation of the Brønsted acid sites of In<sub>2</sub>O<sub>3</sub>-ZnZrOx/SAPO-34 inhibits the secondary hydrogenation reaction, thereby improving the olefin selectivity [27].

## 1.4 The main focus of this review

Even though significant efforts have been made, considerable challenges remain in the development of highly efficient catalysts with selective pathways to light olefins due to the thermodynamically stable nature of the CO<sub>2</sub> molecule, the complexity of reaction networks and catalyst deactivation [8] [47] [48]. Several recent reviews have summarized the CO<sub>2</sub> hydrogenation to value-added products including light olefins [27] [37] [38] [28]. However, it is necessary to present a review focused on the recent advances in mitigating catalyst deactivation of CO<sub>2</sub> hydrogenation to light olefins since catalyst deactivation has been a big challenge that provides economic hurdles to adopt the new technologies.

Since catalysts and mechanisms have been extensively reviewed in numerous review papers [27] [37] [38] [28], the focus of the current article is to identify possible causes that trigger catalyst deactivation and summarize recent advances on catalyst development with enhanced catalyst stability and light olefin selectivity for CO<sub>2</sub> hydrogenation. In this review, we first provide a brief summary of the two dominant reaction pathways (CO<sub>2</sub>-FTS and MeOH-mediated), mechanistic insights and catalytic materials for CO<sub>2</sub> hydrogenation to light olefins. Then we list the deactivation mechanism caused by carbon deposition, water formation, phase transformation and metal sintering/agglomeration. Finally, we summarize the recent progress published within five years on catalyst development that improves catalyst deactivation by the following catalyst functionalities: 1) promoter effect; 2) support effect; 3) hybrid functional effect; and 4) structure effect.

Each one of these aspects is accompanied by a suitable table in which the most significant literature findings are comparatively presented, we attempt to provide a useful resource for researchers to correlate the catalyst deactivation and recent research effort on catalyst development for enhanced olefin yield and catalyst stability.

# 2. Causes of catalyst deactivation

During CO<sub>2</sub> hydrogenation, catalyst deactivation can occur via several mechanisms, resulting in decreased activity and selectivity toward desired olefins. Determining the mechanism of deactivation is an important step toward mitigation. The primary causes for catalyst deactivation are sintering (or agglomeration) of metal particles, phase transformation at the catalyst's surface and catalyst poisoning by water or carbonaceous deposits (i.e., coke). An understanding of the deactivation causes is necessary to develop a mitigation strategy and sustain high selectivity toward desired olefins during CO<sub>2</sub> hydrogenation. For context, we present brief descriptions of each of these causes with a few representative examples from the literature that demonstrate the necessity for robust and novel mitigation studies. More thorough reviews of deactivation causes and their mechanisms can be found elsewhere [49] [50] [51].

# 2.1 Sintering

Catalyst sintering can occur through either Ostwald ripening or particle migration and coalescence as shown in Figure 3. Through sintering, the agglomeration of smaller catalyst crystals into larger ones will bring about the loss of pore structure which lowers the internal surface area of the catalyst, leading to the deactivation. In the area of FT by cobalt catalysts, several groups have determined that particle growth of cobalt is the largest factor causing deactivation [52] [53].

187

188

189

190 191

192

193

194

195

196

197

198

199

200

201

202

203

204

205

206

207

Sun et al. [54] examined how sintering in zinc- and alumina-supported copper catalysts (Cu/ZnO/Al<sub>2</sub>O<sub>3</sub>). It was found that the presence of CO in the process employed for CH<sub>3</sub>OH synthesis strongly contributed to the deactivation of the catalysis over 0 to 50 h. Taken with corroborative evidence from Cu surface area determination, the deactivation was likely attributed to sintering of the Cu metal.

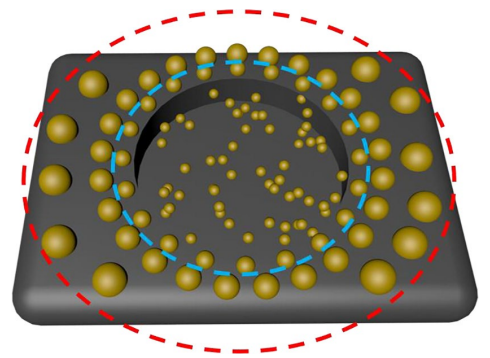


Figure 3. Diagram of active phase sintering occurring over a support material: blue ring - atomic migration to form larger crystallites; Red ring - the coalescence of crystallites . Reproduced with permission from [55]).

As mentioned above, sintering negatively affects the catalytic performance due to many reasons: the overall catalytically active surface area is reduced, loss of support material surface area due to its collapse causing a subsequent catalytic surface area loss and chemical alteration of the catalytically active phases to non-active phases [55] [56] [57]. As this form of deactivation involves the coalescence of larger particles from smaller, it is extremely difficult to reverse. Sintering, therefore, is easier to prevent through careful catalyst design [55] [58]. For example, Li et al. observed the remarkable metal sintering on supported FeCo/ZrO<sub>2</sub> catalysts [58]. As shown in Figure 4A(a), for the 13Fe2Co/ZrO<sub>2</sub> supported catalyst precursor prepared using conventional impregnation method, the Co and Fe are distributed into separate oxide particles, which increased the possibility of sintering as confirmed in Figure 4A(b-c) that aggregates composed of Fe and Co oxide nanoparticles were observed on the ZrO2 fibers, with an average diameter of ca. 15 nm before the reaction. The particle size increased to 48 nm after the reaction, which was responsible for the rapid deactivation of activity (Figure 4A(d-f)). In contrast, Fe-Co-Zr polymetallic fibers obtained by a one-step electrospinning technique depicted that Co and Fe were dispersed in proximity to ZrO<sub>2</sub> as shown in Figure 4C(a), but separately from each other, which helped reduce the possibility of sintering, as demonstrated in Figure 4C(a-f), the Fe and Co oxides nanoparticles successfully dispersed with the ZrO2 particles for the polymetallic oxide fibers, with an average size of roughly 1-2 nm before the reaction, and after the reaction, the particle size barely changed, which contributed to the stable catalytic activity after 500 mins on stream (Figure 4B(a-b)).

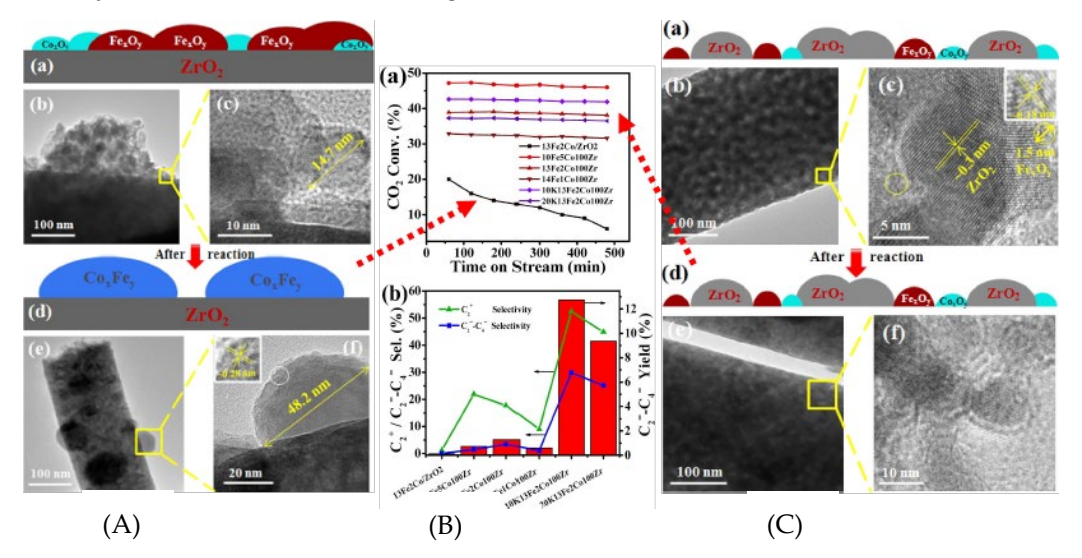


Figure 4. (A): (a-f) Schematic illustration of metal distribution and TEM images of  $13\text{Fe}2\text{Co}/\text{ZrO}_2$  supported catalyst precursor (a-c) and spent catalyst (d-f). (B): CO<sub>2</sub> conversion (a) and C<sub>2+</sub>/C<sub>2</sub>=-C<sub>4</sub>= selectivity and C<sub>2</sub>=-C<sub>4</sub>= yield (b) over different catalysts after 8 h TOS. Reaction conditions: molar ratio of H<sub>2</sub>/CO<sub>2</sub> = 3/1, GHSV = 7200 ml g<sup>-1</sup> h<sup>-1</sup>, P = 3 MPa, T = 673K. (C): (a-f) Schematic illustration of metal distribution and TEM images of 13Fe2Co100Zr polymetallic oxide fibers catalyst (a-c) and spent catalyst (d-f). Reproduced with permission from [58].

# 2.2 Phase Transformations

Phase transformations are processes of deactivation involving the conversion of an active crystalline phase of the catalyst (or one of its components) into a different inactive one. These transformations can involve both metal-supported and metal-oxide catalysts. In the former type of catalysts, atoms from the catalyst's support will diffuse into the catalyst's surface. A reaction at the surface can then result in an inactive phase, deactivating the catalyst.

Riedel et al. demonstrated that the steady states of hydrocarbons synthesis over iron oxides could be divided into five episodes of distinct kinetic regimes. In episode I, the reactants adsorb on the catalyst surface and carbonization of the catalyst takes place dominantly. In episodes II and III, products from the RWGS reaction dominate during ongoing carbon deposition. In episode IV, the FT activity develops up to the steady state and keeps the state in episode V. The iron phases of the reduced catalyst before reaction consist of mainly  $\alpha$ -Fe and Fe<sub>3</sub>O<sub>4</sub>, and small amount of Fe<sub>2</sub>O<sub>3</sub>. With time, Fe<sub>3</sub>O<sub>4</sub> and Fe<sub>2</sub>O<sub>3</sub> phases are consumed and a new amorphous, oxidic iron phase is formed, which appears to be active for the RWGS reaction. FT activity begins under the formation of iron carbide (Fe<sub>3</sub>C<sub>2</sub>) by a reaction of iron with carbon from CO dissociation. The stable but inactive carbide (Fe<sub>3</sub>C) is accountable for the deactivation of the catalyst, which is formed by Fe<sub>5</sub>C<sub>2</sub> carburization [59] [60] [61]. Lee et al. investigated the causes for deactivation of Fe–K/ $\gamma$ -Al<sub>2</sub>O<sub>3</sub> for CO<sub>2</sub> hydrogenation to hydrocarbons and found the causes for deactivation were different at different positions in the reactor. With time, the Fe<sub>2</sub>O<sub>3</sub> was reduced to active phase  $\chi$ -Fe<sub>5</sub>C<sub>3</sub> and then the  $\chi$ -Fe<sub>5</sub>C<sub>3</sub> was transformed to 0-FeC<sub>3</sub>, which is not an active species for CO<sub>2</sub> hydrogenation. The main deactivation reason was the phase transformation at the top of the reactor. Conversely, the main factor at the bottom of the reactor was the deposited coke generated by secondary reactions [59].

Zhang et al. reported the structure evolution of the iron catalyst during its full catalytic life cycle of CO<sub>2</sub> to olefins (CTO), including the catalyst activation, reaction/deactivation (120 h) and regeneration. The phase transition during CO activation is observed to follow the sequence of Fe<sub>2</sub>O<sub>3</sub>  $\rightarrow$  Fe<sub>3</sub>O<sub>4</sub>  $\rightarrow$  Fe  $\rightarrow$  Fe<sub>5</sub>C<sub>2</sub>. The primary deactivation mechanism during CTO is identified as the irreversible transition of iron phases under reaction conditions. Two possible pathways of phase transition of iron catalyst under CTO conditions have been identified, i.e., Fe<sub>5</sub>C<sub>2</sub>  $\rightarrow$  Fe<sub>3</sub>O<sub>4</sub> and Fe<sub>5</sub>C<sub>2</sub>  $\rightarrow$  Fe<sub>3</sub>O<sub>4</sub>. Moreover, carbon deposition and agglomeration of catalyst particle proves to have relatively minor impacts on the catalytic activity compared with phase transition during the 120 h of reaction [62].

It appears that transformation to iron oxides will destroy catalyst activity. There is some question on whether the cementite phase itself is problematic to activity, as higher surface area cementite phases have been reported to do CO<sub>2</sub> hydrogenation quite effectively [63].

### 2.3 Poisoning

Catalytic poisoning is a result of the strong chemisorption of reactants, products or impurities on sites that would otherwise be capable of catalysis. In essence, the poisoning ability of a particular species is related to the strength of its chemisorption to the catalysis relative to the other reactants that are competing for the catalytic active sites. The poisoning has two deactivating effects; a poison physically blocks the active sites from receiving additional reactants

g 221 ne 222 h 223 ne 224

and a poison can alter the electronic or structural properties of the catalytic surface, rendering it partially or completely ineffective toward catalysis [64] [65].

While there are several different poisons which have been reported in the literature that have shown to deactivate CO<sub>2</sub> hydrogenation catalysts [66] [67], we will focus on the two which are the most pervasive, namely, water and carbonaceous deposits or coke.

# 2.3.1 Water Poisoning

As seen in the above CO<sub>2</sub> hydrogenation reactions, water results from the removal of the oxygen atoms from the dissociation of CO<sub>2</sub>, which is a necessary byproduct for thermodynamic favorability, but can be detrimental to catalytic performance. It is because of this unavoidable mechanistic absolute that the mitigation of water poisoning must be part of all catalytic investigations [68].

Wu et al. [69] [70] examined the effect of the produced water on the stability of Cu/ZnO-based catalysts in methanol synthesis from the high temperature hydrogenation of CO<sub>2</sub>. Specifically, Cu/ZnO/ZrO<sub>2</sub>/Al<sub>2</sub>O<sub>3</sub> (40/30/25/5) was subjected to a CO<sub>2</sub>-rich feed, which produces water, and a CO-rich feed, which does not produce water. Examination of the catalysts by x-ray powder diffraction (XRD) after 1 h and 500 h time-on-stream of a CO<sub>2</sub>-rich feed containing steam showed that the Cu and ZnO crystallized more rapidly when compared to identical catalysts exposed to a CO-rich feed not containing steam. In particular, the Cu particle size in the catalyst used with the CO<sub>2</sub>-rich feed containing steam grew from 94Å to 166Å from 1 h to 500 h. The particle size growth under steam might be the key reason to cause catalyst deactivation.

Huber et al. observed the rapid deactivation of Co/SiO<sub>2</sub> during FTS reaction at high water partial pressure and the loss of activity was attributed to the support breakdown by product water accompanied by the formation of stable, inactive cobalt-silicates and the loss of BET surface area [71]. van Steen et al. states that metallic cobalt crystallites with a diameter less than 4.4 nm are more susceptible to oxidation by water to form Co(II)O [72]. This is in agreement with Iglesia's work that small Co metal crystallites (< 5-6 nm diameter) appear to re-oxidize and deactivate rapidly in the presence of water reaction product at typical FTS conditions [73].

Water poisoning has the most dramatic effect on zeolite-based CO<sub>2</sub> hydrogenation catalysts for which the acidic sites of the zeolite are essential for catalysis. Recently, Zhang et al. investigated the water effect over zeolite-based catalysts at high temperatures and found that water caused the loss of crystallinity and modified acid sites, thereby deactivating the catalyst [74]. Their studies show that the tolerance of defective zeolites to hot liquid water can be greatly enhanced by functionalization with organosilanes. This method renders the zeolite hydrophobic, which prevents the wetting of the surface. At the same time, the organosilanes act as a capping agent of Si–OH species reducing their reactivity. Both aspects are important in preventing water attack [74].

It appears then that there are several analogies of Fe catalysts for CO<sub>2</sub> hydrogenation and Co catalysts for conventional FT synthesis. Kliewer et al. for example showed that for supported Co catalyst water can oxidize the surface of Co to an inactive oxide phase and it also plays a large role in sintering. With a high water partial pressure in the Fe system, it appears that this can also oxidize iron carbides to inactive surface oxide phases and also promotes particle growth-sintering [52].

### 2.3.2 Carbonaceous Deposits (Coke)

Coke is produced by the decomposition or condensation of hydrocarbons on the surfaces of catalysts and primarily is comprised of polymerized hydrocarbons. There have been several books and reviews that describe the formation of coke on catalysts and the resulting deactivation [75] [76] [77] [78] [79] [80].

These deposits are most problematic for catalysis involving zeolites because the active sites of the zeolites become blocked or fouled by the coke deposits. Deactivation of MTO reactions over zeolites due to coke deposition results in a reduction in both catalyst activity and product selectivity [81] [82] [83].

Nishiyama et al. [84] studied the effect of SAPO-34 crystal size on catalyst lifetime and found that the amount of coke deposited on the deactivated SAPO-34 catalyst increased with decreasing crystal size, indicating that for larger crystals, the reactants were unable to penetrate further into the larger crystals to reach other acidic sites. Since MTO reactions and coke formation take place simultaneously in the same pores, it seems likely that the effectiveness of the catalyst increased with decreasing crystal size. Their studies demonstrated that the coke formation was inhibited in small-crystal SAPO-34 due to reduced diffusive resistance.

Wei et al.'s work on CO<sub>2</sub> hydrogenation found that the coke is formed and trapped in the cavities and channels of HMCM-22 and HBeta, and blocks the access of the reactants to the acid sites, finally leads to the deactivation of zeolites [11]. Muller et al. investigated the MTO process on H-ZSM-5 catalysts in plug-flow (PFR) and fully back-mixed reactors (CSTR). They found the catalysts deactivated under homogeneous gas phase in the back-mixed reactor show unequivocally that in the early stages of the reaction the zeolite deactivates via blocking of individual Brønsted acid sites and not by coke-induced impeding access to pores. H-ZSM-5 deactivated in the CSTR first rapidly and then at a much slower rate (Figure 6). The fast deactivation was observed in a PFR due to the formation of a larger fraction of the oxygen-containing carbon species. This is followed by the reaction of the oxygenates with olefins to produce a strongly adsorbed aromatic molecule. The formation of conventional aromatic coke takes place mostly by hydride transfer between olefins, and carbon growth to occur via multiple methylations of such aromatic species [85].

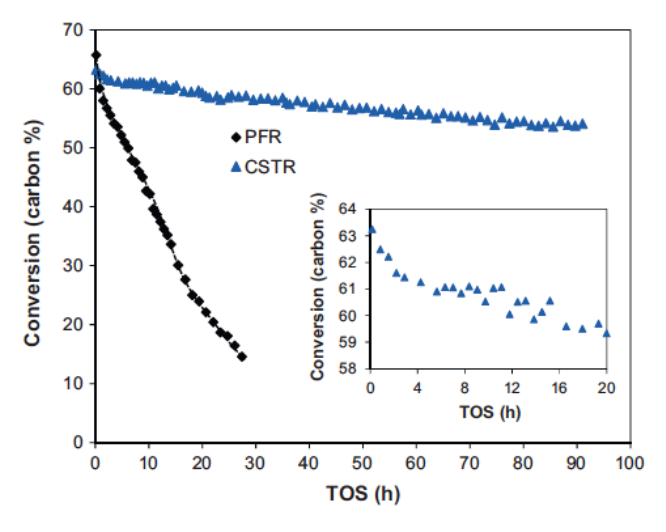


Figure 6. Methanol/DME conversion during MTO reaction of 90 mg catalyst H-ZSM-5-S in the PFR at ambient pressure and 50 mg catalyst H-ZSM-5-S in the CSTR at 6.5 bar, T = 723 K and  $p_{MeOH} = 178$  mbar (enlargement of the conversion change in the CSTR from 0 h to 20 h). Reproduced with permission from [85].

The zeolite-based catalysts that are promising for high olefin selectivity are typically limited by mass transfer, resulting in rapid deactivation due to water poisoning and carbon deposition [85]. The issues with coke deactivation on zeolite catalysts involved in MTO reactions are seen in classical MTO chemistry. Directed transforming of coke to active

intermediates in methanol-to-olefins catalyst was reported to boost light olefins selectivity [86]. Other strategy to mitigate the deactivation was to synthesize nano or hierarchical zeolites to reduce the diffusion limitations within the catalyst [87]. Nanozeolites contain shortened diffusion paths, while mesoporous hierarchical zeolites exhibit longer catalyst lifetimes because of larger pores and improved mass transfer [88] [89].

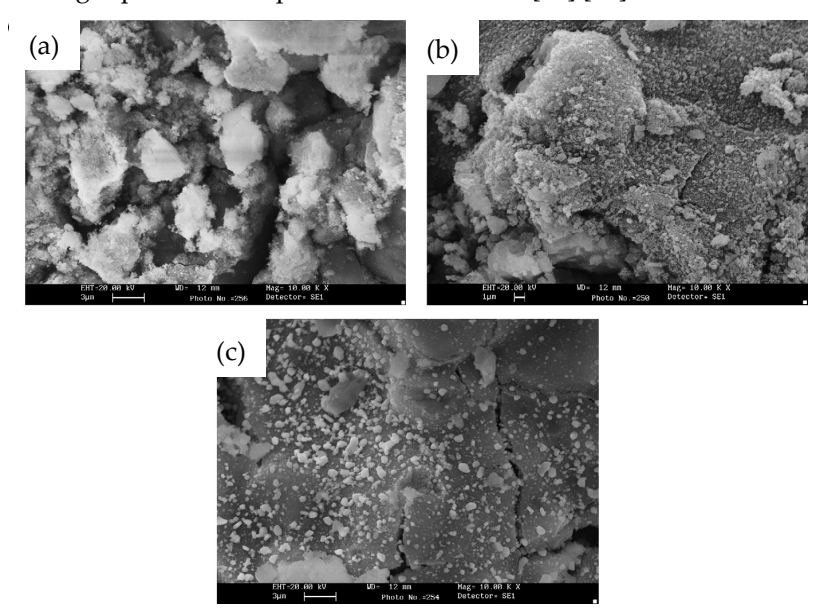


Figure 7. SEM image of the Fe– $K/\gamma$ -Al<sub>2</sub>O<sub>3</sub> catalysts after CO<sub>2</sub> hydrogenation reaction. (a) 100 h, (b) 300 h, and (c) 500 h. Reproduced with permission from [59].

With Fe catalyst, the deactivation by coke is not related to constriction of narrow pores, but several authors have reported formation of carbonaceous residues on active sites. Lee et al. investigated the deactivation behavior of Fe–K/-Al<sub>2</sub>O<sub>3</sub> catalyst and found the deactivation pathway was different with reaction position and reaction time. The main deactivation reason was the phase transformation at the top of the reactor. Conversely, the main factor at the bottom of the reactor was the deposited coke generated by secondary reactions. In particularly, the produced olefins may have been adsorbed on acidic sites and thus the olefins served as major precursors to coke. The SEM micrographs of the used catalysts, clearly showed most of the surface was covered by deposited graphite and graphite clusters protruding on the surface mixed with some fine filamentous carbon (Figure 7) [59].

With these multiple deactivation pathways identified, it now becomes a critical issue to find ways of modifying the catalyst to become more stable. In the section directly below, we will describe the approaches that multiple researchers have examined in an attempt to mitigate deactivation.

# 3. Recent progress on mitigating the catalyst deactivation

We will discuss the effect of promotors, metal oxide support, bifunctional composition and structure on the catalyst design to minimize the catalyst deactivation. We will summarize reports published within five years showing that promoters, supports, and novel morphology designs have mitigated deactivation effects.

# 3.1 Promoter effect

Fe-based catalysts have been widely studied in CO<sub>2</sub> hydrogenation, which usually show unsatisfactory selectivity toward lower olefins. The addition of suitable promotors to increase the yield of light olefins and stability of the catalysts

by controlling the electronic and structural properties have been extensively studied. Alkali metals such as K and Na have been broadly used as promotors to control the electronic properties. Mn, Ce, Ca metals have been used as structural promotors. Transition metals such as Zn, Co, Cu. V, Zr, etc have been used as both electronic and structural promotors. Some representative catalysts on promoter effect for CO<sub>2</sub> hydrogenation to light olefins with improved catalyst stability are presented in Table 1.

Table 1. Some representative catalysts on promoter effect for CO2 hydrogenation to light olefins

|                                        | 60              |       | 6.1               | 0/                |                    | 3/: 11 0/ | O /D  | C+ 1 '1'+ | D (   |
|----------------------------------------|-----------------|-------|-------------------|-------------------|--------------------|-----------|-------|-----------|-------|
| Catalyst                               | CO <sub>2</sub> |       |                   | ivity, %          |                    | Yield, %  | O/P   | Stability | Ref.  |
|                                        | Conv., %        | СО    | CH <sub>4</sub> . | C2-C4=            | C2-C4 <sup>0</sup> | C2-C4=    | ratio |           |       |
| 10Mn-Fe <sub>3</sub> O <sub>4</sub>    | 44.7            | 9.4   | 22.0              | 46.2              | 7.1                | 18.7      | 6.5   | 24 h      | [90]  |
| 0.58% Zn-Fe-                           | 57.8            | 8.8   | 6.2               | 63.2              | 21.8               | 19.9      | 2.9   | 50 h      | [91]  |
| Co/K-Al <sub>2</sub> O <sub>3</sub>    |                 |       |                   |                   |                    |           |       |           |       |
| Na-Zn-Fe                               | 38.0            | 15.0  | 13.0              | 42.0              | 4.9                | 16.0      | 8.5   | 100 h     | [92]  |
| Na-CoFe <sub>2</sub> O <sub>4</sub>    | 41.8            | 10.0  | ~18.0             | 37.2              | ~7.0               | 15.5      | ~5.3  | 100 h     | [93]  |
| Fe-Co/K-Al <sub>2</sub> O <sub>3</sub> | 40.0            | 12.2  | 24.8              | 46.1              | 7.9                | 16.2      | 5.9   | 6 h       | [32]  |
| $0.5\%$ Na-Fe $_5$ C $_2$              | 35.3            | 13.2  | 31.8              | 57.0              | 10.1               | 20.1      | 5.7   | 10 h      | [94]  |
| Fe-Zn-2Na                              | 43.0            | 15.7  | 22.8              | 54.1              | 7.4                | 23.2      | 7.3   | 10 h      | [96]  |
| Fe/C-KHCO <sub>3</sub>                 | 33.0            | 20.8  | 12.7              | 59.8 <sup>b</sup> | 27.3               | 9.0       | 2.2   | 100 h     | [97]  |
| 5Mn-Na/Fe                              | 38.6            | 11.7  | 11.8              | 30.2              | 4.0                | 11.7      | 11.0  | 10 h      | [98]  |
| FeNa(1.18)                             | 40.5            | 13.5  | 15.8              | 46.6              | 7.5                | 15.7      | 6.2   | 60 h      | [30]  |
| Na/Fe-Zn                               | 30.6            | n/a   | 13.0              | 26.8              | 3.9                | 8.4       | 6.9   | 200 h     | [99]  |
| Fe/C-Bio                               | 31.0            | 23.2  | 11.8              | 21.7              | 24.4               | 6.7       | 0.9   | 6 h       | [100] |
| 5%Na/Fe <sub>3</sub> O <sub>4</sub>    | 36.8            | ~11.0 | ~5.0              | 64.3              | ~13.0              | 23.7      | ~4.9  | 10 h      | [101] |
| Fe/C+K(0.75)                           | 40.0            | ~16.0 | ~22.0             | ~39.0             | ~12.0              | ~15.6     | ~3.3  | 50 h      | [102] |
| 35Fe-7Zr-1Ce-K                         | 57.3            | 3.05  | 20.6              | 55.6              | 7.9                | 31.8      | 7.1   | 84 h      | [103] |
| Fe-Mn/K-Al <sub>2</sub> O <sub>3</sub> | 29.4            | 20.2  | 18.7              | 48.7              | 6.5                | 14.3      | 7.4   | > 6 h     | [104] |
| Fe-                                    | 29.3            | 17.0  | 7.0               | 63.8              | 12.2               | 19.1      | 5.2   | 50 h      | [105] |
| Cu(0.17)/K(1.0)                        |                 |       |                   |                   |                    |           |       |           |       |
| Na-                                    | 34.4            | 19.0  | ~5.0              | 38.8              | 18.0               | 13.3      | 12.9  | > 24 h    | [106] |
| CoFe <sub>2</sub> O <sub>4</sub> /CNT  |                 |       |                   |                   |                    |           |       |           |       |
| Fe-Co-                                 | 21.2            | 54.0  | 9.0               | $37.0^{\circ}$    | n/a                | n/a       | 4.1   | 18 h      | [107] |
| K(0.3)/TiO <sub>2</sub>                |                 |       |                   |                   |                    |           |       |           |       |
| $Fe_2Zn_1$                             | 35.0            | ~15.0 | ~20.0             | 57.8 <sup>d</sup> | 7.2                | 20.2      | 8.0   | 200 h     | [29]  |
| $ZnCo_{0.5}Fe_{1.5}O_{4} \\$           | 49.6            | ~7.5  | ~17.5             | 36.1              | ~10.0              | 17.9      | ~3.6  | 80 h      | [108] |

<sup>&</sup>lt;sup>a</sup>CO is not considered when calculating selectivity; <sup>b</sup> refers to high valued olefins (HVO);

<sup>&</sup>lt;sup>c</sup>includes C<sub>2</sub>-C<sub>4</sub> and C<sub>5+</sub> hydrocarbons; <sup>d</sup> refer to C<sub>2</sub>-C<sub>7</sub><sup>=</sup> olefins;

Adding alkali metals (i.e., Na, K) could increase the selectivity towards light olefins due to the enhanced CO<sub>2</sub> adsorption on the more electron rich Fe phases and suppressed H<sub>2</sub> chemisorption which inhibits olefin re-adsorption. Numpilai et al. reported on the effect of varying content of the K promoter on the Fe-Co/K-Al<sub>2</sub>O<sub>3</sub> catalysts via the CO<sub>2</sub>-FTS reaction pathway. Unpromoted catalysts evidenced low light olefin yields when compared to K-promoted ones with ascending K/Fe ratio from 0 to 2.5. The maximum light olefins (C<sub>2</sub>=-C<sub>4</sub>=) distribution of 46.7% and O/P ratio of 7.6 are achieved over the catalyst promoted with a K/Fe atomic ratio of 2.5. (Figure 8). The positive effect of K addition is attributed to the strong interaction of H adsorbed with the catalyst surface caused by the electron donor from K to Fe species. This notion is also rationalized by the fact that the K promoter enhances the bond strength of absorbed CO<sub>2</sub> and H<sub>2</sub>, retarding the hydrogenation of olefins to paraffins. At the same operating condition, the catalyst promoted with a K/Fe atomic ratio of 0.5 provides the maximum light olefins (C<sub>2</sub>=-C<sub>4</sub>=) yield of 16.4% which is significantly higher than that of 2.5 KFe catalysts (13.4%). This is explained by the K enriched surface of 2.5 KFe catalysts significantly reduces the BET surface area and generates a hydrogen-lean environment, ultimately lessening catalytic activity [104].

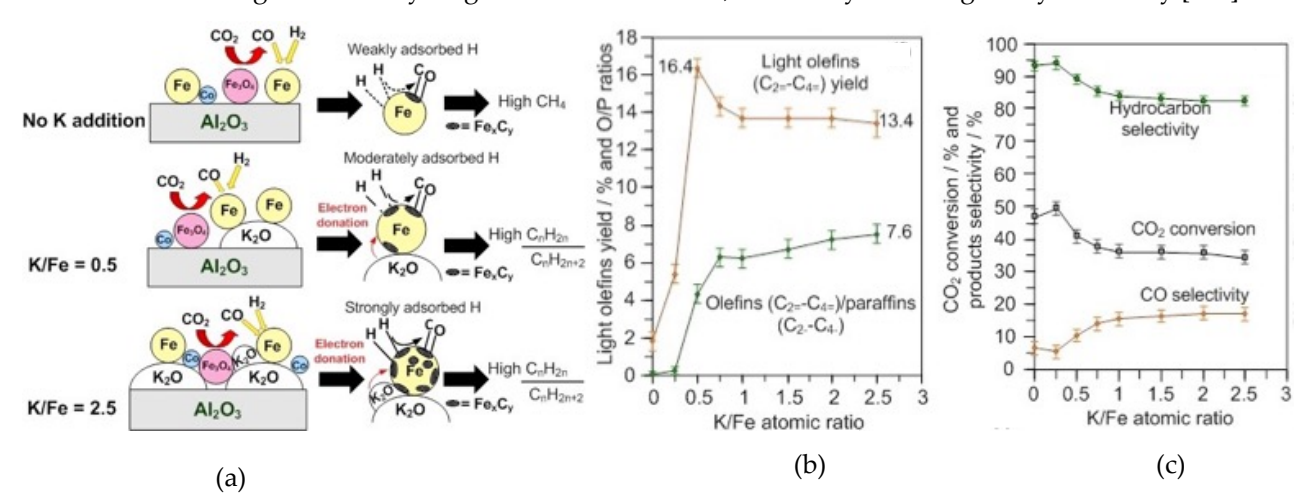


Figure 8. (a) Schematic Illustration of the effect of K addition of Fe-Co/K-Al<sub>2</sub>O<sub>3</sub> catalysts on the formation of olefins. (b) Catalytic performance (CO<sub>2</sub> conversion, CO and hydrocarbon selectivity), and (c) light olefins yield and O/P ratios of different Fe-Co/K-Al<sub>2</sub>O<sub>3</sub> catalysts (testing conditions: 613K, 20 bar, 75 mL min<sup>-1</sup>(CO<sub>2</sub>: H<sub>2</sub>: N<sub>2</sub> = 1: 3: 1). Reproduced with permission from [104].

Different promoter source plays an important role to affect catalytic CO<sub>2</sub> hydrogenation. Han et al. demonstrated that as the series of K-promoters changes from K<sub>2</sub>CO<sub>3</sub>, CH<sub>3</sub>COOK, KHCO<sub>3</sub>, and KOH the electron transfer from potassium to iron species is facilitated which forms a more active and distinct χ-Fe<sub>5</sub>C<sub>2</sub>-K<sub>2</sub>CO<sub>3</sub> interface during CO<sub>2</sub> hydrogenation. This results in a higher selectivity to light olefins (75%) and a higher CO<sub>2</sub> conversion (32%). In contrast, the non-carbonaceous K-promoters do not facilitate iron species to form iron carbides, which causes undesirable catalytic performance (Figure 9a). Additionally, the close proximity between carbonaceous K-promoters and Fe/C catalyst components produced high olefin yields and catalytic stability (Figure 9b) [97]. Guo et al. reported that K derived from bio rather than inorganic precursors showed stronger migration ability during the CO<sub>2</sub> hydrogenation to light olefins. These surface enriched K ions extracted from corncobs could promote the carburization of iron species to form more Fe<sub>5</sub>C<sub>2</sub>, promoting both the reverse water-gas shift reaction and subsequent C-C coupling [100].

Metal organic frameworks as precursors for the preparation of heterogeneous catalysts have been used recently [109] [110] [102]. Ramirez et al. used a metal organic framework as catalyst precursor to synthesize a highly active, selective, and stable catalyst as shown in Figure 10 (a-f) for the hydrogenation of CO<sub>2</sub> to light olefins. Comparing the addition of Cu, Mo, Li, Na, K, Mg, Ca, Zn, Ni, Co, Mn, Fe, Pt, and Rh to an Fe/C composite, only K is able to enhance olefin selectivity as shown in Figure 10c. The presence of K promoted the formation of Fe<sub>5</sub>C<sub>2</sub> and Fe<sub>7</sub>C<sub>3</sub> carbides as

386

387

388

389

390

391

392

393

394

395

396

398

399

400

401

402

403

404

405

406

407

409

410

411

412

confirmed by XRD (Figure 10d). K helped keep a good balance between the iron oxide for RWGS and iron carbide for FTS. Results presented in Figure 10f indicated a trend in which methane formation decreased and olefin selectivity increased as K loading increased. The catalyst Fe/C+K(0.75) exhibited good stability (Figure 10e) and outstanding C<sub>2</sub>–C<sub>4</sub> olefin space time yields of 33.6 mmol· $g_{cat}$ -1·h<sup>-1</sup> at Xco<sub>2</sub> = 40%, 593K, 30 bar, H<sub>2</sub>/CO<sub>2</sub> = 3, and 24,000 mL·g<sup>-1</sup>·h<sup>-1</sup> [102].

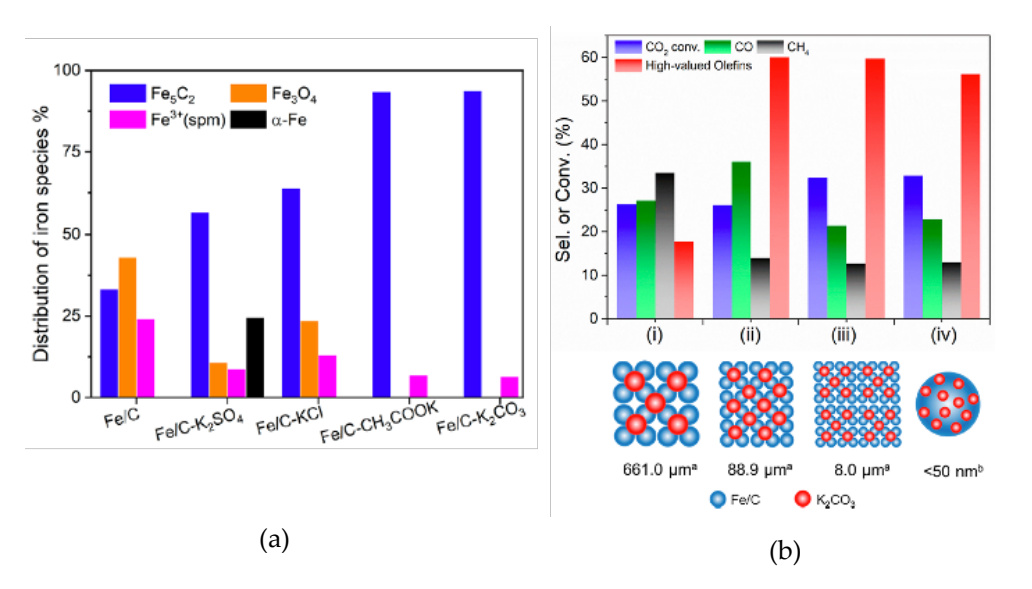


Figure 9. (a) Iron species content of different spent catalysts. (b) CO<sub>2</sub> hydrogenation performance over Fe/C-K<sub>2</sub>CO<sub>3</sub> catalysts with different proximity. Reproduced with permission from [97].

Some work may shed light on how the alkali promoters affect the behavior of iron catalysts. By adding precisely controlled addition of promoters to fine tune the catalytic performance for hydrogenation of CO2 to olefins, Yang et al. investigated the effect of sodium and potassium promoters on the concurrent conversion of CO and CO2 to olefins using a zinc ferrite catalyst system. It was found that the use of promoters altered the balance between iron oxides and iron carbides in the catalyst, which affected the CO and CO2 conversion. The Na- and K-promoted catalysts facilitated the production of C2+ olefins. The Na/Fe-Zn catalyst was found to possess optimal olefin productivity and inhibited the competitive methanation reaction. It showed a total carbon conversion of 34.0%, which decreased by only 12.2% over 200 h [99]. Similarly, Wei et al. unraveled the effect of the Na promoter on the evolution of iron and carbon species and the consequent tuning effect on the hydrogenation of CO<sub>2</sub> to olefins. With the contents of Na promoter increasing from 0 wt% to 0.5 wt%, the ratio of olefins to paraffins (C<sub>2+</sub>) rose markedly from 0.70 to 5.67. In situ XRD and temperature programed surface reaction (TPSR) confirmed that the introduction of Na promoter decreased the particle size of Fe₅C₂ and regulated the distribution of surface carbon species. Furthermore, in situ XRD and Raman demonstrated that the interaction between the Na promoter and the catalysts inhibited the hydrogenation of Fe<sub>5</sub>C<sub>2</sub> and surface graphitic carbon species, consequently, improving the stability of Fe<sub>5</sub>C<sub>2</sub> and enhancing the formation of olefins by inhibiting hydrogenation of intermediate carbon species [94]. Using similar approach, Liang et al. modified the xNa/Fe-based catalysts with tunable amounts of sodium promoter for CO<sub>2</sub> hydrogenation to alkenes with CO<sub>2</sub> conversion at 36.8% and light olefins selectivity of 64.3%. It was found that the addition of Na promoter into Fe-based catalysts boosted the adsorption of CO<sub>2</sub>, facilitated the formation and stability of the active Fe<sub>5</sub>C<sub>2</sub> phase and inhibited the secondary hydrogenation of alkenes under the CO2 hydrogenation reaction conditions (Figure 11a-c). The content of Fe<sub>5</sub>C<sub>2</sub> correlated with the amount of Na is shown in Figure 11d [101].

414

415

416 417

418

419

420

421

422

423

424

425

426

427

428

429

430

431

432

433

434

435

436

437

438

439

440

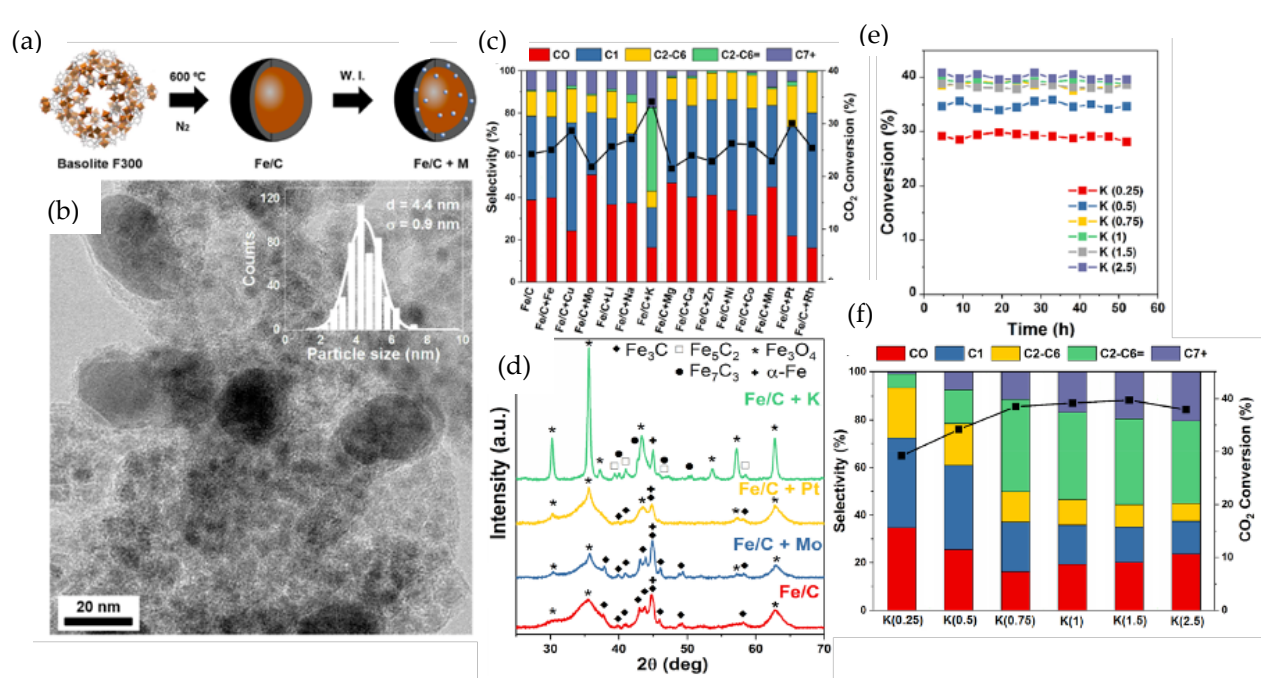


Figure 10. (a) Catalytic performance of promoted and unpromoted Fe catalysts. (b) CO<sub>2</sub> conversion and product distribution after 50 h of TOS. (c) Effect of K loading on CO<sub>2</sub> conversion and product distribution after 50 h of TOS (reaction conditions: 593K, 30 bar,  $H_2/CO_2 = 3$ , and 24 000 mL·g-1·h-1, TOS = 50 h. Reproduced with permission from [102].

Wei et al. synthesized a series of Fe<sub>3</sub>O<sub>4</sub>-based nanocatalysts with varying sodium contents. The residual sodium markedly influenced the textural properties of the Fe<sub>3</sub>O<sub>4</sub>-based catalysts, and faintly hampered the reduction of the catalysts. However, it discernibly promoted the surface basicity and prominently improved the carburization degrees of the iron catalysts, which is favored for olefin production. Compared with the sodium-free Fe<sub>3</sub>O<sub>4</sub> catalysts, the sodium promoted Fe<sub>3</sub>O<sub>4</sub> catalysts displayed higher activity and selectivity for C<sub>2</sub>–C<sub>4</sub> olefins. The catalyst FeNa (1.18) (Na/Fe weight ratio of 1.18/100) exhibited excellent catalytic activity with a high olefin/paraffin ratio (6.2) and selectivity to C2-C4 olefins (46.6%) and low CO and CH4 production at a CO2 conversion of 40.5% (Figure 12a). It also exhibited superb stability during the 100 h test at 593K as shown in Figure 12b. Compare the scanning electron microscopy (SEM) image after reduction, no clear growth of the particle size is observed after catalytic reaction for 100 h, further revealing the excellent reaction stability of these active iron nanoparticles (Figure 12c-d) [30]. Zhang et al. fabricated a Na- and Znpromoted iron catalyst by a sol-gel method and demonstrated high activity, selectivity and stability towards the formation of C2+ olefins in the hydrogenation of CO2 into C2+ olefins. The selectivity of C2+ olefins reached 78%, and the space–time yield of olefins attained as high as 3.4 g g<sub>cat</sub>-1h-1. The catalyst is composed of ZnO and χ-Fe<sub>5</sub>C<sub>2</sub> phases with Na<sup>+</sup> dispersed on both ZnO and χ-Fe<sub>5</sub>C<sub>2</sub>. Zhang et al. unraveled that ZnO functions for the RWGS reaction of CO<sub>2</sub> to CO, while χ-Fe<sub>5</sub>C<sub>2</sub> is responsible for CO hydrogenation to olefins. The presence of Na<sup>+</sup> enhanced the selectivity of C<sub>2+</sub> olefins by regulating the hydrogenation ability and facilitating the desorption of olefins (Figure 13a). The presence of ZnO not only efficiently catalyzes the RWGS reaction but also improves the activity and stability of CO2 hydrogenation by controlling the size of  $\gamma$ -Fe<sub>5</sub>C<sub>2</sub> (Figure 13c-d). It was further discovered that the close proximity between ZnO and χ-Fe<sub>5</sub>C<sub>2</sub> is beneficial for conversion of CO<sub>2</sub> to olefins (Figure 13b). The larger interface could facilitate the diffusion and transfer of CO intermediate from ZnO to χ-Fe<sub>5</sub>C<sub>2</sub>, favoring CO<sub>2</sub> adsorption and subsequent CO hydrogenation to C<sub>2+</sub> olefins [92]. Malhi et al. also investigated the effect of Na and Zn on the iron-based catalysts and found the modified Fe based catalyst exhibited a good performance for CO2 hydrogenation to olefins with a CO2 conversion of 43 %, a selectivity of 54.1 % to C<sub>2+</sub> olefins, and a high olefins-to-paraffins ratio of 7.3 [96].



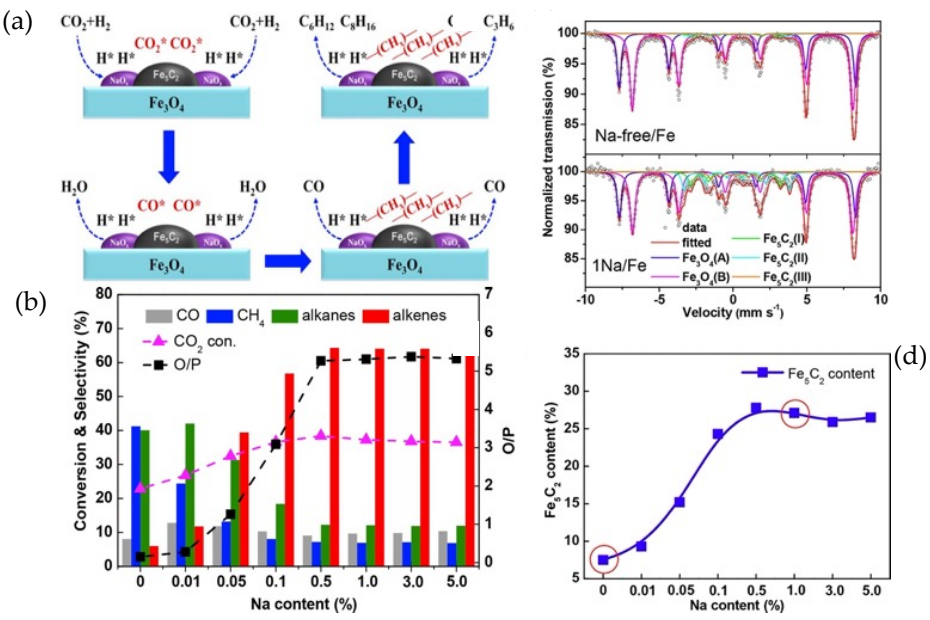


Figure 11. (a) Plausible Scheme of  $CO_2$  Hydrogenation to Alkenes. (b) Catalytic performance of xNa/Fe catalyst for  $CO_2$  hydrogenation (reaction conditions:  $H_2/CO_2 = 3$ ; 3 MPa; 593K; 2040 mLh<sup>-1</sup> $g_{cat}^{-1}$ ; TOS = 10 h). (c) Mossbauer spectra of the Na-free Fe-based and 1Na/Fe catalysts after reaction. (d) Fe<sub>5</sub>C<sub>2</sub> content of xNa/Fe catalyst after reaction as a function of the Na content. Reproduced with permission from [101].

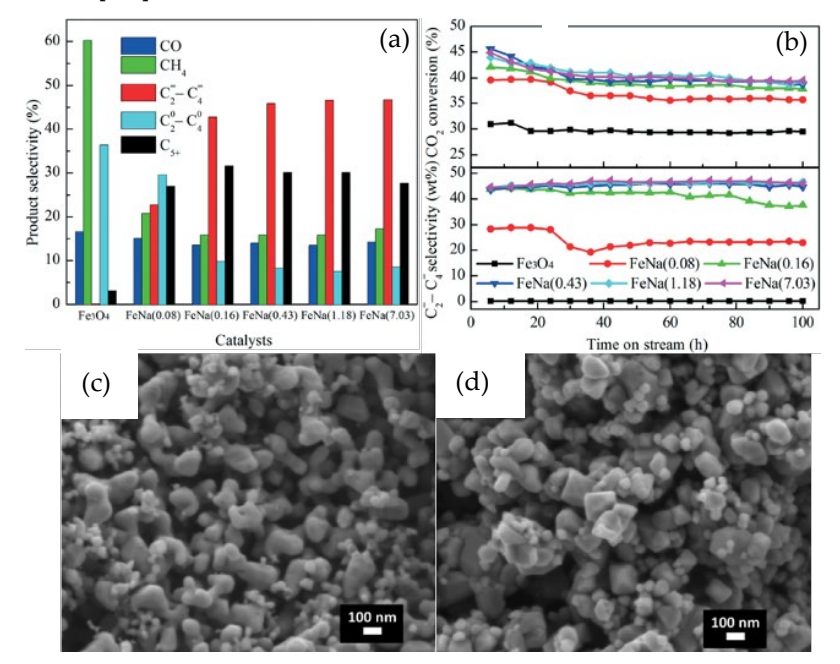


Figure 12. (a) CO and hydrocarbon selectivity; (b) CO<sub>2</sub> conversion and C<sub>2</sub>=-C<sub>4</sub>= selectivity of the FeNa(x) catalysts as a function of time on stream (reaction conditions:  $H_2/CO_2 = 3.0$ , 593K, 3.0 MPa, 2000 ml h<sup>-1</sup> g<sub>cat</sub><sup>-1</sup>); SEM images of the FeNa(1.18) catalysts: (c) after reduction (623K, H<sub>2</sub> and 12 h) and (d) after reaction (593K, 3.0 MPa, H<sub>2</sub>/CO<sub>2</sub> = 3.0 and 100 h). Reproduced with permission from [30].

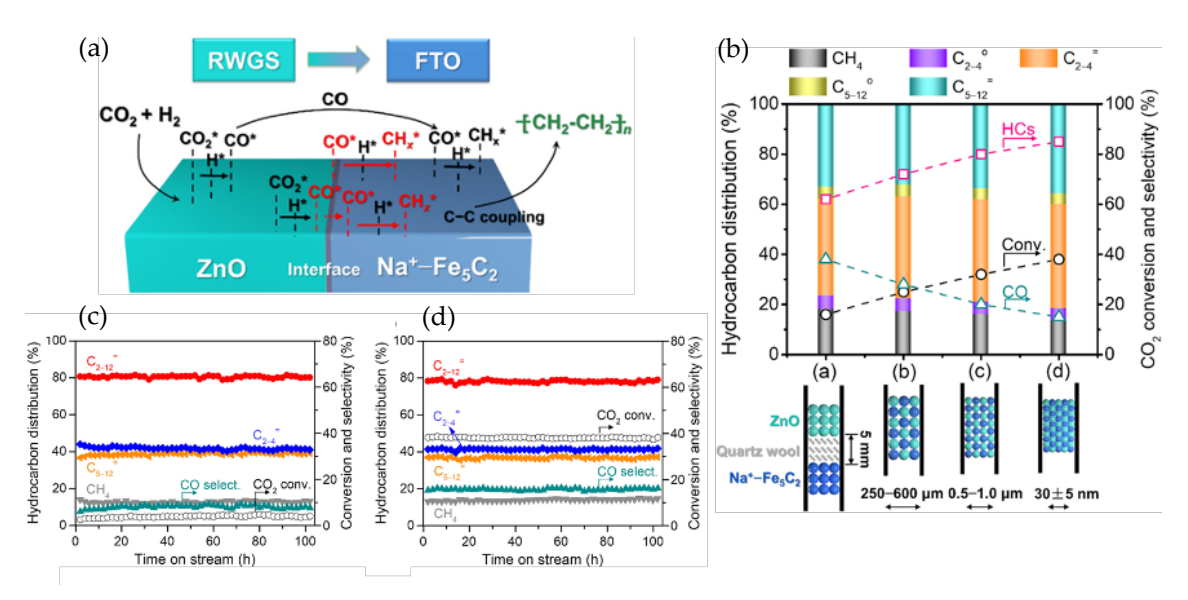


Figure 13. (a) Illustrated reaction mechanism for CO<sub>2</sub> Hydrogenation to olefins over the Na-Zn-Fe Catalyst. (b) Effect of proximity between ZnO and Na $^+$ Fe<sub>5</sub>C<sub>2</sub> on catalytic behaviors for CO<sub>2</sub> hydrogenation. Catalyst stability in CO<sub>2</sub> hydrogenation over (c) Na $^+$ Fe<sub>5</sub>C<sub>2</sub> and (d) Na-Zn-Fe in CO<sub>2</sub> hydrogenation. Reaction conditions: H<sub>2</sub>/CO<sub>2</sub> = 3, P = 2.5 MPa, W = 0.10 g, F = 25 mL min1, T = 613 K. Reproduced with permission from [92].

Chaipraditgul et al. investigated the effect of transition metals (Cu, Co, Zn, Mn or V) to Fe/K-Al<sub>2</sub>O<sub>3</sub> catalyst and found the addition of each transition metal remarkably altered the interaction between the adsorptive CO<sub>2</sub> and H<sub>2</sub> and the catalysts surface. The Fe/K-Al<sub>2</sub>O<sub>3</sub> promoted with Cu, Co or Zn showed the markedly increased number of weakly adsorbed H atom, promoting the hydrogenation ability to lower the olefin to paraffin ratio. On the contrary, the addition of Mn promoter to Fe/K-Al<sub>2</sub>O<sub>3</sub> reduced the number of weakly adsorbed H atom, lowering the hydrogenation ability to result in high olefin to paraffin ratio of 7.4. The presence of either Mn or V inhibited the CO hydrogenation to hydrocarbon, leading to the low CO<sub>2</sub> conversion, while the CO<sub>2</sub> conversion was enhanced by incorporating either Co or Cu onto the Fe/K-Al<sub>2</sub>O<sub>3</sub> catalyst [32]. Gong et al. investigated the effect of Cu promoter on Fe-Mn-based catalysts in production of light olefins via the CO<sub>2</sub>-FTS process. The Cu promoter was found to facilitate the reduction process and enhance CO dissociative adsorption by changing the interactions between Fe, Mn and the SiO<sub>2</sub> binder, which led to an improved activity. The overall weakened surface basicity instigated by Cu decreased the chain growth probability and led to a higher selectivity of light olefins [95].

Jiang et al. reported the synthesis of Mn-modified Fe<sub>3</sub>O<sub>4</sub> microsphere catalysts. It exhibited excellent catalytic performance with a CO<sub>2</sub> conversion (44.7%), light olefin selectivity (46.2 %), and light olefin yield (18.7%) over the 10Mn–Fe<sub>3</sub>O<sub>4</sub> catalyst. The O/P ratio increased from 3.7 for unpromoted Fe<sub>3</sub>O<sub>4</sub> catalyst to 6.5 for Mn-promoted catalyst. Manganese was evenly distributed over the surface of Fe<sub>3</sub>O<sub>4</sub> microsphere. Such homogeneous dispersion allows for an increase in the basicity of the catalyst, which prevents the further hydrogenation of olefins into paraffins. It was noted that the synergistic effects between Fe and Mn improve the dissociation and conversion of CO<sub>2</sub> to hydrocarbons. The addition of Mn was found to promote the production of Fe carbides and enhance CO<sub>2</sub> hydrogenation active phases and the FTS reaction, as well as prevent the hydrogenation of light olefins into paraffins and chain growth into longer hydrocarbons [90]. Similar effect of the addition of Mn to Na/Fe catalysts was also observed by Liang et al [98].

Zhang et al. synthesized uniform microspheres of Fe-Zr-Ce-K catalysts by the microwave assisted homogeneous precipitation and found the reducibility, surface basicity and surface atom composition of the catalysts was tuned by varying the Ce content. CeO<sub>2</sub> as structural promoter restrained the growth of Fe<sub>2</sub>O<sub>3</sub> crystallite, weakened the

484

485

486

487

488

489

490

491

492

493

494

495

496

497

498

500

501

502

503

504

505 506

interaction between Fe species and zirconia and enabled the reduction of Fe<sub>2</sub>O<sub>3</sub> easier. The best performance was obtained on catalyst 35Fe-7Zr-1Ce-K at 593K and 2 MPa with CO<sub>2</sub> conversion of 57.34%, C<sub>2</sub>-C<sub>4</sub> olefins selectivity of 55.67%, and the ratio of olefin/paraffin of 7 [103].

Extensive research efforts have exerted on the development of bi-metallic catalysts for converting CO2 to light olefins. Yuan et al. demonstrated the influence of Na, Co and intimacy between Fe and Co on the catalytic performance of Fe-Co bimetallic catalysts for CO<sub>2</sub> hydrogenation that offers C<sub>2</sub>-C<sub>4</sub>= space time yield of 2.88 µmol C<sub>2</sub>-C<sub>4</sub>= gcat<sup>-1</sup>s-1 and olefin to paraffin ratio of 6 at CO<sub>2</sub> conversion of 41 %. With the introduction of Co into the Fe catalyst, the CO<sub>2</sub> conversion is significantly enhanced. The intimate contact between Fe and Co sites favored the production of C₂-C₄<sup>∓</sup>. When Na was added to the system, the surface of the catalyst became carbon-rich and hydrogen-poor, allowing C-C coupling to form light olefins and suppress the methane formation. Moreover, the addition of Na promoter facilitated the generation of  $\chi$ -(Fe<sub>1-x</sub>Co<sub>x</sub>)<sub>5</sub>C<sub>2</sub> under the CO<sub>2</sub> hydrogenation reaction conditions and thus further improves the catalytic performances. A superb stability over 100 h was observed (Figure 14) [93]. Witoon et al. investigated the effect of Zn addition into Fe-Co/K-Al<sub>2</sub>O<sub>3</sub> catalysts. The addition of Zn improved the dispersion and the reducibility of iron oxides. The 0.58 wt% Znpromoted Fe-Co/K-Al<sub>2</sub>O<sub>3</sub> catalyst offered a large number for active sites for adsorption of CO and H<sub>2</sub> due to a higher dispersion and an eased reducibility (Figure 15a), which exhibited superior activity for light olefins formation with yield of 19.9% under the optimum testing conditions of 613K, 25 bar, 9,000 mL gcat-1h-1 and H2/CO2 ratio of 4. A gradual decrease in olefin to paraffin ratio with an almost constant CO2 conversion as a function of time-on-stream was observed in Figure 15b. The x-ray photoelectron spectroscopy (XPS) analysis of the spent catalyst showed the continuous growth of iron carbide with time-on-stream, suggesting that the iron carbide may be the active site for the paraffin production (Figure 15c). The formation of Fe-C phases over the spent 0.58 wt% Zn promoted Fe-Co/K-Al<sub>2</sub>O<sub>3</sub> catalyst at time-onstream was also confirmed by XRD (Figure 15d) [91].

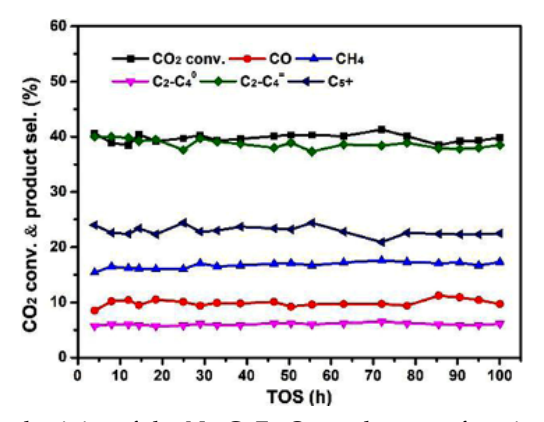


Figure 14.  $CO_2$  conversion and product selectivity of the Na-CoFe<sub>2</sub>O<sub>4</sub> catalyst as a function of time on stream (reaction conditions:  $H_2/CO_2 = 3$ , 593K, 3 MPa, 7200 mL  $h^{-1}gcat^{-1}$ , TOS = 100 h). Reproduced with permission from [93].

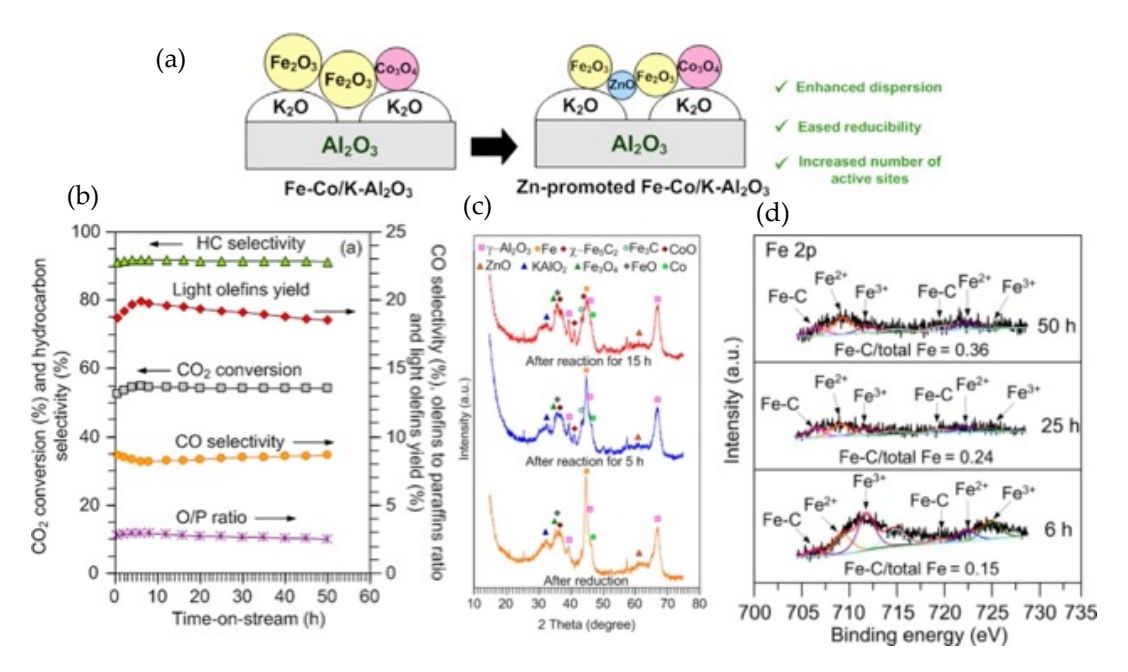
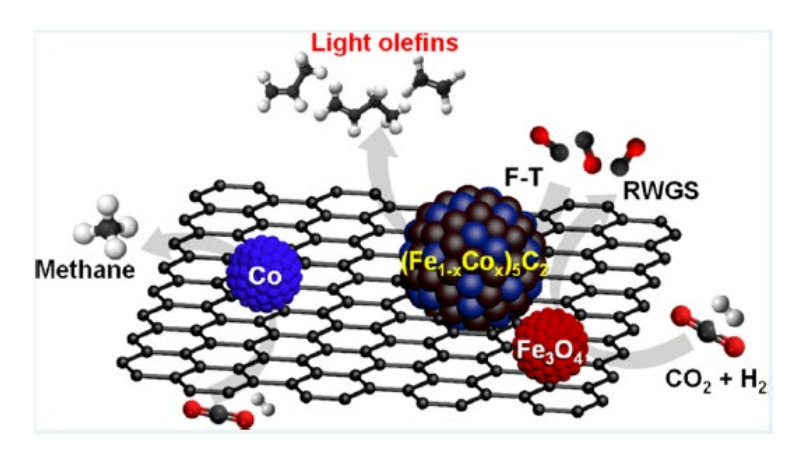


Figure 15. (a) Illustrated reaction mechanism. (b) CO<sub>2</sub> conversion, hydrocarbon and CO selectivity, light olefins yield and O/P ratio. (c) XRD pattern of the reduced and the spent 0.58 wt% Zn-promoted Fe-Co/K-Al<sub>2</sub>O<sub>3</sub> catalyst at different time-on-stream. (d) XPS spectra of Fe 2p region of the 0.58 wt% Zn-promoted Fe-Co/K-Al<sub>2</sub>O<sub>3</sub> catalysts under operating parameters: T = 613K, P = 25 bar, space velocity = 9,000 mLg<sub>cat</sub>-1h-1 and H<sub>2</sub>/CO<sub>2</sub> ratio = 4. Reproduced with permission from [91].

Wang et al. reported the synthesis of  $\gamma$ -alumina supported Fe-Cu bimetallic catalysts and found that the combination of Fe and Cu at specific composition led to a strong bimetallic promotion for selective CO<sub>2</sub> conversion to olefin-rich C<sub>2+</sub> hydrocarbons formation. The addition of Cu to Fe successfully suppressed the undesired CH<sub>4</sub> formation while enhancing C-C coupling for C<sub>2+</sub> hydrocarbon formation. XRD results suggested the formation of Fe-Cu alloy in Fe-Cu(0.17)/Al<sub>2</sub>O<sub>3</sub> catalyst. Furthermore, the addition of K into Fe-Cu considerably enhanced the production of light olefins C<sub>2</sub>-C<sub>4</sub><sup>\*</sup> and O/P ratio over Fe-Cu bimetallic catalysts. The Fe-Cu/K catalysts exhibited superior selectivity of C<sub>2+</sub> hydrocarbons than Fe-Co/K catalysts under the same reaction conditions [105]. Kim et al. synthesized monodisperse nanoparticles (NPs) of CoFe<sub>2</sub>O<sub>4</sub> by the thermal decomposition of metal-oleate complexes as shown in Scheme 4. The prepared NPs were supported on carbon nanotubes (CNTs) and Na was added to investigate the promoter and support effects on the catalyst for CO<sub>2</sub> hydrogenation to light olefins. The resulting Na-CoFe<sub>2</sub>O<sub>4</sub>/CNT exhibited superior CO<sub>2</sub> conversion of 34% and light olefin selectivity of 39% to other reported Fe-based catalysts under similar reaction conditions. The superb performance of Na-CoFe<sub>2</sub>O<sub>4</sub>/CNT was attributed to the facile formation of a unique bimetallic alloy carbide (Fe<sub>1-x</sub>Co<sub>x</sub>)<sub>5</sub>C<sub>2</sub>, which results in higher CO<sub>2</sub> conversion and better light olefins selectivity in comparison with conventional  $\chi$ - Fe<sub>5</sub>C<sub>2</sub> active sites derived from Fe-only catalysts and drastically improved C<sub>2+</sub> hydrocarbon formation in comparison with the Co<sub>2</sub>C sites of Co-only catalysts [106].

Song et al. investigated titania supported monometallic and bimetallic Fe-based catalysts for CO<sub>2</sub> conversion and found the mono-metallic catalyst (Fe-, Co-, Cu-) performed poorly on C-C coupling reactions. But the addition of a small amount of second metal (Co and Cu) to Fe revealed the synergetic promotion on the CO<sub>2</sub> conversion and the space-time yields (STY) of hydrocarbon products. The incorporation of K and La as promoters further improved the activity, higher hydrocarbons selectivity and O/P ratio, indicating that the promotor facilitated the CO<sub>2</sub> activation and C-C couplings over bi-metallic catalysts [107]. Zhang et al. investigated Fe-Zn bimetallic catalysts for CO<sub>2</sub> hydrogenation to C<sub>2+</sub> olefins. High C<sub>2+</sub> olefins selectivity of 57.8% after 200 h of time-on-stream at a CO<sub>2</sub> conversion of 35.0% was obtained over

Fe<sub>2</sub>Zn<sub>1</sub> catalyst. The relationship of performance and structure has been established to unravel the role of ZnO in bimetallic Fe<sub>5</sub>C<sub>2</sub>-ZnO catalysts. The dominant mechanism of deactivation was ascribed to phase transformation from FeC<sub>x</sub> to FeO<sub>x</sub> over Fe<sub>2</sub>O<sub>3</sub>, but the addition of Zn to Fe<sub>2</sub>O<sub>3</sub> remarkably suppressed the phase transformation and the carbon deposits over Fe<sub>2</sub>Zn<sub>1</sub>. Furthermore, the addition of Na suppressed the oxidation of active species  $\chi$ -Fe<sub>5</sub>C<sub>2</sub> for Fe-Zn bimetallic catalysts. Zn and Na were proved to migrate onto the surface during the activation process. The interaction between Zn and Na suppressed the oxidation of FeC<sub>x</sub> by H<sub>2</sub>O and CO<sub>2</sub>. This study revealed the deactivation mechanism and stabilization effects of Zn on the active phase of FeC<sub>x</sub> during CO<sub>2</sub> hydrogenation [29].



Scheme 4. Schematic demonstration of CO<sub>2</sub> hydrogenation over CNT supported bi-metallic catalyst CoFe<sub>2</sub>O<sub>4</sub>. Reproduced with permission from [106].

Xu et al. investigated the roles of Fe-Co interactions over ternary spinel-type ZnCo<sub>x</sub>Fe<sub>2-x</sub>O<sub>4</sub> catalysts for CO<sub>2</sub> hydrogenation to produce light olefins. A high light olefins selectivity of 36.1%, low CO selectivity of 5.8% at high CO<sub>2</sub> conversion of 49.6% and an unprecedentedly high Fe time yield (FTY) = value of 29.1 μmolco<sub>2</sub>g<sub>Fe</sub>-1s-1 was obtained on the ZnCo<sub>0.5</sub>Fe<sub>1.5</sub>O<sub>4</sub> via RWGS-FTS reaction pathway. It was unveiled that during the CO<sub>2</sub> hydrogenation over ternary ZnCo<sub>0.5</sub>Fe<sub>1.5</sub>O<sub>4</sub> catalysts, the formation of electron-rich Fe<sup>0</sup> atoms in the CoFe alloy phase significantly boosted the generation of active χ-Fe<sub>5</sub>C<sub>2</sub>, Co<sub>2</sub>C, and θ-Fe<sub>3</sub>C phases, in which χ-Fe<sub>5</sub>C<sub>2</sub> phase facilitated the C-C coupling, the Co<sub>2</sub>C species suppressed the formation of CH<sub>4</sub> and the formation of θ-Fe<sub>3</sub>C phase with lower hydrogenation activity inhibited the second hydrogenation of light olefins [108].

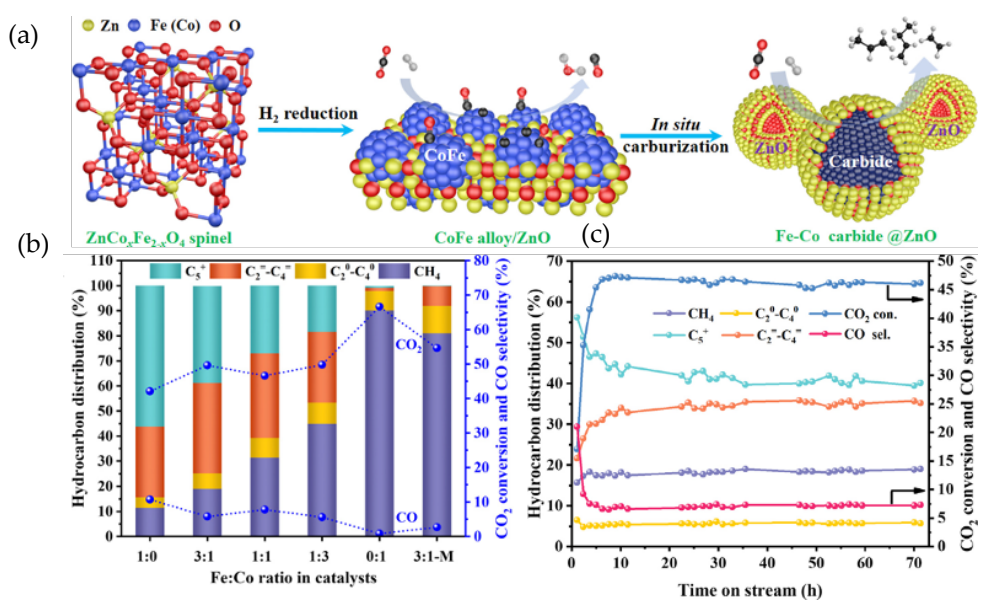


Figure 16. (a) Schematic illustration of structural transformations of as-formed ZnCo<sub>x</sub>Fe<sub>2-x</sub>O<sub>4</sub> catalysts during the reduction and reaction steps. (b) CO<sub>2</sub> conversion and product distributions over K-containing ZnCo<sub>x</sub>Fe<sub>2-x</sub>O<sub>4</sub> catalysts with various Fe/Co molar ratio. (c) The stability of the K-containing ZnCo<sub>0.5</sub>Fe<sub>1.5</sub>O<sub>4</sub> catalyst in CO<sub>2</sub> hydrogenation (reaction conditions: 583K, 2.5 MPa, 4800 mLh<sup>-1</sup>g<sub>cat</sub><sup>-1</sup>, CO<sub>2</sub>/H<sub>2</sub> = 1:3). Reproduced with permission from [108].

In summary, the use of appropriate K or Na promoter and the inclusion of Cu, Co, Zn, Mn or Ce to the Fe phase and the bi-metallic formation have played important roles for enhanced catalytic performance and stability.

# 3.2 Support effect

Catalyst supports also have a significant effect on the activity and selectivity due to the strong interactions between active phases and the support during CO<sub>2</sub>-FTS. Some representative catalysts on support effect for CO<sub>2</sub> hydrogenation to light olefins with improved catalyst stability are presented in Table 1.

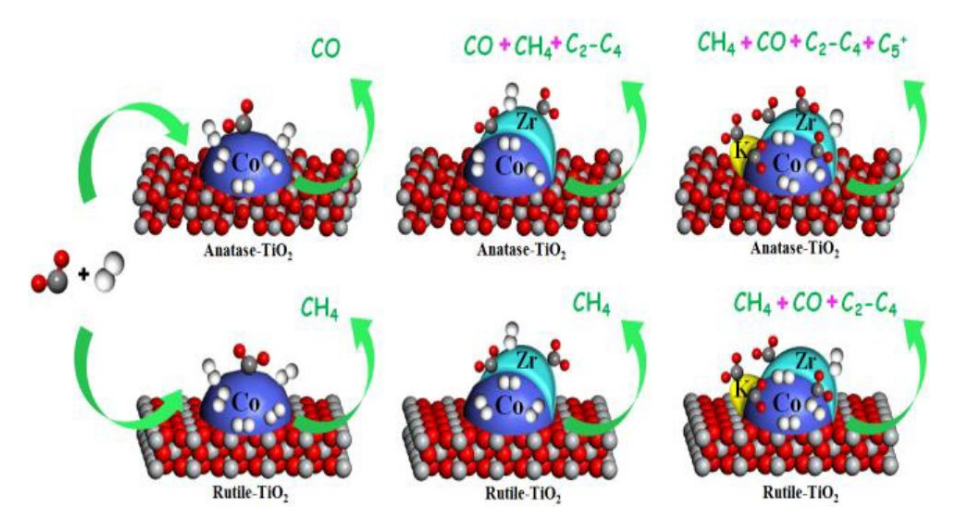
Table 2. Some representative catalysts on support effect for CO2 hydrogenation to light olefins

|                                        | CO <sub>2</sub> |       | Selectivity, %    |                 |                            | Yield, %        | O/P   |           |       |
|----------------------------------------|-----------------|-------|-------------------|-----------------|----------------------------|-----------------|-------|-----------|-------|
| Catalyst                               | Conv., %        | CO    | CH <sub>4</sub> . | $C_2$ - $C_4$ = | $C_2$ - $C_4$ <sup>0</sup> | $C_2$ - $C_4$ = | ratio | Stability | Ref.  |
| Fe-K/HPCMs-1                           | 33.4            | 38.9  | 13.5              | 18.0            | 11.5                       | 6.0             | 1.6   | 35 h      | [111] |
| $ZIF-8(a)/Fe_2O_3$                     | ~24.0           | ~24.0 | ~21.0             | ~20.0           | ~24.0                      | ~4.8            | 0.83  | n/a       | [112] |
| $Fe(0.5)$ - $Mo_2C^c$                  | 9.8             | 0.5   | 2.1               | 92.0            | 3.5                        | 9.0             | 26.3  | 2 h       | [113] |
| K-Zr-Co/aTiO2                          | 70.0            | n/a   | n/a               | 17.0            | n/a                        | 11.9            | n/a   | 8h        | [58]  |
| Fe-Cr-K/Nb <sub>2</sub> O <sub>5</sub> | 31.0            | 57.0  | 32.0              | 10.0            | 1.0                        | 3.1             | 3.1   | n/a       | [114] |
| 15Fe-K/m-ZrO <sub>2</sub>              | 38.8            | 19.9  | 30.1              | 42.8            | 12.8                       | 16.6            | 3.3   | 12 h      | [115] |
| 20%Fe/CeO <sub>2</sub> -NC             | 18.9            | 73.5  | 75.5              | 18.2            | 4.0                        | 3.4             | 4.1   | n/a       | [116] |
| 10Fe-1K/m-ZrO <sub>2</sub>             | 40.5            | n/a   | n/a               | 15.0            | n/a                        | 6.1             | n/a   | 100 h     | [117] |
| $Fe_5C_2-10K/a-Al_2O_3$                | 40.9            | n/a   | n/a               | 73.5            | n/a                        | 30.1            | n/a   | 100 h     | [15]  |
| Co-Na-Mo/CeO <sub>2</sub>              | 15.1            | 70.2  | 22.1              | 10.7            | 36.0                       | 1.6             | 0.03  | n/a       | [118] |

Owen et al. investigated the effect of Co-Na-Mo on various supports (SiO<sub>2</sub>, CeO<sub>2</sub>, ZrO<sub>2</sub>,  $\gamma$ -Al<sub>2</sub>O<sub>3</sub>, TiO<sub>2</sub>, ZSM-5 (NH<sub>4</sub>\*) and MgO) for CO<sub>2</sub> hydrogenation. It was found that the surface area of the support and the metal-support interaction played a key role in determining the cobalt crystallite size which strongly affected the catalytic activity. Cobalt particles with sizes < 2 nm supported on MgO depicted low RWGS conversion with negligible FT activity, which is in agreement with the work of de Jong et al. [53]. When the cobalt particle size increased to 15 nm supported on SiO<sub>2</sub> and ZSM-5, both CO<sub>2</sub> conversion and C<sub>2+</sub> hydrocarbon selectivity increased markedly. When the cobalt particle size further increased to 25-30 nm, lower CO<sub>2</sub> conversion but higher C<sub>2+</sub> light olefins selectivity was obtained. The authors reported that the higher the metal-support interaction, the higher the growth chain probability of the hydrocarbons. By altering the TiO<sub>2</sub> /SiO<sub>2</sub> ratio in the support, CO<sub>2</sub> conversion and C<sub>2+</sub> light olefins selectivity could be tuned [118]. Li et al. evaluated cobalt catalysts supported on TiO<sub>2</sub> with different crystal forms of anatase (a-TiO<sub>2</sub>) and rutile (r-TiO<sub>2</sub>) and it was found that the addition of Zr, K, and Cs improved the CO, CO<sub>2</sub>, and H<sub>2</sub> adsorption in both the capacity and strength over a-TiO<sub>2</sub> and r-TiO<sub>2</sub> supported catalysts. The surface C/H ratio increased drastically in the presence of promoters, leading to high C<sub>2+</sub> selectivity of 17% with 70% CO<sub>2</sub> conversion over K-Zr-Co/a-TiO<sub>2</sub> catalyst. As a result, the product

582

distribution could be tuned by adjusting the metal-support interaction and surface C/H ratio through Zr, K, and Cs modification over Co-based catalysts for CO<sub>2</sub> hydrogenation as shown in Scheme 7 [58].



Scheme 7. Schematic illustration of un-promoted and Zr, K promoted cobalt catalysts supported on a-TiO<sub>2</sub> and r-TiO<sub>2</sub> for CO<sub>2</sub> hydrogenation. Reproduced with permission from [58].

Da Silva et al. found the Fe-Cr catalyst, promoted with K and supported on niobium oxide was more active (CO<sub>2</sub> conversion = 20%) and selective to light olefins (25%) than the same composition supported on silica (CO<sub>2</sub> conversion = 11%, light olefins selectivity = 18%) under the same testing conditions. Alkali metal promotion increased the selectivity of olefins probably due to electron-donor effects and the basicity of niobium oxide. Niobium oxide supported Fe-Cr catalyst presented higher activity and selectivity to olefins, which is probably due to strong metal-support interactions when compared with traditional SiO<sub>2</sub> [114]. Very recently, Huang et al. revealed the dynamic evolution of active Fe and carbon species over different (monoclinic and tetragonal) zirconia supports (m-ZrO2 and t-ZrO2) on CO2 hydrogenation to light olefins as shown in Scheme 6. Fe-K/m-ZrO2 catalysts performed better than the corresponding Fe-K/t-ZrO2 catalysts under the optimal reaction conditions. Among them, the 15Fe-K/m-ZrO2 catalyst showed remarkable catalytic activity with a CO<sub>2</sub> conversion of 38.8% and C<sub>2</sub>-C<sub>4</sub>= selectivity of 42.8%. More active species (Fe<sub>3</sub>O<sub>4</sub> and χ-Fe<sub>5</sub>C<sub>2</sub>) with smaller particle sizes were obtained for the Fe-K/m-ZrO<sub>2</sub> catalysts. The larger specific surface area facilitated the highly dispersed Fe species on the surface of m-ZrO2 support when compared to the t-ZrO2 support. In addition, the m-ZrO2 support provided relatively more strong basic sites, reducing the physically deposited carbon species and coke generation. Moreover, more oxygen vacancies (Ov) and the electron-donating ability of iron elements enhanced the charge transfer between Fe and ZrO2. The synergy effect between K2O and ZrO2 fostered the generation of active carbide species. The formation of more χ-Fe<sub>5</sub>C<sub>2</sub> species contributed to the high yield of light olefins [115]. Similarly, Gu et al. investigated Fe-K supported on ZrO2 with different crystal phases revealing 40.5% of CO2 conversion, 15.0% of light olefins selectivity and excellent stability (Figure 17) over the 10Fe-1K/m-ZrO2 (10 wt% Fe and 1 wt% K) at 2.0 MPa and 613K. The CO<sub>2</sub> conversion was almost 200% higher than that of 10Fe-1K/t-ZrO<sub>2</sub> [117].

583

584

585 586

587

588

589

590

591

592

593

594

595

596

598

599

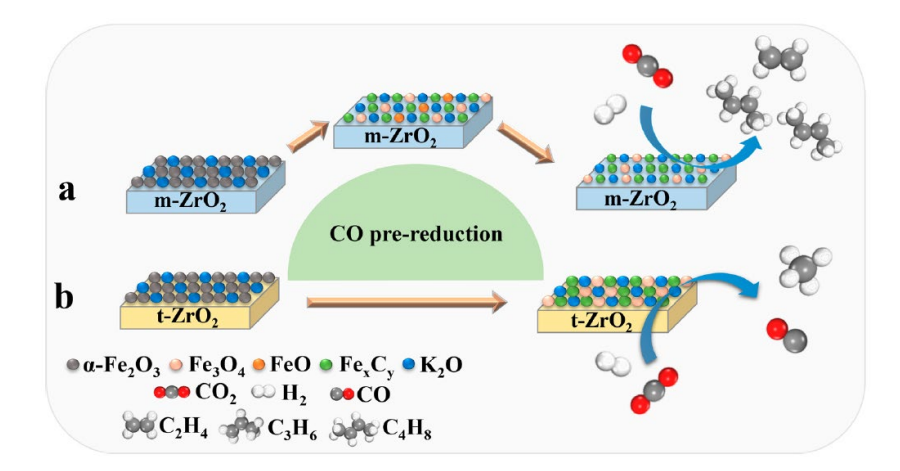
600

601

602

603

604



Scheme 6. CO Pre-reduction and CO<sub>2</sub> hydrogenation process on (a) m-ZrO<sub>2</sub> and (b) t-ZrO<sub>2</sub> supported Fe-Zr catalysts. Reproduced with permission from [115].

Torrente-Murciano demonstrated that the iron-based catalysts could be modified not only by the addition of promoters, but also by careful control of the morphology of the ceria support (nanoparticle, nanorods, nanocubes) for CO<sub>2</sub> hydrogenation to light olefins. 20 wt% Fe/CeO<sub>2</sub> cubes provided better catalytic performance (CO<sub>2</sub> conversion = 15.2%, C<sub>2</sub>-C<sub>4</sub><sup>=</sup> selectivity = 20.2%) when compared with nanorods and nano particles counterparts. TPR showed the ceria reducibility decreased in the order of rods > particles > cubes, suggesting that the catalytic effect was directly related to the reducibility of the different nanostructured ceria supports and their interaction with the iron particles [116]. By physical mixing Fe<sub>5</sub>C<sub>2</sub> and K modified Al<sub>2</sub>O<sub>3</sub>, Liu et al. discovered that Fe<sub>5</sub>C<sub>2</sub>-10K/a-Al<sub>2</sub>O<sub>3</sub> exhibited CO<sub>2</sub> conversion of 40.9% and C<sub>2+</sub> selectivity of 73.5% containing 37.3% C<sub>2</sub>-C<sub>4</sub><sup>=</sup> and 31.1% C<sub>5+</sub> (Figure 18). The superior catalytic performance was due to the potassium migrated into Fe<sub>5</sub>C<sub>2</sub> during reaction and the intimate contact between Fe<sub>5</sub>C<sub>2</sub> and K/a-Al<sub>2</sub>O<sub>3</sub>. Among various supports tested as shown in Figure 18, alkaline Al<sub>2</sub>O<sub>3</sub> is the best support for high selectivity of value-added hydrocarbons [15].

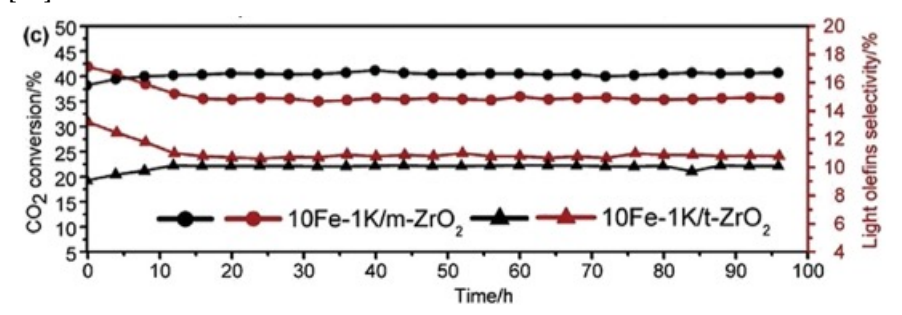


Figure 17. The stability of 10Fe1K/m-ZrO<sub>2</sub> and 10Fe1K/t-ZrO<sub>2</sub> for the conversion of CO<sub>2</sub> and the selectivity of light olefins for 100 h at 613K. Reproduced with permission from [117].

Dai et al. synthesized hierarchical porous carbon monoliths (HPCMs) by a versatile strategy involving one-step desilication of coke-deposited spent zeolite catalyst. Such hierarchical porous carbon was found to be a superior support for reducing the nanoparticle size and boosting the synergism of the Fe–K catalyst for CO<sub>2</sub> hydrogenation with CO<sub>2</sub> conversion of 33.4% and C<sub>2</sub>=-C<sub>4</sub>= selectivity of 18.0% [111].

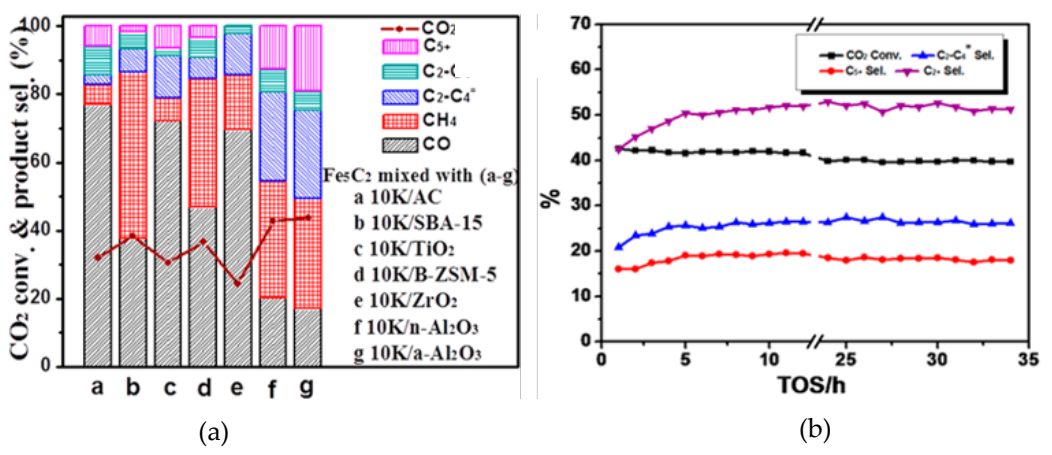


Figure 18. (a) CO<sub>2</sub> conversion and product selectivity over Fe<sub>5</sub>C<sub>2</sub>-based catalysts on various supports. (b) Catalytic performance and stability over Fe<sub>5</sub>C<sub>2</sub>-10K/a-Al<sub>2</sub>O<sub>3</sub> catalyst (reaction conditions: 673K, 3.0 MPa, 3600 mLg<sup>-1</sup>h<sup>-1</sup>, H<sub>2</sub>/CO<sub>2</sub> = 3). Reproduced with permission from [15].

Metal organic frameworks (MOFs) as a novel porous materials had a significant impact on the activity and selectivity of Fe based catalysts. Hu et al. synthesized a type of hydrothermally stable MOFs, Zeolitic imidazolate frameworks (ZIF-8) with different size and morphology, and used as supports for CO2 hydrogenation. The acidity, internal diffusion process and crystal size enabled the ZIF-8 supports to depict different levels of substantial light olefins selectivity [112]. Raghav et al. developed a facile method for the synthesis of hierarchical molybdenum carbide (β-Mo<sub>2</sub>C). The β-Mo<sub>2</sub>C phase exhibited the strongest metallic and some ionic character and it behaved as both a support and cocatalyst for CO<sub>2</sub> hydrogenation to light olefins. The Fe(0.5)-Mo<sub>2</sub>C catalyst exhibited conversion of CO<sub>2</sub> of 7.3% and C<sub>2</sub>= olefins selectivity of 79.4% at 300 °C and 4.0 mPa. The XRD patterns of the fresh and used Fe(0.5)-Mo<sub>2</sub>C catalyst does not show a noticeable difference indicating the stability of the catalysts to achieve high olefin selectivity [113].

In summary, various supports (SiO<sub>2</sub>, CeO<sub>2</sub>, m-ZrO<sub>2</sub>, γ-Al<sub>2</sub>O<sub>3</sub>, TiO<sub>2</sub>, ZSM-5, MgO, NbO HPCMs, MOFs, β-Mo<sub>2</sub>C) have been used for dispersing active species. The surface area, basicity, reducibility, oxygen vacancies, and morphology of the support played important roles, in most cases with the presence of promoters (K, Zr, Cs), in affecting the amount and particle size of the active carbide species, the synergy effect, the metal-support interaction, the strength and capacity of CO, CO2, and H2 adsorption on support, and the surface C/H ratio for CO2 hydrogenation. By tuning what abovementioned properly, the physically deposited carbon species, coke generation and metal sintering could be mitigated as reported.

### 3.4 Bifunctional composite catalyst effect

The zeolite- methanol composite catalyst can also be improved by compositional modifications. The composite catalyst composed of two functional components: one is target for methanol synthesis, mainly Cu, Zn, In metal oxide catalysts; another one is for MTO process, mainly zeolite catalysts. Herein in this section the recent progress on composite catalysts for improved catalytic performance and stability are described accordingly. Some representative catalysts on bifunctional composite catalyst effect for CO2 hydrogenation to light olefins with improved catalyst stability are presented in Table 3.

Table 3. Some representative catalysts on bifunctional composite catalyst effect for CO2 hydrogenation to light olefins

| Catalyst | $CO_2$   | Selectivity, % |                   |                 |                            | Yield, %        | O/P   | Stability |      |
|----------|----------|----------------|-------------------|-----------------|----------------------------|-----------------|-------|-----------|------|
|          | Conv., % | CO             | CH <sub>4</sub> . | $C_2$ - $C_4$ = | $C_2$ - $C_4$ <sup>0</sup> | $C_2$ - $C_4$ = | ratio |           | Ref. |

630 631 632

629

633 634

635

636

637

644

645

646

647

648

649 650

651

652 653 654

655

656 657

658

| CuO-ZnO/                           | 41.3  | 9.3   | 11.8  | 63.4           | 15.5       | 26.2 | 4.1  | 13 h    |       |
|------------------------------------|-------|-------|-------|----------------|------------|------|------|---------|-------|
| SAPO-34                            |       |       |       |                |            |      |      |         | [119] |
| (CuO-ZnO)-                         | 57.6  | 9.6   | 11.4  | 63.8           | 15.2       | 36.7 | 4.2  | 20 h    | [119] |
| kaolin/SAPO-34                     |       |       |       |                |            |      |      |         |       |
| In2O3/ZrO2                         | 19.0  | 87.0  | ~17.0 | $90.0^{a}$     | n/a        | 17.1 | n/a  | > 50 h  | [44]  |
| &SAPO                              |       |       |       |                |            |      |      |         |       |
| In2O3/ZrO2                         | ~14.0 | < 5.0 | < 5.0 | 70.0           | n/a        | 9.8  | n/a  | > 100 h | [46]  |
| &SAPO                              |       |       |       |                |            |      |      |         |       |
| In-Zr/SAPO-34                      | 26.7  | n/a   | 4.3   | $76.4^{\rm a}$ | ~14.0a     | 20.4 | 5.5  | > 150 h | [19]  |
| $Zn_{0.5}Ce_{0.2}Zr_{1.8}O_{4}/$   | 10.7  | 28.3  | 2.9   | 83.4           | 5.4        | 8.9  | 15.4 | > 30 h  |       |
| H-RUB-13 (200)                     |       |       |       |                |            |      |      |         | [120] |
| $ZnZrO_x$                          | 10.0  | ~80.0 | 5.5   | 64.4           | 30.1       | 6.4  | 2.1  | 60 h    |       |
| &bio-ZSM-Si                        |       |       |       |                |            |      |      |         | [121] |
| InCrOx(0.13)&                      | 33.6  | 55.0  | 35.0  | $75.0^{a}$     | $20.0^{a}$ | 11.3 | 3.8  | > 120 h |       |
| SAPO-34                            |       |       |       |                |            |      |      |         | [122] |
| ZnZrO/SAPO-34                      | 12.6  | 47.0  | 3.0   | 80.0a          | $14.0^{a}$ | 10.1 | 5.7  | > 100 h | [14]  |
| CZZ@Zn                             | ~7.0  | n/a   | ~18.0 | 72.0           | 8.0        | 1.3  | 8.6  | > 120 h | [123] |
| &SAPO-34                           |       |       |       |                |            |      |      |         |       |
| $In_2O_3$ - $ZnZrO_x$ /            | 17.0  | 55.8  | 1.6   | $85.0^{a}$     | 11.1a      | 14.5 | 7.7  | > 90 h  | [43]  |
| SAPO-34-S-a                        |       |       |       |                |            |      |      |         |       |
| $In_2O_3$ - $ZnZrO_x$ /            | 17.0  | 53.4  | 1.2   | 84.5a          | $11.0^a$   | 14.4 | 7.7  | > 90 h  | [43]  |
| SAPO-34-H-a                        |       |       |       |                |            |      |      |         |       |
| ZnAl <sub>2</sub> O <sub>4</sub> / | 15.0  | 49.0  | 0.7   | 87.0a          | $10.0^{a}$ | 13.1 | 8.7  | 10 h    |       |
| SAPO-34                            |       |       |       |                |            |      |      |         | [124] |
| ZnGa <sub>2</sub> O <sub>4</sub> / | 13.0  | 46.0  | 1.0   | 86.0a          | 11.0a      | 11.2 | 7.8  | 10 h    | [124] |
| SAPO-34                            |       |       |       |                |            |      |      |         |       |
| 13%ZnO-ZrO <sub>2</sub> /          | 24.4  | 42.2  | 3.7   | 61.7           | 33.6       | 15.1 | 1.8  | 10 h    |       |
| Mn <sub>0.1</sub> SAPO-34          |       |       |       |                |            |      |      |         | [125] |
| In-Zr (4:1)/                       | 26.2  | 63.9  | 2.0   | 74.5a          | 21.5a      | 19.5 | 3.5  | > 140 h | [39]  |
| SAPO-34                            |       |       |       |                |            |      |      |         |       |

<sup>&</sup>lt;sup>a</sup> CO is not considered when calculating selectivity;

Wang et al. prepared kaolin-supported CuO-ZnO/SAPO-34 catalysts using kaolin as support and raw material to prepare SAPO-34 molecular sieves. It was found that the resulted SAPO-34 molecular sieves showed lamellar structure, relatively high crystallinity and larger specific surface area, which enabled the well dispersion of CuO-ZnO on the surface of kaolin and exposed more active sites for CO<sub>2</sub> conversion. The confinement effect of (CuO-ZnO)-kaolin/SAPO-34 catalysts could prevent methanol dissipation and provided an increased driving force for the conversion of CO<sub>2</sub>. Furthermore, the lamellar structure of SAPO-34 molecular sieves shortened the diffusion path of intermediate product and therefore enhanced the catalytic lifetime [119].

Gao et al. demonstrated a selective hydrogenation process to directly convert  $CO_2$  to light olefins via a bifunctional catalyst composed of a methanol synthesis ( $In_2O_3$ - $ZrO_2$ ) catalyst and a methanol-to-olefins (SAPO-34) catalyst by physical mixing. This bifunctional exhibited outstanding light olefin ( $C_2$ - $C_3$ =) selectivity of 80-90% with a  $CO_2$  conversion

of ~20% and superior catalyst stability for running 50 hours without obvious deactivation. The excellent catalytic performance was ascribed to the hybrid catalyst that suppress uncontrollable surface polymerization of CH*x* in conventional CO<sub>2</sub>-FT synthesis. This was the highest selectivity reported to date, which significantly surpassed the value obtained over conventional iron or cobalt CO<sub>2</sub>-FT synthesis catalysts (typically less than 50%) [44].

Similarly, Tan et al. evaluated CO<sub>2</sub> to light olefins over In<sub>2</sub>O<sub>3</sub>-ZrO<sub>2</sub>/SAPO-34 hybrid catalyst. This hybrid catalyst combined In<sub>2</sub>O<sub>3</sub>-ZrO<sub>2</sub> component giving the oxygen vacancy to benefit CO<sub>2</sub> activation for hydrogenation into methanol and SAPO-34 component for further dehydrates the formed methanol into light olefins (Figure 19a). The light olefins selectivity reached 77.6% with less than 5% CO formation, which was attributed to strong adsorption of CO<sub>2</sub> to defective In<sub>2</sub>O<sub>3</sub> and ZrO<sub>2</sub>, creating a large energy barrier that suppressed CO<sub>2</sub> dissociation into CO. The weaker acidity from In<sub>2</sub>O<sub>3</sub>-ZrO<sub>2</sub> suppressed the generated light olefins to be further hydrogenated to paraffins. The catalyst displayed excellent stability for running 100 hours without obvious deactivation (Figure 19b) [46].

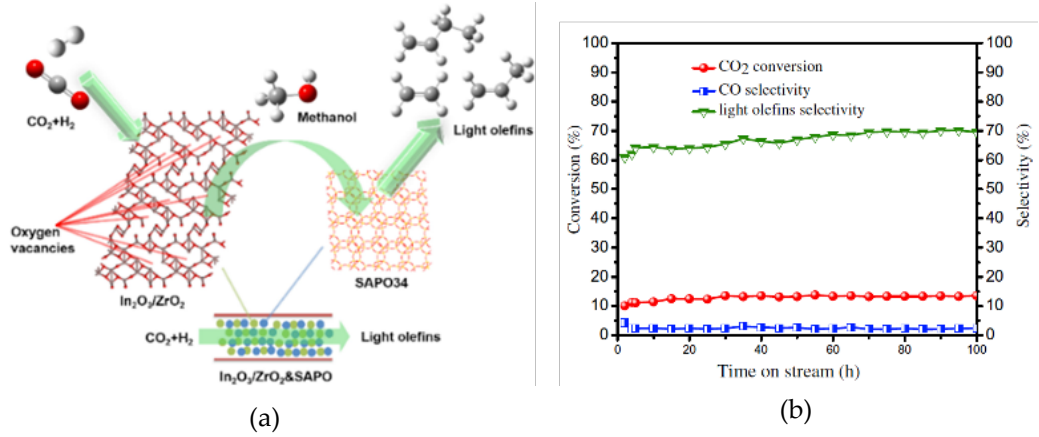
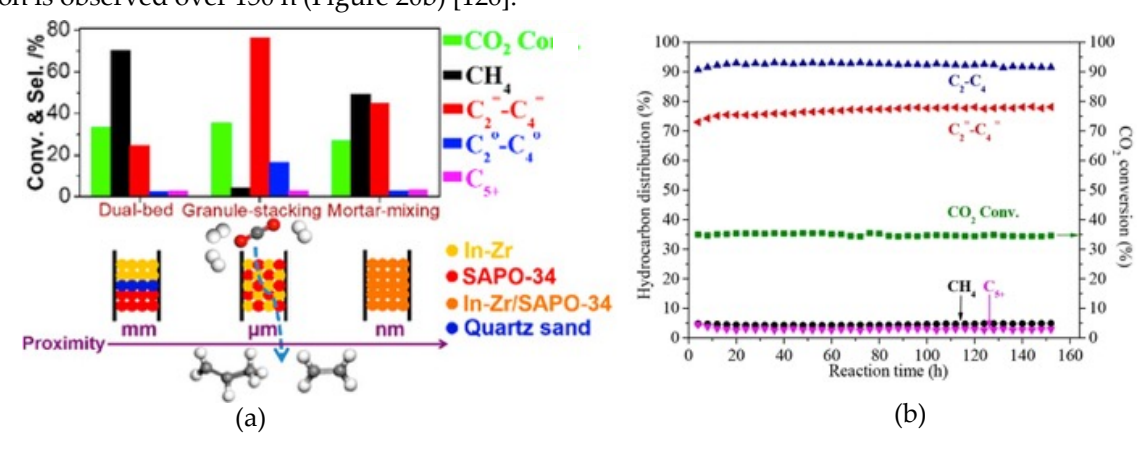


Figure 19. (a) Illustrated reaction mechanism over the hybrid catalyst  $In_2O_3$ - $ZrO_2/SAPO$ -34 and (b) Stability of  $In_2O_3$ - $ZrO_2/SAPO$ -34 hybrid catalyst for  $CO_2$  conversion to light olefins (testing conditions: 2.0 MPa, 573K, 2160 cm<sup>3</sup>h<sup>-1</sup>g<sub>cat</sub><sup>-1</sup>). Reproduced with permission from [46].

Furthermore, Gao et al. discovered that a bifunctional catalyst with an appropriate proximity contained In–Zr oxide and SAPO-34, which was responsible for the CO<sub>2</sub> activation and the selective C–C coupling, respectively, could enhance the CO<sub>2</sub> hydrogenation to lower olefins with excellent selectivity (80%) and high activity (35% CO<sub>2</sub> conversion) (Figure 20a). They demonstrated that the incorporation of zirconium significantly boosted the surface oxygen vacancies and remarkably improved the catalytic stability by preventing the sintering of the oxide nanoparticles. No obvious deactivation is observed over 150 h (Figure 20b) [126].



698

699

700

701

702

703

704

705

706

707

708

709

710

711

712

713

714

715

716

717

718

719

720

721

722

Figure 20. (a) Effect of the integration manner of the active components on catalytic performances and (b) Catalytic stability test of composite In-Zr/SAPO-34 catalyst (reaction conditions: 673K, 3.0 MPa, 9000 mLg<sub>cat</sub><sup>-1</sup> h<sup>-1</sup>, H<sub>2</sub>/CO<sub>2</sub>/N<sub>2</sub> = 73/24/3, and oxide/zeolite mass ratio = 2). Reproduced with permission from [126].

Wang et al. developed a new catalyst system composed of  $Zn_{0.5}Ce_{0.2}Zr_{1.8}O_4$  solid solution and H-RUB-13 zeolite. This composite exhibited a remarkable  $C_2$ = $-C_4$ = yield as high as 16.1% with a CO selectivity of only 26.5% due to hindering RWGS reaction. It was demonstrated that methanol was first generated on the  $Zn_{0.5}Ce_{0.2}Zr_{1.8}O_4$  solid solution via the formate-methoxyl intermediates mechanism and was then converted into light olefins on H-RUB-13. By adjusting the H-RUB-13 acidity, the light olefins distribution can be effectively regulated with propene and butene accounting for 90% of light olefins [120].

Li et al. proposed a new synthetic strategy to prepare bifunctional catalysts ZnZrO<sub>x</sub>/bio-ZSM-5. The hierarchically porous structured bio-ZSM-5 was prepared by using natural rice husk as a template, which was then integrated with ZnZrO<sub>x</sub> solid solution nanoparticles by physical mixing. The derived bifunctional catalysts ZnZrO<sub>x</sub>&bio-ZSM-5 catalysts exhibited superior light olefins selectivity and stability due to the unique pore structure which were beneficial for the mass transportation and inhibition of coke formation. \*CH<sub>x</sub>O was found to be the key intermediate formed on the ZnZrO<sub>x</sub> surface and was transferred to the Brønsted acid sites in the bio-ZSM-5 for the subsequent conversion to light olefins. The addition of a Si promoter to the ZnZrO<sub>x</sub>/bio-ZSM-5 catalyst prominently enhanced the light olefins selectivity. The ZnZrO<sub>x</sub>/bio-ZSM-5-Si catalyst exhibited an outstanding light olefins selectivity of 64.4% with CO<sub>2</sub> conversion of 10% and an excellent stability without noticeable deactivation during 60 h on stream (Figure 21a). In addition, the proximity of the catalyst components plays a key role in light olefin selectivity. As seen in Figure 21b, increasing the proximity resulted in a greater olefin selectivity [121]. By incorporating proper amounts of Ce or Cr ions into indium oxides, the methanol selectivity is increased, along with a reduction in the CH<sub>4</sub> amount as shown in Figure 22. Upon complexing with SAPO-34, a CO<sub>2</sub> conversion of 33.6% and a C<sub>2</sub>=-C<sub>4</sub>= selectivity of 75.0% were achieved over InCrO<sub>x</sub>(0.13)/ SAPO-34, which was about 1.5-2.0 times of those obtained on In<sub>2</sub>O<sub>3</sub>/SAPO-34 and In-Zr/SAPO-34. This is because incorporation of Ce or Cr ions into In<sub>2</sub>O<sub>3</sub> lattice sites promoted generation of more surface oxygen vacancies as shown in Figure 22a and enhanced the electronic interaction of HCOO\* with  $InCeO_x(0.13)$  and  $InCrO_x(0.13)$  surfaces, which decreased the free energy barrier and enthalpy barrier for the formation of HCOO\* and CH<sub>3</sub>OH. The composite catalysts also displayed excellent stability after 120 hours on stream (Figure 22b) [122].

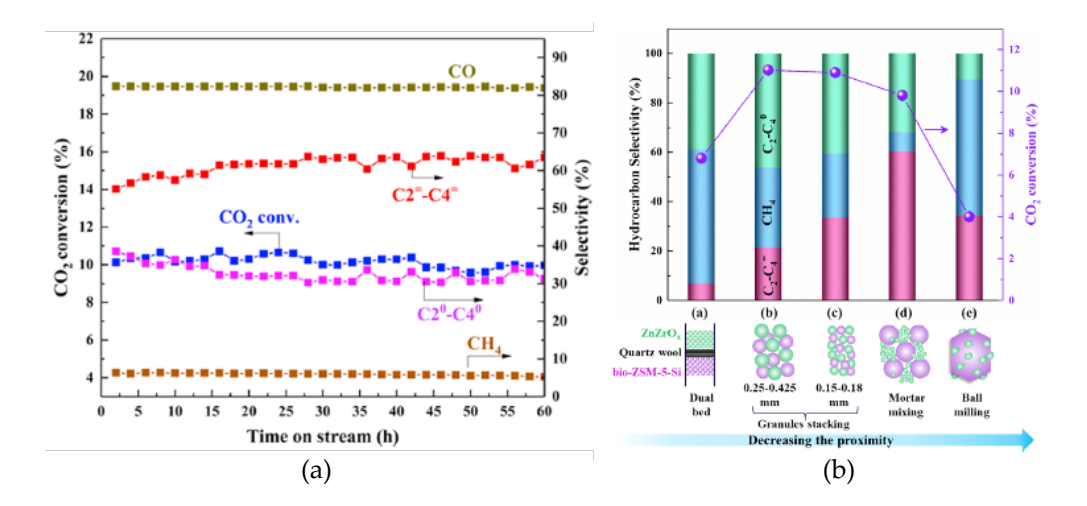


Figure 21. (a) CO<sub>2</sub> conversion and product selectivity over bifunctional catalysts ZnZrO<sub>x</sub>/bio-ZSM-5–Si as a function of time on stream (reaction conditions: 0.6 g catalyst, 653K, 3 MPa, feed gas flow rate =  $20 \text{ mLmin}^{-1}$ ). (b) Effect of integration manner of ZnZrO<sub>x</sub>/bio-ZSM-5-Si on the catalytic activity of the bifunctional catalysts. Reproduced with permission from [121].

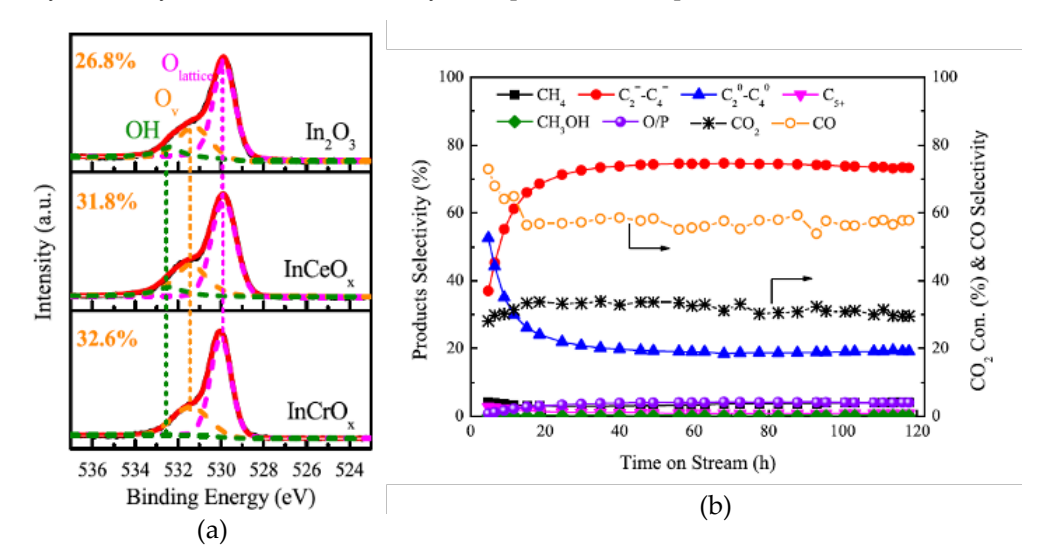


Figure 22. (a) The concentration of surface oxygen vacancies ( $O_v$ ) from O(1s) XPS spectra for In<sub>2</sub>O<sub>3</sub>, InCeO<sub>x</sub>(0.13), and InCrO<sub>x</sub>(0.13). (b) Catalytic stability test for InCrO<sub>x</sub>(0.13)&SAPO-34 (reaction conditions: H<sub>2</sub>/CO<sub>2</sub> = 3/1, 623K, 3.5 MPa, GHSV = 1140 mLg<sub>cat</sub>-1h-1). Reproduced with permission from [122].

Similarly, Li et al. developed a bifunctional composite catalyst ZnZrO/SAPO-34 containing a component ZnOZrO<sub>2</sub> to activate CO<sub>2</sub> and H<sub>2</sub> to form methanol and a component SAPO-34 to perform C-C bond formation for converting produced methanol to light olefins. The derived dual function tandem catalyst exhibited an outstanding light olefins selectivity of 80% with good stability and CO<sub>2</sub> conversion of 12.6% (Figure 23a-b). The thermodynamic and kinetic coupling between the tandem reactions enabled the highly efficient conversion of CO<sub>2</sub> to lower olefins through the transferring and migrating of CH<sub>x</sub>O intermediate species [45].

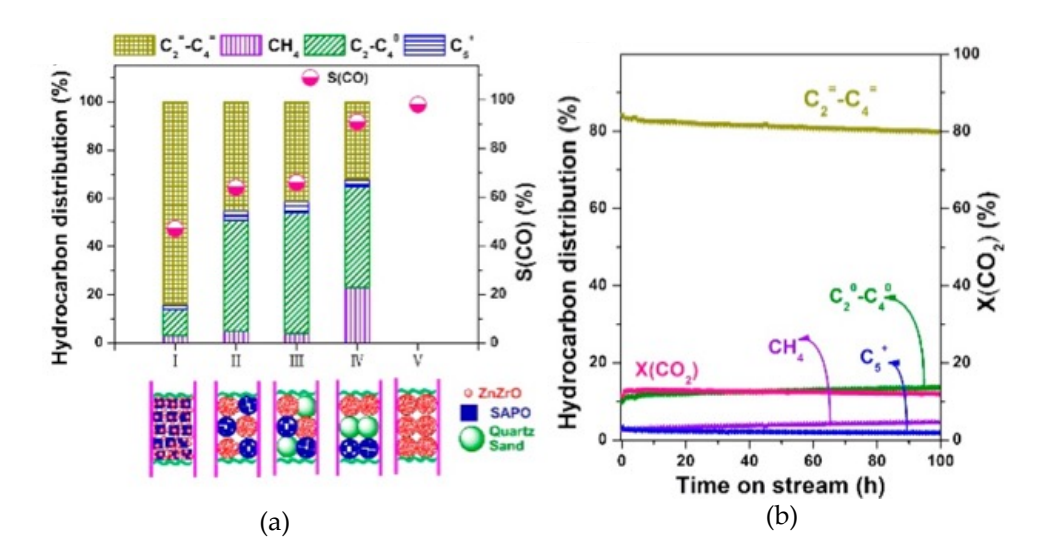


Figure 23. (a) CO<sub>2</sub> hydrogenation over ZnZrO/SAPO-34, integrated catalyst components ZnZrO and SAPO with different proximity. (b) Catalytic stability test for ZnZrO/SAPO-34 (reaction conditions: 653K, 2 MPa, 3600 mLg<sub>cat</sub>-1h-1and 2 MPa. Reproduced with permission from [45].

[43].

747

745

757

758

759

760

761 762

763

765

766

767

768

769

770

771

772

773

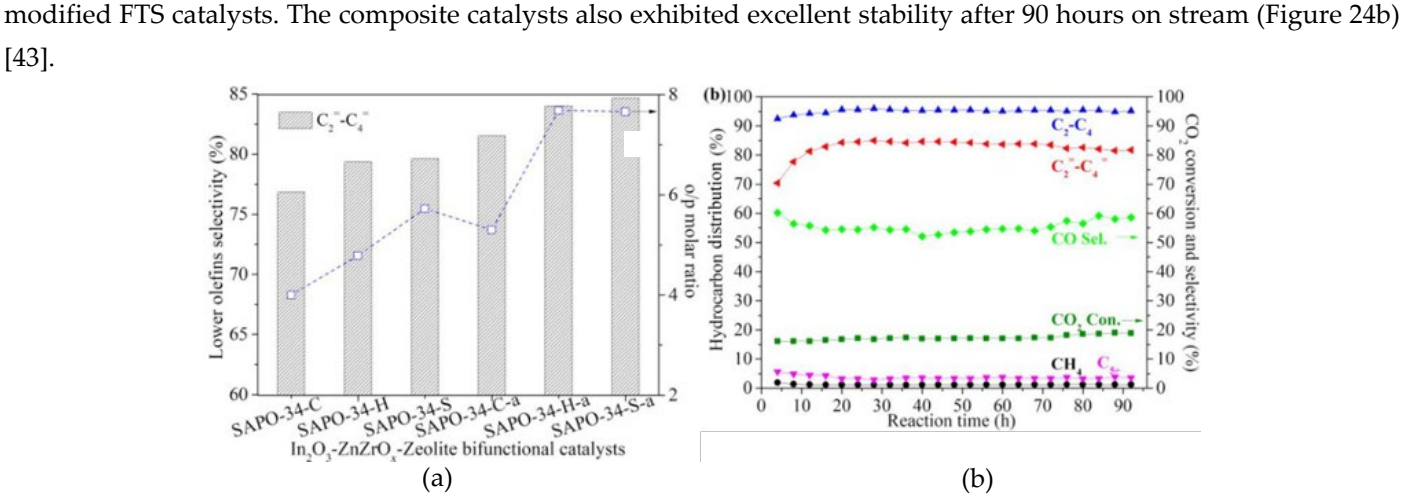
774

775

776

777

778



Dang et al. developed a series of dual function tandem catalysts containing In<sub>2</sub>O<sub>3</sub>-ZnZrOx oxides and various

SAPO-34 zeolites with varying crystal sizes (0.4-1.5 mm) and pore structures. It was found that decreasing the crystal

size of SAPO-34 could shorten the diffusion path from the surface to the acid sites inside the zeolite pores, thus favoring

the mass transfer of intermediate species for efficient C-C coupling to produce lower olefins and enhance the selectivity

of C<sub>2</sub>-C<sub>4</sub>. Interestingly, further HNO<sub>3</sub> post-treatment caused the formation of the SAPO-34 zeolites with a hierarchical

structure comprised of micro-/meso-/macropores, and reduced the amount of the Brønsted acid sites, both of which led

to a significant increase in the catalytic performance with the C2=-C4= selectivity reached as high as 85% among all

hydrocarbons (Figure 24a), very low CH4 selectivity of only 1% and O/P ratio of 7.7 at a CO2 conversion of 17 %. The

C2=-C4= selectivity is much higher than the maximum predicted by the Anderson-Schulz-Flory distribution over

Figure 24. (a) Lower olefins selectivity and O/P molar ratio of hydrocarbons for CO<sub>2</sub> hydrogenation over In<sub>2</sub>O<sub>3</sub>-ZnZrO<sub>x</sub> with various SAPO-34. (b) Stability tests of bifunctional catalysts In<sub>2</sub>O<sub>3</sub>-ZnZrO<sub>x</sub>/SAPO-34-H-a (reaction conditions: 653K, 3.0 MPa, 9000 mLg<sub>cat</sub>-1h-<sup>1</sup>, H<sub>2</sub>/CO<sub>2</sub>/N<sub>2</sub>=73:24:3, catalysts with oxide/zeolite mass ratio = 0.5). Reproduced with permission from [43].

Liu et al. synthesized bifunctional composite catalysts composed of a spinel binary metal oxide ZnAl<sub>2</sub>O<sub>4</sub>/ZnGa<sub>2</sub>O<sub>4</sub> and SAPO-34 with the selectivity of C<sub>2</sub>-C<sub>4</sub> olefins reached 87% at CO<sub>2</sub> conversions of 15%. This study revealed that the oxygen vacancy site on metal oxides played a pivotal role in the adsorption and activation of CO<sub>2</sub>, while the -Zn-O- domain accounted for H2 activation. It was demonstrated that methanol formed on the metal oxide as reaction intermediates, then subsequently converted to lower olefins by the Brønsted acid sites in SAPO-34 zeolite [124]. Tong et al. developed a dual function composite catalyst 13%ZnO-ZrO<sub>2</sub>/Mn<sub>0.1</sub>SAPO-34 and attained a high CO<sub>2</sub> conversion of 21.3% with a light olefins selectivity of 61.7% and suppressed selectivity of CO below 43% and CH<sub>4</sub> selectivity below 4%. The fine-tuned acidity of zeolite by the addition of Mn and the granule stacking arrangement contributed to the excellent catalytic performance. Mn was embedded into the zeolite ionic structure to tune the acidity of the molecular sieve and limit secondary hydrogenation reactions. The granule stacking arrangement facilitated the tandem catalysis [125]. Dang et al. reported a series of bifunctional catalysts contained indium-zirconium composite oxides with different In/Zr atomic ratios and SAPO-34 zeolite for CO2 conversion to light olefins. It was demonstrated that the incorporation of a certain amount of zirconium could create more oxygen vacancy sites (Figure 25a), stabilize the intermediates in CO2 hydrogenation and prevent the sintering of the active nanoparticles, thus leading to significantly enhanced catalytic activity, selectivity of hydrocarbons and stability for direct CO2 hydrogenation to lower olefins at the relatively high reaction temperature of 653K. As high as 80% of light olefins selectivity at CO2 conversion

of 27% and less than 2.5% of methane selectivity was obtained over the optimized Indium-zirconium/SAPO-34 bifunctional catalyst. The catalyst exhibited excellent stability for over 140 hours without showing obvious deactivation (Figure 25b) [39].

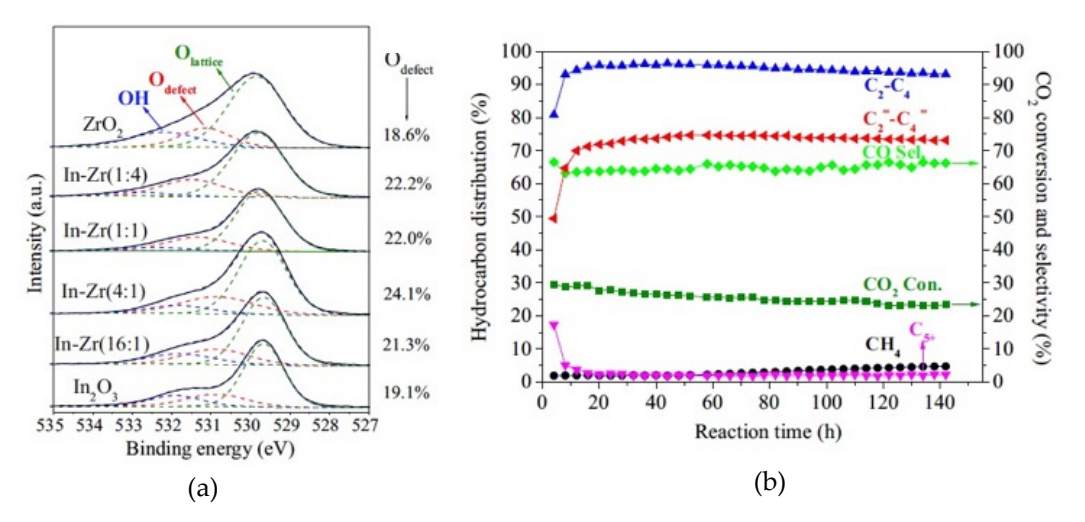


Figure 25. (a) The XPS spectra of O1s of various oxides after pretreated at 673 K for 1 h with pure Ar. (b) The stability tests of composites In-Zr(4:1)/SAPO-34 (reaction conditions: 653K, 3.0 MPa, 9000 mL gcat $^{-1}h^{-1}$ ,H<sub>2</sub>/CO<sub>2</sub>/N<sub>2</sub> = 73/24/3, catalysts with oxide/zeolite mass ratio = 0.5). Reproduced with permission from [39].

In summary, the majority of the catalysts tested for CO<sub>2</sub> hydrogenation to light olefins via MeOH mediated route involve two active components (metal oxides and zeolite), so called bifunctional composite catalysts. In this section, multiple variations (acidity, particle size, proximity, oxygen vacancy) in combining methanol synthesis catalysts (Cu, Zn, In, Ce, Zr, etc. metal oxides) with various zeolites (SAPO-34 and ZSM5) have been reported to give improved olefin selectivity and catalyst stability by mitigating coke formation, reducing particle size growth of active carbide species, and inhibiting inactive species formation for CO<sub>2</sub> hydrogenation to light olefins.

# 3.5 Structure Effect

Structure of the catalysts plays an important role in converting CO<sub>2</sub> to light olefins. In this section, we will report the recent progress on how morphology changes in both the Fe- based and methanol zeolite composite catalysts can improve the catalytic performance. Some representative catalysts on structure effect for CO<sub>2</sub> hydrogenation to light olefins with improved catalyst stability are presented in Table 4.

Table 4. Some representative catalysts on structure effect for CO<sub>2</sub> hydrogenation to light olefins

| Catalyst                            | CO <sub>2</sub> | Selectivity, % |                   |                 |                            | Yield, %        | O/P   |           |       |
|-------------------------------------|-----------------|----------------|-------------------|-----------------|----------------------------|-----------------|-------|-----------|-------|
|                                     | Conv., %        | CO             | CH <sub>4</sub> . | $C_2$ - $C_4$ = | $C_2$ - $C_4$ <sup>0</sup> | $C_2$ - $C_4$ = | ratio | Stability | Ref.  |
| 0.8K-2.4Fe-1.3Ti                    | 35.0            | 36.3           | 22.0              | 60.0            | 8.0                        | 21.0            | 7.5   | 200 h     | [127] |
| Fe@NC-400                           | 29.0            | 17.5           | 27.0              | 21.0            | 12.0                       | 6.1             | 1.7   | > 15 h    | [35]  |
| K/Fe-Al-O Spinel                    | 48.0            | 16.0           | 10.0              | 52.0            | 5.0                        | 24.0            | 3.1   | 120 h     | [128] |
| E.1 nanobelts                       |                 |                |                   |                 |                            |                 |       |           |       |
| MgH <sub>2</sub> /Cu <sub>x</sub> O | 20.7            | n/a            | 40.0              | 54.8            | 7.0                        | 11.3            | 7.8   | 210 h     | [129] |
| CZA/SAPO-                           | 50.0            | 3.0            | 10.0              | 62.0            | 25.0                       | 33.0            | 2.5   | 12 h      | [130] |
| 34(TEAOH)HCI                        |                 |                |                   |                 |                            |                 |       |           |       |

| Carbon-confined       10.5       27.6       17.5       50.9       4.0       5.3       12.7       > 2 h       [132]         MgH2 nano-lamellae       80.0       12.4       33.7       41.1       6.4       14.4       6.4       50 h       [36]         K-(CM-Al2O3)       85.0       1.8       83.9a       12.9a       23.2       6.5       n/a       [41]         Y2O3& SAPO-34       93.0       12.9a       12.9a       23.2       6.5       n/a       [41] | FeK1.5/HSG                              | 50   | 39   | 31   | 56                | 9.9   | 28                | 5.7  | > 120 h | [131] |
|---------------------------------------------------------------------------------------------------------------------------------------------------------------------------------------------------------------------------------------------------------------------------------------------------------------------------------------------------------------------------------------------------------------------------------------------------------------|-----------------------------------------|------|------|------|-------------------|-------|-------------------|------|---------|-------|
| lamellae Fe-Co/ 41.0 12.4 33.7 41.1 6.4 14.4 6.4 50 h [36] K-(CM-Al <sub>2</sub> O <sub>3</sub> ) 6.7 wt% ZnO- 27.6 85.0 1.8 83.9 <sup>a</sup> 12.9 <sup>a</sup> 23.2 6.5 n/a [41]                                                                                                                                                                                                                                                                            | Carbon-confined                         | 10.5 | 27.6 | 17.5 | 50.9              | 4.0   | 5.3               | 12.7 | > 2 h   | [132] |
| Fe-Co/ 41.0 12.4 33.7 41.1 6.4 14.4 6.4 50 h [36]<br>K-(CM-Al <sub>2</sub> O <sub>3</sub> )<br>6.7 wt% ZnO- 27.6 85.0 1.8 83.9 <sup>a</sup> 12.9 <sup>a</sup> 23.2 6.5 n/a [41]                                                                                                                                                                                                                                                                               | MgH2 nano-                              |      |      |      |                   |       |                   |      |         |       |
| K-(CM-Al <sub>2</sub> O <sub>3</sub> ) 6.7 wt% ZnO- 27.6 85.0 1.8 83.9 <sup>a</sup> 12.9 <sup>a</sup> 23.2 6.5 n/a [41]                                                                                                                                                                                                                                                                                                                                       | lamellae                                |      |      |      |                   |       |                   |      |         |       |
| 6.7 wt% ZnO- 27.6 85.0 1.8 83.9 <sup>a</sup> 12.9 <sup>a</sup> 23.2 6.5 n/a [41]                                                                                                                                                                                                                                                                                                                                                                              | Fe-Co/                                  | 41.0 | 12.4 | 33.7 | 41.1              | 6.4   | 14.4              | 6.4  | 50 h    | [36]  |
|                                                                                                                                                                                                                                                                                                                                                                                                                                                               | K-(CM-Al <sub>2</sub> O <sub>3</sub> )  |      |      |      |                   |       |                   |      |         |       |
| Y <sub>2</sub> O <sub>3</sub> & SAPO-34                                                                                                                                                                                                                                                                                                                                                                                                                       | 6.7 wt% ZnO-                            | 27.6 | 85.0 | 1.8  | 83.9ª             | 12.9a | 23.2              | 6.5  | n/a     | [41]  |
|                                                                                                                                                                                                                                                                                                                                                                                                                                                               | Y <sub>2</sub> O <sub>3</sub> & SAPO-34 |      |      |      |                   |       |                   |      |         |       |
| Cu-Zn-Al (6:3:1) 27.6 53.4 0.7 45.5 <sup>b</sup> n/a 12.6 <sup>b</sup> n/a 9 h [133]                                                                                                                                                                                                                                                                                                                                                                          | Cu-Zn-Al (6:3:1)                        | 27.6 | 53.4 | 0.7  | 45.5 <sup>b</sup> | n/a   | 12.6 <sup>b</sup> | n/a  | 9 h     | [133] |
| oxide +HB zeolite                                                                                                                                                                                                                                                                                                                                                                                                                                             | oxide +HB zeolite                       |      |      |      |                   |       |                   |      |         |       |

<sup>&</sup>lt;sup>a</sup> refer to hydrocarbon distribution %; <sup>b</sup> refer to C<sub>2-C5+</sub> hydrocarbons

Wang et al. developed layered metal oxides (LMO) structure K-Fe-Ti that displayed high catalytic activity, olefin selectivity and decent stability toward CO<sub>2</sub>-FTS. The light olefin selectivity achieved approximately 60% with an olefin/paraffin ratio of 7.3 over catalyst 0.8K-2.4Fe-1.3Ti (Figure 26). The exfoliated LMO through acid treatment was found to weaken the interaction between Fe and Ti, which enabled the reduction and activation of iron oxides easier to form active iron carbide species that favored a shift from the RWGS to FTS reaction. Meantime, C<sub>2</sub>H<sub>4</sub> adsorption was hindered due to the low surface area of LMO structure, contributing to higher olefin selectivity by inhibiting the secondary hydrogenation of primary olefins. The acid treatment played a key role in the formation of slice structure that favored for CO<sub>2</sub> conversion to light olefins with lower CO selectivity [127]. Fujiwara et al. found the composite catalysts obtained by the physical mixing of Cu–Zn–Al oxide with HB zeolite that was modified with 1,4-bis(hydroxydimethylsilyl) benzene to be very effective for CO<sub>2</sub> hydrogenation to C<sub>2+</sub> hydrocarbons. The modification of zeolite with the disilane compound altered the surface property from hydrophilic to hydrophobic, a characteristic effective in preventing catalyst deactivation by the formation of water during CO<sub>2</sub> hydrogenation. The highest yield of C<sub>2+</sub> hydrocarbons over the modified composite catalysts reached about 12.6 C-mol% at 573K under a pressure of 0.98 Mpa. The enhanced catalytic activity is caused by suppressing the deactivation of the strong acid sites of HB zeolite with the hydrophobic surface [133].

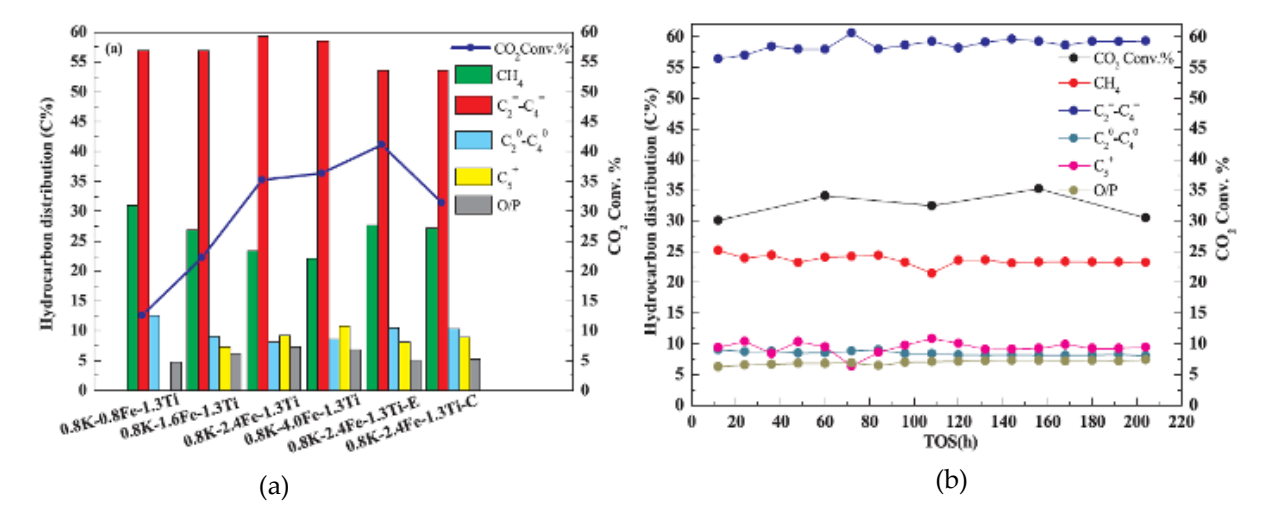


Figure 26. (a) Catalytic activity over different catalysts. (b) Stability of 0.8K-2.4Fe-1.3Ti with time on stream (reaction conditions:  $H_2/CO_2 = 3/1$ , 593K, 2.0 MPa and 10000 mL gcat<sup>-1</sup>h<sup>-1</sup>). Reproduced with permission from [127].

Liu et al. synthesized a unique structure with ZnO and nitrogen-doped carbon (NC) overcoated Fe-based catalysts (Fe@NC) (Figure 27) and found the reaction rate increased by  $\sim$ 25%, while the O/P ratio increased from 0.07 to 1.68 when compared with the benchmark Fe<sub>3</sub>O<sub>4</sub> catalyst. The inactive  $\theta$ -Fe<sub>3</sub>C phase disappeared, and the active phases (Fe<sub>3</sub>O<sub>4</sub> and Fe<sub>5</sub>C<sub>2</sub>) formed for CO<sub>2</sub> hydrogenation. The introduction of NC to the surface of the Fe catalysts significantly boosted the catalyst activity, selectivity toward light olefins, and stability due to the enhanced metal-support-reactant interaction and interfacial charge transfer [35].

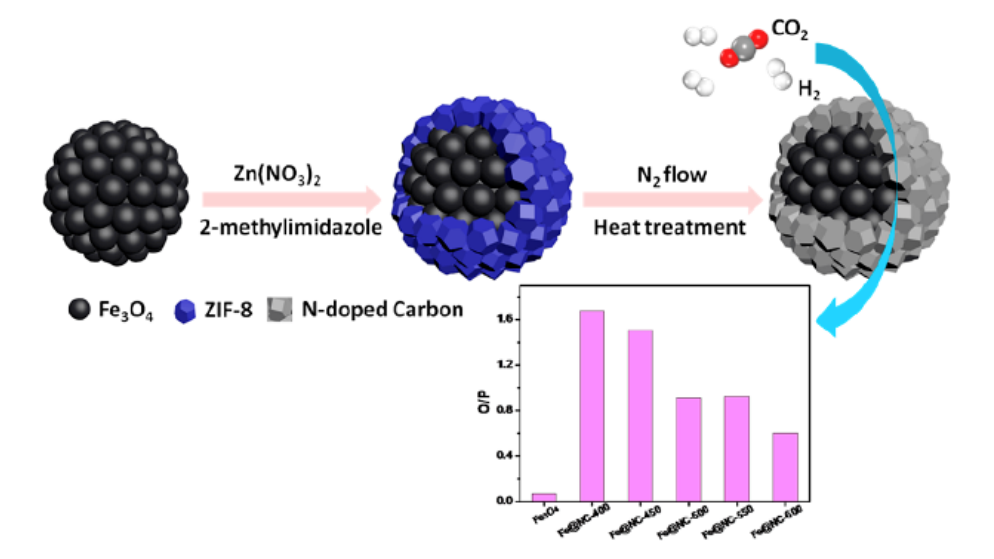


Figure 27. Schematic illustration of formation of Fe@NC catalysts and reaction for CO<sub>2</sub> hydrogenation. Reproduced with permission from [35].

Numpilai et. al studied the hydrogenation of CO<sub>2</sub> to light olefins over the Fe-Co/K-Al<sub>2</sub>O<sub>3</sub> catalysts and discovered that the pore sizes of the Al<sub>2</sub>O<sub>3</sub> support had the profound effects on the Fe<sub>2</sub>O<sub>3</sub> crystallite size, the reducibility, the adsorption-desorption of CO<sub>2</sub> and H<sub>2</sub> and the catalytic performances. The largest pore catalyst (CL-Al<sub>2</sub>O<sub>3</sub>) gave the highest olefins to paraffins ratio of 6.82 due to the suppression of the hydrogenation of olefins to paraffins by increasing the pore sizes of Al<sub>2</sub>O<sub>3</sub> to eliminate diffusion limitation. The maximum light olefins yield of 14.38% is obtained over the catalyst having appropriated Al<sub>2</sub>O<sub>3</sub> pore size (49.7 nm) owing to the suppression of the olefins hydrogenation and chain growth reaction [36].

The electrospun ceramic K/Fe-Al-O nanobelt catalysts synthesized by Elishav et al. showed a superior carbon dioxide conversion of 48%, a C<sub>2</sub>-C<sub>5</sub> olefin selectivity of 52%, and a high olefin/paraffin ratio of 10.4, while the K/Fe-Al-O spinel powder catalyst produced mainly C<sub>6+</sub> hydrocarbons. The enhanced olefin selectivity of the electrospun materials is related to a high degree of reduction of surface iron atoms due to the more efficient interaction with the potassium promoter [128].

A defect-rich MgH<sub>2</sub>/Cu<sub>x</sub>O hydrogen storage composite might inspire the catalysts design for the hydrogenation of CO<sub>2</sub> to lower olefins. Chen et al. reported a defect-rich MgH<sub>2</sub>/Cu<sub>x</sub>O composite catalyst that achieved a C<sub>2</sub>=-C<sub>4</sub>= selectivity of 54.8% and a CO<sub>2</sub> conversion of 20.7% at 623K under a low H<sub>2</sub>/CO<sub>2</sub> ratio of 1:5. It was found that the defective structure of MgH<sub>2</sub>/Cu<sub>x</sub>O could promote CO<sub>2</sub> molecule adsorption and activation, while the electronic structure of MgH<sub>2</sub> was beneficial for offering lattice H<sup>-</sup> for CO<sub>2</sub> molecule hydrogenation. The lattice H<sup>-</sup> could combine the C site of CO<sub>2</sub> molecule to promote the formation of Mg formate, which was further hydrogenated to lower olefins under a low H<sup>-</sup> concentration [129]. The same group reported carbon-confined MgH<sub>2</sub> nano-lamellae storing solid hydrogen for

hydrogenation of CO<sub>2</sub> to lower olefins with a high selectivity under low H<sub>2</sub>/CO<sub>2</sub> ratios. The high selectivity of lower olefins was ascribed to the low concentration of solid hydrogen under low H<sub>2</sub>/CO<sub>2</sub> ratios that suppressed the further hydrogenation of light olefins from Mg formate [132].

SAPO-34 molecular sieves were considered to be the best catalysts due to their excellent structure selectivity, suitable acidity, favorable thermal stability, and hydrothermal stability as well as their high selectivity for light olefins. Tian, *et al.* used Palygorskite as a silicon and partial aluminum source and DEA, TEA, MOR and TEAOH as template agents to prepare SAPO-34 molecular sieves with higher purity. Composite catalysts of CuO-ZnO-Al<sub>2</sub>O<sub>3</sub>/SAPO-34 were prepared by mechanically mixing SAPO-34 molecular sieves with CuO-ZnO-Al<sub>2</sub>O<sub>3</sub> (CZA) and a superb CO<sub>2</sub> conversion of 53.5%, light olefin selectivity of 62.1% and yield of 33.2% was obtained over the CZA/SAPO-34(TEAOH)HCl composite catalyst [130]. CO<sub>2</sub> conversion and product distribution are strongly dependent on the oxide composition and structure. Li *et al.* developed a bifunctional catalyst composed of ZnO-Y<sub>2</sub>O<sub>3</sub> oxide and SAPO-34 zeolite that offered CO<sub>2</sub> conversion of 27.6% and light olefin selectivity of 83.6% [41].

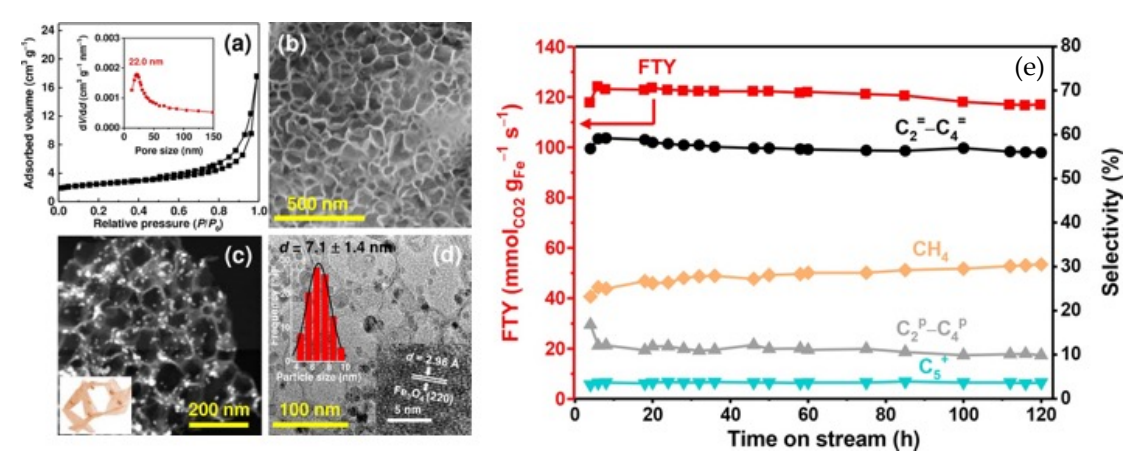


Figure 28. (a)  $N_2$  physisorption isotherms and pore size distribution, (b) SEM image, (c) HAADF-STEM image, and (d) TEM image and particle distribution histogram of the as-prepared FeK1.5/HSG catalyst (Inset in d shows the lattice fringes of the nanoparticle on the catalyst), (e) CO<sub>2</sub> hydrogenation over the FeK1.5/HSG catalyst during 120 h on stream (reaction conditions: 0.15 g catalyst, T = 613 K, P = 20 bar,  $H_2/CO_2 = 3$ , GHSV = 26 Lh<sup>-1</sup>g<sup>-1</sup>). Reproduced with permission from [131].

Some Fe-containing catalysts can also be improved by creating unique architectures. Wei et al. devised iron-based catalysts with honeycomb-structured graphene (HSG) as the support and potassium as the promoter and achieved 59% selectivity of light olefins over FeK<sub>1.5</sub>/HSG catalyst. No obvious deactivation was observed within 120 h on stream (Figure 28). The excellent catalytic performance was attributed to the confinement effect of HSG and the potassium promotion effect on the activation of inert CO<sub>2</sub> and the formation of iron carbide. The unique three-dimensional (3D) architecture of the porous HSG effectively impeded the sintering of the active sites iron carbide nanoparticles (NPs). Meantime, H<sub>2</sub> and CO<sub>2</sub> could more easily infiltrate into the mesoporous-macroporous hierarchical framework of HSG and get access to the active sites, and the generated light olefins could more easily escape from the catalyst so as to avoid over hydrogenation [131].

Consequently, multiple reports indicate that modifying the morphology of zeolite-methanol synthesis composites by creating core-shell configurations can have a beneficial effect [16] [134] [123]. For example, Dual function composite catalysts containing CuZnZr (CZZ) and SAPO-34 were prepared by Chen et .al for the tandem reactions of CO<sub>2</sub> to methanol and methanol to olefins. The assembled core–shell CZZ@SAPO-34 as shown in Figure 29 exhibited enhanced light olefins selectivity of 72% olefins and inhibited CH<sub>4</sub> formation due to reduced contact interface between CZZ and

SAPO-34 and hydrogenation ability on the metal sites. Furthermore, the addition of Zn reduced the acidity of SAPO-34, as a result greatly restrained secondary reactions of the primary olefins (Figure 29) [123].

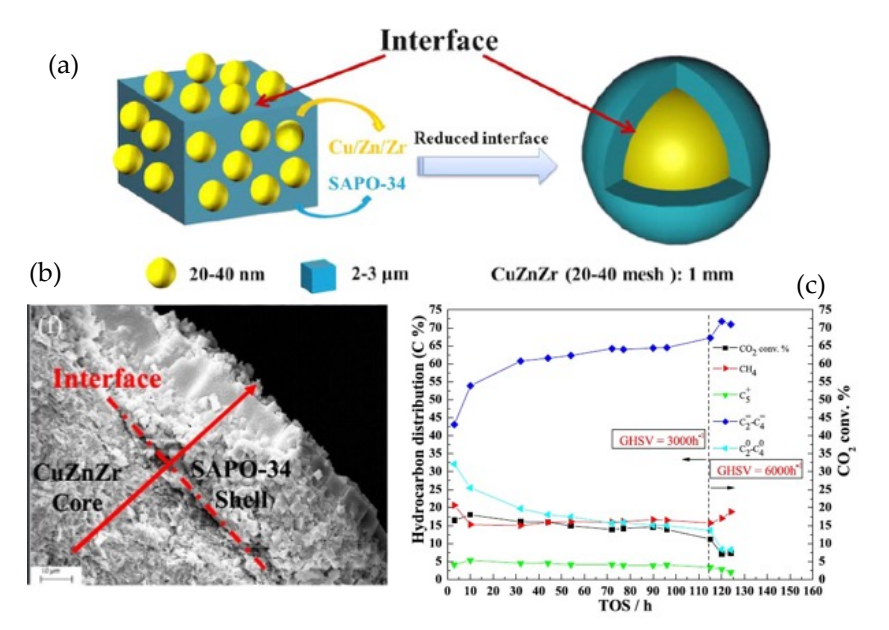


Figure 29. (a) Schematic diagram of the interface between CZZ and SAPO-34. (b) Core-shell interface of CZZ and SAPO-34. (c) Stability of CZZ@Zn-SAPO-34 catalyst with time on stream (reaction conditions:  $H_2/CO_2 = 3$ , 673K). Reproduced with permission from [123].

In summary of this section, the structure and the properties associated with the structure of the catalysts are pivotal towards CO<sub>2</sub> hydrogenation to light olefins. The low surface area of LMO structure could hinder the C<sub>2</sub>H<sub>4</sub> adsorption contributing to higher olefin selectivity. The surface modification of zeolite from hydrophilic to hydrophobic could prevent catalyst deactivation caused by the formation of water. A unique structure of Fe@NC enables phase transformation from inactive (θ-Fe<sub>3</sub>C) phase to active species (Fe<sub>3</sub>O<sub>4</sub> and Fe<sub>5</sub>C<sub>2</sub>). Increase the pore sizes of Al<sub>2</sub>O<sub>3</sub> could eliminate diffusion limitation for CO<sub>2</sub> and H<sub>2</sub>. The electrospun ceramic K/Fe-Al-O nanobelt catalysts led to a high degree of reduction of surface iron atoms. The defective structure of MgH<sub>2</sub>/Cu<sub>x</sub>O and carbon-confined MgH<sub>2</sub>/C nano-lamellae could promote CO<sub>2</sub> adsorption and activation while the electronic structure of MgH<sub>2</sub> offering lattice H-for CO<sub>2</sub> hydrogenation. The 3D architecture of the porous HSG could impede the sintering of the active sites iron carbide NPs. The confinement of core-shell CZZ@SAPO-34 could increase the frequency of methanol intermediate to access to the active zeolite sites so that to improve the light olefine selectivity.

#### 4. Conclusions

There is an urgent need to control CO<sub>2</sub> emission to mitigate its negative impact on the environment. Catalytic conversion of CO<sub>2</sub> is an encouraging approach to mitigate CO<sub>2</sub> emissions by producing chemicals and fuels. A highly promising route is the selective CO<sub>2</sub> hydrogenation to produce light olefins. The huge market demand for the lower olefins offers a great opportunity for the target technology to profoundly impact the scale of CO<sub>2</sub> utilization once it is developed with renewable hydrogen. Currently, there are two primary pathways (CO<sub>2</sub>–FT route and MeOH mediated route) to produce light olefins from CO<sub>2</sub> hydrogenation in a one-step process. In the CO<sub>2</sub>-FT path, Fe is one of the most widely used components, while in the MeOH path, Cu/zeolite has been mostly used. Even though significant efforts have been made, considerable challenges remain in the development of highly efficient catalysts with selective pathways to light olefins due to the thermodynamically stable nature of the CO<sub>2</sub> molecule, the complexity of reaction

networks and catalyst deactivation. During CO<sub>2</sub> hydrogenation, the primary causes for catalyst deactivation are sintering (or agglomeration) of metal particles, phase transformation at the catalyst's surface and catalyst poisoning by water or carbonaceous deposits (i.e., coke). An understanding of the deactivation causes is necessary to develop a mitigation strategy and sustain high selectivity toward desired olefins during CO<sub>2</sub> hydrogenation. In this review, we summarized the reports published within five years on the effect of promotors, metal oxide support, bifunctional composites and structure on the catalyst design to minimize the catalyst deactivation.

*Promoter effect:* Alkali metals such as K and Na have been broadly used as promotors to control the electronic properties. Mn, Ce, Ca metals have been used as structural promotors. Transition metals such as Zn, Co, Cu. V, Zr, etc have been used as both electronic and structural promotors. When modified with alkali promoters, Fe-based catalysts exhibit higher olefin selectivity. The alkali metals perform as electron donors to Fe metal centers, facilitating CO<sub>2</sub> adsorption while lowering their affinity with H<sub>2</sub>, and consequently lead to higher olefins yield. Doping the catalyst with a second metal may promote olefin yields by forming a highly active interface. The second metal components account for tuning the CO<sub>2</sub> and H<sub>2</sub> adsorption and activation, shifting the product distribution towards desired hydrocarbons.

Support effect: Supporting the Fe-based species on supports such as SiO<sub>2</sub>, CeO<sub>2</sub>, m-ZrO<sub>2</sub>,  $\gamma$ -Al<sub>2</sub>O<sub>3</sub>, TiO<sub>2</sub>, ZSM-5, MgO, NbO HPCMs, MOFs, and β-Mo<sub>2</sub>C may enhance the catalytic performance by improving the active metal dispersion and retarding the sintering of the active particles. The surface area, basicity, reducibility, oxygen vacancies, and morphology of the support played important roles, in most cases with the presence of promoters (K, Zr, Cs), in affecting the amount and particle size of the active carbide species, the synergy effect, the metal-support interaction, the strength and capacity of CO, CO<sub>2</sub>, and H<sub>2</sub> adsorption on support, and the surface C/H ratio for CO<sub>2</sub> hydrogenation. By tuning what abovementioned properly, the physically deposited carbon species, coke generation and metal sintering could be mitigated.

Bifunctional composite catalysts effect: The catalysts tested for CO<sub>2</sub> hydrogenation to light olefins via MeOH mediated route mainly involve two active components (metal oxides and zeolite), so called bifunctional composite catalysts. In this review, multiple variations (acidity, particle size, proximity, oxygen vacancy) in combining methanol synthesis catalysts (Cu, Zn, In, Ce, Zr, etc. metal oxides) with various zeolites (SAPO-34 and ZSM5) have been reported for enhanced olefin selectivity and catalyst stability by mitigating coke formation, reducing particle size growth of active carbide species, and inhibiting inactive species formation for CO<sub>2</sub> hydrogenation to light olefins.

Structure effect: The structure of the catalysts plays a pivotal role towards CO<sub>2</sub> hydrogenation to light olefins. The structures and properties (for example, LMO, surface modification of zeolite from hydrophilic to hydrophobic, Fe@NC, pore sizes of Al<sub>2</sub>O<sub>3</sub>, defective structure of MgH<sub>2</sub>/Cu<sub>x</sub>O and carbon-confined MgH<sub>2</sub>/C nano-lamellae, 3D architecture of the porous HSG, core-shell CZZ@SAPO-34) could be tuned to mitigate catalyst deactivation by retarding sintering of active species and coke deposition, tolerating water formation and enabling favorable phase transformation for enhanced light olefins yield and catalyst stability.

Despite the many advances made in catalytic development, especially with light olefins yield and stability, a novel catalytic system that is both economically viable and resistant to deactivation has not yet been achieved. Most research efforts have focused on the development of catalytic materials and adjustment of properties and metal interactions for the desired catalyst activity and long-term stability. Future research directions for CO<sub>2</sub> hydrogenation should consider:

1) to regulate the catalyst surface H/C ratio and facilitate C-C coupling; 2) to tune the support basicity and oxygen vacancies to facilitate the CO<sub>2</sub> adsorption and activation; 3) to explore more novel catalytic materials/structures and improve the catalyst stability, and 4) to explore more low-temperature and energy-saving catalysts for CO<sub>2</sub> hydrogenation. In addition, in situ measurements using synchrotron-based techniques, such as x-ray adsorption

954

955

956

957

958

960

961 962

963

964

spectroscopy (XAS), should be performed to understand how the local environment of the catalysts affects activity and stability and efficient mitigation.

**Author Contributions:** Conceptualization, C.Z.; writing-original draft, C.Z., N.R., T.H., D.W., M.W., C.M. A.Z., N.F.; writing-review and editing, C.Z. and N.R.; funding acquisition, C.Z.; re-sources, C.Z.; supervision, C.Z. All authors have read and agreed to the published version of the manuscript.

Funding: This work was supported by the National Science Foundation under Grant No. 1955521.

**Acknowledgement:** The authors are grateful for the U.S. Department of Energy, Office of Science, Office of Workforce Development for Teachers and Scientists (WDTS) under the Science Undergraduate Laboratory Internships Program (SULI) and Visiting Faculty Program (VFP).

Conflicts of Interest: The authors declare no conflict of interest.

## Abbreviations and Symbols

FTS Fisch-Tropsch Synthesis

MeOH methanol

RWGS reverse water-gas shift MTO MeOH-to-olefins

ASF Anderson-Schulz-Flory

CTO CO<sub>2</sub> to olefins

XRD x-ray powder diffraction

PFR plug-flow

CSTR fully back-mixed reactors

TPSR temperature programed surface reaction

XPS x-ray photoelectron spectroscopy
SEM scanning electron microscopy
TEM transmission electron microscopy

HAADF-STEM high-angle annular dark-field- scanning transmission electron microscopy

O/P ratio olefins/paraffin ratio

NPs nanoparticles
CNT carbon nanotubes
FTY Fe time yield
STY space-time yields

HPCMs hierarchical porous carbon monoliths

LMO layered metal oxides
MOF Metal organic framework

References

- [1] Zhang, X.; Zhang, A.; Jiang, X.; Zhu, J.; Liu, J.; Li, J.; Zhang, G.; Song, C.; Guo, X. Utilization of CO<sub>2</sub> for aromatics production over ZnO/ZrO<sub>2</sub>-ZSM-5 tandem catalyst. *J. CO<sub>2</sub> Util.* **2019**, 29, 140 45.
- [2] Center for Climate and Energy Solutions. Available Online: https://www.c2es.org/content/heat-waves-and-climate-change.

- [3] Monastersky, R. Global carbon dioxide levels near worrisome milestone. *Nature* **2013**, 497, 13 4.
- [4] Igor, A.; da Silva, I.; Mota, C. Conversion of CO<sub>2</sub> to light olefins over iron-based catalysts supported on niobium oxide. *Front. Energy Res.* **2019**, *7*, 49.
- [5] Keith, D.; Holmes, G.; St. Angelo, D.; Heidel, K. A process for capturing CO<sub>2</sub> from the atmosphere. *Joule* 2018, 2, 1573–1594.
- [6] Centi, G.; Quadrelli, E.A.; Perathoner, S. Catalysis for CO<sub>2</sub> conversion: a key technology for rapid introduction of renewable energy in the value chain of chemical industries. *Energy Environ. Sci.* **2013**, *6*, 1711.
- [7] Dutta, A.; Farooq, S.; Karimi, I.A.; Khan, S.A. Assessing the potential of CO<sub>2</sub> utilization with an integrated framework for producing power and chemicals. *J. CO<sub>2</sub> Util.* **2017**, *19*, 49–57.
- [8] Ma, Z.; Porosoff, M. Development of tandem catalysts for CO<sub>2</sub> hydrogenation to olefins. ACS Catal. 2019, 9, 2639–2656.
- [9] Science Daily. Available Online: https://www.sciencedaily.com/releases/2018/11/181108130533.htm.
- [10] Galvis, H.M.T.; de Jong, K.P. Catalysts for production of lower olefins from synthesis gas: A review. ACS Catal. 2013, 3, 2130–2149.
- [11] Wei, J.; Yao, R.W.; Ge, Q.J.; Wen, Z.Y.; Ji, X.W.; Fang, C.Y.; Zhang, J.X.; Xu, H.Y.; Sun, J. Catalytic hydrogenation of CO<sub>2</sub> to isoparaffins over Fe-based multifunctional catalysts. *ACS Catal.* **2018**, *8*, 9958–9967.
- [12] Wei, J.; Ge, Q.J.; Y.R.W.; Wen, Z.Y.; Fang, C.Y.; G. L. S.; Xu, H.Y.; Sun, J. Directly converting CO₂ into a gasoline fuel. *Nat. Commun.* 2018, 8, 15174.
- [13] Li, Z.L.; Wang, J.J.; Q. Y. Z.; Liu, H.L.; Tang, C.Z.; Miao, S.; Feng, Z.C.; An, H.Y.; Li, C. Highly selective conversion of carbon dioxide to lower olefins. ACS Catal. 2017, 7, 8544–8548.
- [14] Li, Z.L.; Qu, Y.Z.; Wang, J.J.; Liu, H.L.; Li, M.R.; Miao, S.; Li, C. Highly selective conversion of carbon dioxide to aromatics over tandem catalysts. *Joule* **2019**, *3*, 570–583.
- [15] Liu, J.H.; Zhang, A.F.; Jiang, X.; Liu, M.; Zhu, J.; Song C.S.; Guo, X.W. Direct transformation of carbon dioxide to value-added hydrocarbons by physical mixtures of Fe<sub>5</sub>C<sub>2</sub> and K-modified Al<sub>2</sub>O<sub>3</sub>. *Ind. Eng. Chem. Res.* 2018, 57, 9120–9126.
- [16] Xie, C.L.; Chen, C.; Yu, Y.; Su, J.; Li, Y.F.; Somorjai, G.A.; Yang, P.D. Tandem catalysis for CO<sub>2</sub> hydrogenation to C<sub>2</sub>–C<sub>4</sub> hydrocarbons. *Nano Lett.* **2017**, *17*, 3798–3802.
- [17] Liu, M.; Yi, Y.H.; Wang, L.; Guo, H.C.; Bogaerts, A. Hydrogenation of carbon dioxide to value-added chemicals by heterogeneous catalysis and plasma catalysis. *Catalysts* **2019**, *9*, 275.
- [18] Dang, S.S.; Gao, P.; Liu, Z.Y.; Chen, X.Q.; Yang, C.G.; Wang, H.; Zhong, L.S.; Li, S.G.; Sun, Y.H.; Role of zirconium in direct CO<sub>2</sub> hydrogenation to lower olefins on oxide/zeolite bifunctional catalysts. *J. Catal.* 2018, 364, 382–393.
- [19] Gao, P.; Dang, S.S.; Li, S.G.; Bu, X.N.; Liu, Z.Y.; Qiu, M.H.; Yang, C.G.; Wang, H.; Zhong, L.S.; Han, Y.; Liu, Q.; Wei, W.; Sun, Y.H.; Direct production of lower olefins from CO₂ conversion via bifunctional catalysis. *ACS Catal.* **2018**, *8*, 571–578.
- [20] You, Z.Y.; Deng, W.P.; Zhang Q.H.; Wang, Y. Hydrogenation of carbon dioxide to light olefins over non-supported iron catalyst. *Chinese J. Catal.* **2013**, *34*, 956–963.
- [21] Gnanamani, M.K.; Jacobs, G.; Hamdeh, H.H.; Shafer, W.D.; Liu, F.; Hopps, S.D.; Thomas, G.A.; Davis, B.H. Hydrogenation of carbon dioxide over Co–Fe bimetallic catalysts. *ACS Catal.* **2016**, *6*, 913–927.

- [22] Ren, T.; Patel, M.; Blok, K. Olefins from conventional and heavy feedstocks: Energy use in steam cracking and alternative processes. *Energy* **2006**, 31, 4, 425 451.
- [23] Amghizar, I.; Vandewalle, L.A.; Geem, K.M.V.; Marin, G.B. New trends in olefin production. *Engineering* **2017**, 3, 171 78.
- [24] One, O.; Niziolek, A.M.; Floudas, C.A. Optimal production of light olefins from natural gas via the methanol intermediate. *Ind. Eng. Chem. Res.* **2016**, *5511*, 3043 3063.
- [25] Li, W.H.; Wang, H.Z.; Jiang, X.; Zhu, J.; Liu, Z.M.; Guo, X.W.; Song, C.S. A short review of recent advances in CO2 hydrogenation to hydrocarbons over heterogeneous catalysts. *RCS Adv.* **2018**, *8*, 7651.
- [26] Porosoff, M.; Yan, B.; Chen, J. Catalytic reduction of CO<sub>2</sub> by H<sub>2</sub> for synthesis of CO, methanol and hydrocarbons: challenges and opportunities. *Energy Environ. Sci.* **2016**, *9*, 62 3.
- [27] Wang, D.; Xie, Z.; Porosoff, M.D.; Chen, J. Recent advances in carbon dioxide hydrogenation to produce olefins and aromatics. *Chem* **2021**, *7*, 1 35.
- [28] Li, W.; Wang, H.; Jiang, X.; Zhu, J.; Liu, Z.; Guo, X.; Song, C. A short review of recent advances in CO₂ hydrogenation to hydrocarbons over heterogeneous catalysts. RSC Adv. 2018, 8, 7651 [7669.]
- [29] Zhang, C.; Cao, C.; Zhang, Y.; Liu, X.; Xu, J.; Zhu, M.; Tu, W.; Han, Y. Unraveling the role of zinc on bimetallic Fe<sub>5</sub>C<sub>2</sub>–ZnO catalysts for highly selective carbon dioxide hydrogenation to high carbon α-olefins. ACS Catal. 2021, 11, 2121–2133.
- [30] Wei, J.; Sun, J.; Wen, Z.; Fang, C.; Ge, Q.; Xu, H. New insights into the effect of sodium on Fe<sub>3</sub>O<sub>4</sub>- based nanocatalysts for CO<sub>2</sub> hydrogenation to light olefins. *Catal. Sci. Technol.* **2016**, *6*, 4786.
- [31] Wezendonk, T.A.; Sun, X.; Duglan, A.I.; van Hoof, A.J.F.; Hensen, E.J.M.; Kapteijn, F.; Gascon, J. Controlled formation of iron carbides and their performance in Fischer-Tropsch synthesis. *J. Catal.* **2018**, 362, 106–117.
- [32] Chaipraditgul, N.; Numpilai, T.; Cheng, C.K.; Siri-Nguan, N.; Sornchamni, T.; Wattanakit, C.; Limtrakul, J.; Witoon, T. Tuning interaction of surface-adsorbed species over Fe/K-Al<sub>2</sub>O<sub>3</sub> modified with transition metals (Cu, Mn, V, Zn or Co) on light olefins production from CO<sub>2</sub> hydrogenation. Fuel 2021, 283, 119248.
- [33] Gnanamani, M. K.; Jacobs, G.; Hamdeh, H. H.; Shafer, W. D.; Liu, F.; Hopps, S. D.; Thomas, G. A.; Davis, B H. Hydrogenation of carbon dioxide over iron carbide prepared from alkali metal promoted iron oxalate. *Appl. Catal. A: Gen.* 2018, 564, 243–249.
- [34] Guo, L.; Sun, J.; Ge, Q.; Tsubaki, N. Recent advances in direct catalytic hydro-genation of carbon dioxide to valuable C<sub>2</sub>-hydrocarbons. *J. Mater. Chem. A* **2018**, *6*, 23244–23262.
- [35] Liu, J.; Zhang, A.; Jiang, X.; Zhang, G.; Sun, Y.; Liu, M.; Ding, F.; Song, C.; Guo, X. Overcoating the surface of Fe-based catalyst with ZnO and nitrogen-doped carbon toward high selectivity of light olefins in CO<sub>2</sub> Hydrogenation. *Ind. Eng. Chem. Res.* **2019**, *58*, 4017 4023.
- [36] Numpilai, T.; Chanel, N.; Poo-Arporn, Y.; Cheng, C.; Siri-Nguan, N.; Sornchamni, T.; Chareonpanich, M.; Kongkachuichay, P.; Yigit, N.; Rupprechter, G.; Limtrakul, J.; Witoon, T. Pore size effects on physicochemical properties of Fe-Co/K-Al<sub>2</sub>O<sub>3</sub> catalysts and their catalytic activity in CO<sub>2</sub> hydrogenation to light olefins. *Appl. Surf. Sci.* 2019, 483, 581 392.
- [37] Numpilai, T.; Cheng, C.K.; Limtrakul, J.; Witoon, T. Recent advances in light olefins production from catalytic hydrogenation of carbon dioxide. *Proc. Saf. Environ. Prot.* 2021, 151, 401–427.

- [38] Yang, H.; Zhang, C.; Gao, P.; Wang, H.; Li, X.; Zhong, L.; Wei, W.; Sun, Y. A review of the catalytic hydrogenation of carbon dioxide into value-added hydrocarbons. *Catal. Sci. Technol.* **2017**, *7*, 4580.
- [39] Dang, S.; Gao, P.; Liu, Z.; Chen, X.; Yang, C.; Wang, H.; Zhong, L.; Li, S.; Sun, Y. Role of zirconium in direct CO<sub>2</sub> hydrogenation to lower olefins on oxide/zeolite bifunctional catalysts. *J. Catal.* **2018**, 364, 382 393.
- [40] Jiao, F.; Li, J.; Pan, X.; Xiao, J.; Li, H.; Ma, H.; Wei, M.; Pan, Y.; Zhou, Z.; Li, M.; Miao, S.; Li, J.; Zhu, Y.; Xiao, D.; He, T.; Yang, J.; Qi, F.; Fu, Q.; Bao, X. Selective conversion of syngas to light olefins. Science 2016, 351, 1065–1068.
- [41] Li, J.; Yu, T.; Miao, D.; Pan, X.; Bao, X. Carbon dioxide hydrogenation to light olefins over ZnO/Y<sub>2</sub>O<sub>3</sub> and SAPO-34 bifunctional catalysts. *Catal. Commun.* **2019**, *129*, 105711.
- [42] Liu, X.; Wang, M.; Zhou, C.; Zhou, W.; Cheng, K.; Kang, J.; Zhang, Q.; Deng, W.; Wang, Y. Selective transformation of carbon dioxide into lower olefins with a bifunctional catalyst composed of ZnGa<sub>2</sub>O<sub>4</sub> and SAPO-34. *Chem. Commun.* **2018**, *54*, 140–143.
- [43] Dang, S.; Li, S.; Yang, C.; Chen, X.; Li, X.; Zhong, L.; Gao, P.; Sun, Y. Selective transformation of CO₂ and H₂ into lower olefins over In₂O₃-ZnZrOx/SAPO-34 bifunctional catalysts. *ChemSusChem* **2019**, 12, 3582☐3591.
- [44] Gao, J.; Jia, C.; Liu, B. Direct and selective hydrogenation of CO<sub>2</sub> to ethylene and propene by bifunctional catalysts. *Catal. Sci. Technol.* **2017**, *7*, 5602 607.
- [45] Li, Z.; Wang, J.; Qu, Y.; Liu, H.; Tang, C.; Miao, S.; Feng, Z.; An, H.; Li, C. Highly selective conversion of carbon dioxide to lower olefins. *ACS Catal.* **2017**, *7*, 8544[\$548.
- [46] Tan, L.; Zhang, P.; Cui, Y.; Suzuki, Y.; Li, H.; Guo, L.; Yang, G.; Tsubaki, N. Direct CO<sub>2</sub> hydrogenation to light olefins by suppressing CO by-product formation. *Fuel Process. Technol.* **2019**, *196*, 106174 06178.
- [47] Porosoff, M.D.; Kattel, S.; Li, W.; Liu, P.; Chen, J.G. Identifying trends and descriptors for selective CO<sub>2</sub> conversion to CO over transition metal carbides. *Chem. Commun.* 2015, 51, 6988 6991.
- [48] Porosoff, M.D.; Chen, J.G. Trends in the catalytic reduction of CO<sub>2</sub> by hydrogen over supported monometallic and bimetallic catalysts. *J. Catal.* **2013**, 301, 30[37.
- [49] Butt, J.B.; Petersen, E. Activation, deactivation and poisoning of catalysts; Academic Press: 1988.
- [50] Bartholomew, C. Mechanisms of catalyst deactivation. *Appl. Catal. A: Gen.* **2001**, 212, 17**6**0.
- [51] Moulijn, J.A.; van Diepen, A.E.; Kapteijn, F. Catalyst deactivation: is it predictable?: What to do? *Appl. Catal. A: Gen.* **2001**, 212, 3 6.
- [52] Kliewer, C.E.; Soled, S.L.; Kiss, G. Morphological transformations during Fischer-Tropsch synthesis on a titania-supported cobalt catalyst. *Catal. Today* **2019**, 323, 233 **2**56.
- [53] Eschemann, T.O.; de Jong, K.P. Deactivation behavior of Co/TiO<sub>2</sub> catalysts during Fischer–Tropsch synthesis. ACS Catal. 2015, 5, 3181–3188.
- [54] Sun, J.T.; Metcalfe, I.S.; Sahibzada, M. Deactivation of Cu/ZnO/Al<sub>2</sub>O<sub>3</sub> methanol synthesis catalyst by sintering, Ind. Eng. Chem. Res. 1999, 38, 3868 3872.
- [55] Price, C.A.H.; Reina, T.R.; Liu, J. Engineering heterogenous catalysts for chemical CO<sub>2</sub> utilization: Lessons from thermal catalysis and advantages of yolk@shell structured nanoreactors. *J. Energy Chem.* **2021**, *57*, 304[324.
- [56] Argyle, M.; Bartholomew, C. Heterogeneous catalyst deactivation and regeneration: A review. *Catalyst* **2015**, *5*, 145–269.
- [57] Hansen, T.W.; Delariva, A.T.; Challa, S.R.; Datye, A.K. Sintering of catalytic nanoparticles: particle migration or Ostwald ripening. *Acc. Chem. Res.* **2013**, *46*, 1720**7**30.

- [58] Li, W.; Zhang, G.; Jiang, X.; Liu, Y.; Zhu, J.; Ding, F.; Liu, Z.; Guo, X.; Song, C. CO<sub>2</sub> hydrogenation on unpromoted and M-promoted Co/TiO<sub>2</sub> catalysts (M = Zr, K, Cs): Effects of crystal phase of supports and metal–support interaction on tuning product distribution. *ACS Catal.* **2019**, *9*, 2739 **27**51.
- [59] Lee, S.-C.; Kim, J.-S.; Shin, W.C.; Choi, M.-J.; Choung, S.-J. Catalyst deactivation during hydrogenation of carbon dioxide: Effect of catalyst position in the packed bed reactor. *J. Mol. Catal. A: Chem.* **2009**, *301*, 98**1**05.
- [60] Riedel, T.; Schulz, H.; Schaub, G.; Jun, K.W.; Hwang, J.S.; Lee, K.W. Fischer–Tropsch on iron with H<sub>2</sub>-CO and H<sub>2</sub>-CO<sub>2</sub> as synthesis gases: the episodes of formation of the Fischer–Tropsch regime and construction of the catalyst. *Top. Catal.* **2003**, *26*, 41–54.
- [61] Wang, W.; Wang, S.P.; Ma, X.B.; Gong, J.L. Recent advances in catalytic hydrogenation of carbon dioxide. *Chem. Soc. Rev.* **2011**, 40, 3703–3727.
- [62] Zhang, Y.; Cao, C.; Zhang, C.; Zhang, Z.; Liu, X.; Yng, Z.; Zhu, M.; Meng, B.; Jing, X.; Han, Y.-F. The study of structure-performance relationship of iron catalyst during a full life cycle for CO<sub>2</sub> hydrogenation. *J. Catal.* **2019**, 378, 51 62.
- [63] Fiato, R.A.; Rice, G.W.; Miseo, S.; Soled, S.L. Laser produced iron carbide-based catalysts. US Patent 4,687,753, filed 25 Oct 1985 and issued 8 Aug 1987.
- [64] Hegedus, L.L.; McCabe, R.W. Catalyst poisoning. In Catalyst Deactivation 1980 (Studies in Surface Science and Catalysis); Delmon, B., Froment, G.F., Eds.; Elsevier: Amsterdam, The Netherlands, 1980; Volume 6, pp. 471 505.
- [65] Bartholomew, C.H. Mechanisms of nickel catalyst poisoning. In *Catalyst Deactivation 1987 (Studies in Surface Science and Catalysis)*; Delmon, B., Froment, G.F., Eds.; Elsevier: Amsterdam, The Netherlands, 1987; Volume 34, pp. 81 104.
- [66] Schühle, P.; Schmidt, M.; Schill, L.; Rilsager, A.; Wasserscheid, P.; Albert, J. Influence of gas impurities on the hydrogenation of CO<sub>2</sub> to methanol using indium-based catalysts. *Catal. Sci. Technol.* **2020**, *10*, 7309 322.
- [67] Szailer, T.; Novák, É.; Oszkó, A.; Erdőhelyi, A. Effect of H<sub>2</sub>S on the hydrogenation of carbon dioxide over supported Rh catalysts. *Top. Catal.* **2007**, *46*, 79 **8**6.
- [68] Rytter, E.; Holmen, A. Perspectives on the effect of water in cobalt Fischer–Tropsch synthesis. *ACS Catal.* **2017**, 7, 5321 328.
- [69] Wu, J.; Luo, S.; Toyir, J.; Saito, M.; Takeuchi, M.; Watanabe, T. Optimization of preparation conditions and improvement of stability of Cu/ZnO-based multicomponent catalysts for methanol synthesis from CO<sub>2</sub> and H<sub>2</sub>. Catal. Today, 1998, 45, 215 20.
- [70] Wu, J.; Saito, M.; Takeuchi, M.; Watanabe, T. The stability of Cu/ZnO-based catalysts in methanol synthesis from a CO<sub>2</sub>-rich feed and from a CO-rich feed, *Appl. Catal. A.* **2001**, 218, 235 **2**40.
- [71] Huber, G.W.; Guymon, C.G.; Conrad, T.L.; Stephenson, B.C.; Bartholomew, C.H. Hydrothermal stability of Co/SiO<sub>2</sub> Fischer-Tropsch Synthesis Catalysts. *Stud. Surf. Sci. Catal.* **2001**, *139*, 423 429.
- [72] van Steen, E.; Claeys, M.; Dry, M.E.; van de Loosdrecht, J.; Viljoen, E.L.; Visagie, J.L. Stability of nanocrystals: thermodynamic analysis of oxidation and re-reduction of cobalt in water/hydrogen mixtures. *J. Phys. Chem. B* **2005**, *109*, 3575 3577.
- [73] Iglesia, E. Design, synthesis, and use of cobalt-based Fischer-Tropsch synthesis catalysts. *Appl. Catal. A: Gen.* 1997, 161, 59 78.

- [74] Zhang, L.; Chen, K.; Chen, B.; White, J.L.; Resasco, D.E. Factors that determine zeolite stability in hot liquid water. *J. Am. Chem. Soc.* **2015**, 137, 11810 1819.
- [75] Rostrup-Neilson, J.; Trimm, D.L. Mechanisms of carbon formation on nickel-containing catalysts. *J. Catal.* **1977**, 48, 155 165.
- [76] Trimm, D.L. The formation and removal of coke from nickel catalyst. Catal. Rev. Sci. Eng. 1977, 16, 155 89.
- [77] Trimm, D.L. Catalyst design for reduced coking (review). Appl. Catal. 1983, 5, 263–290.
- [78] Bartholomew, C.H. Carbon deposition in steam reforming and methanation. *Catal. Rev. Sci. Eng.* **1982**, 24, 67 12.
- [79] Albright, L.F.; Baker, R.T.K. Eds. Coke Formation on Metal Surfaces, ACS Symposium Series; American Chemical Society: Washington, DC, USA, 1982, Volume 202: pp. 1 200.
- [80] Menon, P.G. Coke on catalysts-harmful, harmless, invisible and beneficial types. J. Mol. Catal. 1990, 59, 207 220.
- [81] Chen, D.; Moljord, K.; Holmen, A. Methanol to olefins: Coke formation and deactivation. In *Deactivation and Regeneration of Zeolite Catalysts*; Guisnet, M., Ribeiro, F., Eds.; Imperial College Press: London, UK, 2011, Volume 9, pp. 269 292.
- [82] Chen, D.; Rebo, H.P., Grønvold, A.; Moljord, K.; Holmen, A. Methanol conversion to light olefins over SAPO-34: kinetic modeling of coke formation. *Micropor. Mesopor. Mat.* **2000**, 35 [36, 121 ]35.
- [83] Chen, D.; Moljord, K.; Fuglerud, T.; Holmen, A. The effect of crystal size of SAPO-34 on the selectivity and deactivation of the MTO reaction. *Micropor. Mesopor. Mat.* **1999**, 29, 191–203.
- [84] Nishiyama, N.; Kawaguchi, M.; Hirota, Y.; Van Vu, D.; Egashira, Y.; Ueyama, K. Size control of SAPO-34 crystals and their catalyst lifetime in the methanol-to-olefin reaction. Appl. Catal. A: Gen. 2009, 362, 193 99.
- [85] Müller, S.; Liu, Y.; Vishnuvarthan, M.; Sun, X.; van Veen, A.C.; Haller, G.L.; Sanchez-Sanchez, M.; Lercher, J.A. Coke formation and deactivation pathways on H-ZSM-5 in the conversion of methanol to olefins. *J. Catal.* **2015**, 325, 48 39.
- [86] Zhou, J.; Gao, M.; Zhang, J.; Liu, W.; Zhang, T.; Li, H.; Xu, Z.; Ye, M.; Liu, Z. Directed transforming of coke to active intermediates in methanol-to-olefins catalyst to boost light olefins selectivity. *Nat. Commun.* **2021**, *12*, 17.
- [87] Yang, M.; Tian, P.; Wang, C.; Yuan, Y.; Yang, Y.; Xu, S.; He, Y.; Liu, Z. A top-down approach to prepare silicoaluminophosphate molecular sieve nanocrystals with improved catalytic activity. *Chem. Commun.* **2014**, 50, 1845 847.
- [88] Xi, D.; Sun, Q.; Chen, X.; Wang, N.; Yu, J. The recyclable synthesis of hierarchical zeolite SAPO-34 with excellent MTO catalytic performance. *Chem. Commun.* **2015**, *51*.
- [89] Guo, G.; Sun, Q.; Wang, N.; Bai, R.; Yu, J. Cost-effective synthesis of hierarchical SAPO-34 zeolites with abundant intracrystalline mesopores and excellent MTO performance. *Chem. Commun.* **2018**, *54*, 3697 3700.
- [90] Jiang, J.; Wen, C.; Tian, Z.; Wang, Y.; Zhai, Y.; Chen, L.; Li, Y.; Liu, Q.; Wang, C.; Ma, L. Manganese-promoted Fe<sub>3</sub>O<sub>4</sub> microsphere for efficient conversion of CO<sub>2</sub> to light olefins. *Ind. Eng. Chem. Res.* **2020**, *59*, 2155 2162.
- [91] Witoon, T.; Chaipraditgul, N.; Numpilai, T.; Lapkeatseree, V.; Ayodele, B.; Cheng, C.; Siri-Nguan, N.; Sornchamni, T., Limtrakul, J. Highly active Fe-Co-Zn/K-Al<sub>2</sub>O<sub>3</sub> catalysts for CO<sub>2</sub> hydrogenation to light olefins. Chem. Eng. Sci. 2021, 233, 116428.
- [92] Zhang, Z.; Yin, H.; Yu, G.; He, S.; Kang, J.; Liu, Z.; Cheng, K.; Zhang, Q.; Wang, Y. Selective hydrogenation of CO<sub>2</sub> and CO into olefins over sodium- and zinc-promoted iron carbide catalysts. *J. Catal.* **2021**, *395*, 350 **3**61.

- [93] Yuan, F.; Zhang, G.; Zhu, J.; Ding, F.; Zhang, A.; Song, C.; Guo, X. Boosting light olefin selectivity in CO<sub>2</sub> hydrogenation by adding Co to Fe catalysts within close proximity. *Catal. Today* **2021**, *371*, 142 49.
- [94] Wei, C.; Tu, W.; Jia, L.; Liu, Y.; Lian, H.; Wang, P.; Zhang, Z. The evolutions of carbon and iron species modified by Na and their tuning effect on the hydrogenation of CO<sub>2</sub> to olefins. *Appl. Surf. Sci.* **2020**, 525, 146622.
- [95] Gong, W.; Ye, R.-P.; Ding, J.; Wang, T.; Shi, X.; Russell, C.K.; Tang, J.; Eddings, E.G.; Zhang, Y.; Fan, M. Effect of copper on highly effective Fe-Mn based catalysts during production of light olefins via Fischer-Tropsch process with low CO<sub>2</sub> emission. *Appl. Catal.* **2020**, *278*, 119302.
- [96] Malhi, H.S.; Sun, C.; Zhang, Z.; Liu, Y.; Liu, W.; Ren, P.; Tu, W.; Han, Y.-F. Catalytic consequences of the decoration of sodium and zinc atoms during CO<sub>2</sub> hydrogenation to olefins over iron-based catalyst. *Catal. Today* **2021**, *in press*.
- [97] Han, Y.; Fang, C.; Ji, X.; Wei, J.; Ge, Q.; Sun, J. Interfacing with carbonaceous potassium promoters boosts catalytic CO<sub>2</sub> hydrogenation of iron. ACS Catal. 2020, 10, 12098 2108.
- [98] Liang, B.; Sun, T.; Ma, J.; Duan, H.; Li, L.; Yang, X.; Zhang, Y.; Su, X.; Huang, Y.; Zhang, T. Mn decorated Na/Fe catalysts for CO₂ hydrogenation to light olefins. *Catal. Sci. Technol.* **2019**, *9*, 456 46.
- [99] Yang, S.; Chun, H.; Lee, S.; Han, S.J.; Lee, K.; Kim, Y.T. Comparative study of olefin production from CO and CO<sub>2</sub> Using Na-and K-promoted zinc ferrite. *ACS Catal.* **2020**, *10*, 10742 0759.
- [100] Guo, L.; Sun, J.; Ji, X.; Wei, J.; Wen, Z.; Yao, R.; Xu, H.; Ge, Q. Directly converting carbon dioxide to linear  $\alpha$ -olefins on bio-promoted catalysts. *Commun. Chem.* **2018**, *1*, 11.
- [101] Liang, B.; Duan, H.; Sun, T.; Ma, T.; Liu, X.; Xu, J.; Su, X.; Huang, Y.; Zhang, T. Effect of Na promoter on Febased catalyst for CO<sub>2</sub> hydrogenation to alkenes. *ACS Sustain. Chem. Eng.* **2019**, 7, 925 32.
- [102] Ramirez, A.; Gevers, L.; Bavykina, A.; Ould-Chikh, S.; Gascon, J. Metal organic framework-derived iron catalysts for the direct hydrogenation of CO<sub>2</sub> to short chain olefins. *ACS Catal.* **2018**, *8*, 9174 182.
- [103] Zhang, J.; Su, X.; Wang, X.; Ma, Q.; Fan, S.; Zhao, T. Promotion effects of Ce added Fe–Zr–K on CO<sub>2</sub> hydrogenation to light olefins. *Reac. Kinet. Mech. Cat.* **2018**, 124, 575 **3**85,.
- [104] Numpilai, T.; Chanlek, N.; Poo-Arporn, Y.; Cheng, C.K.; Siri-Nguan, N.; Sornchamni, T.; Chareonpanich, M.; Kongkachuichay, P.; Yigit, N.; Rupprechter, G.; Limtrakul, J.; Witoon, T. Tuning interactions of surface-adsorbed species over Fe-Co/K-Al₂O₃ catalyst by different K content: selective CO₂ hydrogenation to light olefins. ChemCatChem 2020, 12, 3306 3320.
- [105] Wang, W.; Jiang, X.; Wang, X.; Song, C. Fe-Cu bimetallic catalysts for selective CO<sub>2</sub> hydrogenation to olefin-rich C<sub>2+</sub> hydrocarbons. *Ind. Eng. Chem. Res.* **2018**, *57*, 4535 4542.
- [106] Kim, K.Y.; Lee, H.; Noh, W.Y.; Shin, J.; Han, S.J.; Kim, S.K.; An, K.; Lee, J.S. Cobalt ferrite nanoparticles to form a catalytic Co–Fe alloy carbide phase for selective CO<sub>2</sub> hydrogenation to light olefins. ACS Catal. 2020, 10, 8660 8671.
- [107] Boreriboon, N.; Jiang, X.; Song, C.; Prasassarakich, P. Fe-based bimetallic catalysts supported on TiO<sub>2</sub> for selective CO<sub>2</sub> hydrogenation to hydrocarbons, *J. CO<sub>2</sub> Util.* **2018**, 25, 330 37.
- [108] Xu, Q.; Xu, X.; Fan, G.; Yang, L.; Li, F. Unveiling the roles of Fe-Co interactions over ternary spinel-type ZnCo<sub>x</sub>Fe<sub>2-x</sub>O<sub>4</sub> catalysts for highly efficient CO<sub>2</sub> hydrogenation to produce light olefins. J. Catal. 2021, 400, 355□366.

- [109] Numpilai, T.; Witoon, T.; Chanlek, N.; Limphirat, W.; Bonura, G.; Chareonpanich, M.; Limtrakul, J. Structure–activity relationships of Fe-Co/K-Al<sub>2</sub>O<sub>3</sub> catalysts calcined at different temperatures for CO<sub>2</sub> hydrogenation to light olefins. Appl. Catal. A: Gen. 2017, 547, 219 229.
- [110] Rodemerck, U.; Holena, M.; Wagner, E.; Smejkal, Q.; Barkschat, A.; Baerns, M. Catalyst development for CO<sub>2</sub> hydrogenation to fuels. *ChemCatChem* **2013**, *5*, 1948 955.
- [111] Dai, C.; Zhang, A.; Liu, M.; Song, F.; Song, C.; Guo, X. Facile one-step synthesis of hierarchical porous carbon monoliths as superior supports of Fe-based catalysts for CO<sub>2</sub> hydrogenation. *RSC Adv.* **2016**, *6*, 10831–10836.
- [112] Hu, S.; Liu, M.; Ding, F.; Song, C.; Zhang, G.; Guo, X. Hydrothermally stable MOFs for CO<sub>2</sub> hydrogenation over iron-based catalyst to light olefins. *J. CO*<sub>2</sub> *Util.* **2016**, *15*, 89 5.
- [113] Raghav, H.; Siva Kumar Konathala, L.N.; Mishra, N.; Joshi, B.; Goyal, R.; Agrawal, A.; Sarkar, B. Fe-decorated hierarchical molybdenum carbide for direct conversion of CO<sub>2</sub> into ethylene: Tailoring activity and stability. *J. CO*<sub>2</sub> *Util.* **2021**, *50*, 101607.
- [114] da Silva, I.A.; Mota, C.J.A. Conversion of CO<sub>2</sub> to light olefins over iron-based catalysts supported on niobium oxide. *Front. Energy Res.* **2019**, *7*, 49.
- [115] Huang, J.; Jiang, S.; Wang, M.; Wang, X.; Gao, J.; Song, C. Dynamic evolution of Fe and carbon species over different ZrO<sub>2</sub> supports during CO prereduction and their effects on CO<sub>2</sub> hydrogenation to light olefins," ACS Sustain. Chem. Eng. 2021, 9, 7891 7903.
- [116] Torrente-Murciano, L.; Chapman, R.S.L.; Narvaez-Dinamarca, A.; Mattia, D.; Jones, M.D. Effect of nanostructured ceria as support for the iron catalysed hydrogenation of CO<sub>2</sub> into hydrocarbons. *Phys. Chem. Phys.* **2016**, *18*, 15496 5500.
- [117] Gu, H.; Ding, J.; Zhong, Q.; Zeng, Y.; Song, F. Promotion of surface oxygen vacancies on the light olefins synthesis from catalytic CO<sub>2</sub> hydrogenation over Fe–K/ZrO<sub>2</sub> catalysts. *Int. J. Hydrog. Energy* **2019**, 44, 11808 1816.
- [118] Owen, R.E.; Pluckinski, P.; Mattia, D.; Torrente-Murciano, L.; Ting, V.; Jones, M.D. Effect of support of Co-Na-Mo catalysts on the direct conversion of CO<sub>2</sub> to hydrocarbons, *J. CO<sub>2</sub> Util.* **2016**, *16*, 97 3.
- [119] Wang, P.; Zha, F.; Yao, L.; Chang, Y. Synthesis of light olefins from CO<sub>2</sub> hydrogenation over (CuO-ZnO)-kaolin/SAPO-34 molecular sieves. *Appl. Clay Sci.* **2018**, *163*, 249 256.
- [120] Wang, S.; Zhang, L.; Zhang, W.; Wang, P.; Qin, Z.; Yan, W.; Dong, M.; Li, J.; Wang, J.; He, L.; Olsbye, U.; Fan, W.; Selective conversion of CO<sub>2</sub> into propene and butene. Chem. 2020, 6, 3344 363.
- [121] Li, W.; Wang, K.; Zhan, G.; Huang, J.; Li, Q. Design and synthesis of bioinspired ZnZrOx & bio-ZSM-5 integrated nanocatalysts to boost CO<sub>2</sub> hydrogenation to light olefins. *ACS Sustain. Chem. Eng.* **2021**, *9*, 6446–6458.
- [122] Wang, S.; Wang, P.; Qin, Z.; Yan, W.; Dong, M.; Li, J.; Wang, J.; Fan, W. Enhancement of light olefin production in CO<sub>2</sub> hydrogenation over In<sub>2</sub>O<sub>3</sub>-based oxide and SAPO-34 composite. *J. Catal.* **2020**, *391*, 459–470.
- [123] Chen, J.; Wang, X.; Wu, D.; Zhang, J.; Ma, Q.; Gao, X.; Lai, X.; Xia, H.; Fan, S.; Zhao, T. Hydrogenation of CO<sub>2</sub> to light olefins on CuZnZr@(Zn-)SAPO-34 catalysts: Strategy for product distribution. *Fuel* **2019**, 239, 44 32.
- [124] Liu, X.; Wang, M.; Yin, H.; Hu, J.; Cheng, K.; Kang, J.; Zhang, Q.; Wang, Y. Tandem catalysis for hydrogenation of CO and CO<sub>2</sub> to lower olefins with bifunctional catalysts composed of spinel oxide and SAPO-34. *ACS Catal.* **2020**, *10*, 8303 [3314.

- [125] Tong, M.; Chizema, L.G.; Chang, X.; Hondo, E.; Dai, L.; Zeng, Y.; Zeng, C.; Ahmad, H.; Yang, R.; Lu, P. Tandem catalysis over tailored ZnO-ZrO<sub>2</sub>/MnSAPO-34 composite catalyst for enhanced light olefins selectivity in CO<sub>2</sub> hydrogenation. *Micropor. Mesopor. Mater.* 2021, 320, 111105.
- [126] Gao, P.; Dang, S.; Li, S.; Bu, X.; Liu, Z.; Qiu, M.; Yang, C.; Wang, H.; Zhong, L.; Han, Y.; Liu, Q.; Wei, W.; Sun, Y. Direct production of lower olefins from CO<sub>2</sub> conversion via bifunctional catalysis. ACS Catal. 2018, 8, 571 378.
- [127] Wang, X.; Wu, D.; Zhang, J.; Gao, X.; Ma, Q.; Fan, S.; Zhao, T. Highly selective conversion of CO₂ to light olefins via Fischer-Tropsch synthesis over stable layered K–Fe–Ti catalysts. *Appl. Catal. A: Gen.* **2019**, *573*, 32 40.
- [128] Elishav, O.; Shener, Y.; Beilin, V.; Langau, M.V.; Herskowitz, M.; Shter, G.E.; Grader, G.S. Electrospun Fe–Al–O nanobelts for selective CO<sub>2</sub> hydrogenation to light olefins. *ACS Appl. Mater. Interfaces* **2020**, *12*, 24855 [24867.
- [129] Chen, H.; Liu, P.; Li, J.; Wang, Y.; She, C.; Liu, J.; Zhang, L.; Yang, Q.; Zhou, S.; Feng, X. MgH<sub>2</sub>/Cu<sub>x</sub>O hydrogen storage composite with defect-rich surfaces for carbon dioxide hydrogenation. *ACS Appl. Mater. Interfaces* **2019**, 11, 31009 31017.
- [130] Tian, H.; Yao, J.; Zha, F.; Yao, L.; Chang, Y. Catalytic activity of SAPO-34 molecular sieves prepared by using palygorskite in the synthesis of light olefins via CO<sub>2</sub> hydrogenation. *Appl. Clay Sci.* **2020**, *184*, 105392.
- [131] Wu, T.; Lin, J.; Cheng, Y.; Tian, J.; Wang, S.; Xie, S.; Pei, Y.; Yan, S.; Qiao, M.; Xu, H.; Zong, B. Porous graphene-confined Fe–K as highly efficient catalyst for CO<sub>2</sub> direct hydrogenation to light olefins. ACS Appl. Mater. Interfaces 2018, 10, 23439 23443.
- [132] Chen, H.; Liu, J.; Liu, P.; Wang, Y.; Xiao, H.; Yang, Q.; Feng, X.; Zhou, S. Carbon-confined magnesium hydride nano-lamellae for catalytic hydrogenation of carbon dioxide to lower olefins. *J. Catal.* **2019**, 379, 121 28.
- [133] Fujiwara, M.; Satake, T.; Shiokawa, K.; Sakurai, H. CO<sub>2</sub> hydrogenation for C<sub>2+</sub> hydrocarbon synthesis over composite catalyst using surface modified HB zeolite. *Appl. Catal. B: Environ.* **2015**, *179*, 37—33.

971

965 966 967

**Graphical Abstract** 

